Engineering a Temperature-Responsive, Local and Sustained Release System for the Paranasal Sinuses

by

Andrea Leigh Schilling

Bachelor of Science, Rensselaer Polytechnic Institute, 2011

Master of Science, Rutgers University, 2015

Submitted to the Graduate Faculty of the

Swanson School of Engineering in partial fulfillment

of the requirements for the degree of

Doctor of Philosophy

University of Pittsburgh

2021

UNIVERSITY OF PITTSBURGH

SWANSON SCHOOL OF ENGINEERING

This dissertation was presented

by

Andrea Leigh Schilling

It was defended on

September 16, 2021

and approved by

Ipsita Banerjee, Ph.D. Associate Professor, Department of Chemical and Petroleum Engineering

Tagbo H.R. Niepa, Ph.D. Assistant Professor, Department of Chemical and Petroleum Engineering

Eric W. Wang, M.D. Associate Professor, Department of Otolaryngology—Head and Neck Surgery

Stella E. Lee, M.D. Section Chief, Rhinology, Division of Otolaryngology—Head and Neck Surgery, Department of Surgery, Harvard Medical School

Dissertation Director: Steven R. Little, Ph.D. William Kepler Whiteford Professor, Department of Chemical and Petroleum Engineering

Engineering a Temperature-Responsive, Local and Sustained Release System for the Paranasal Sinuses

Andrea Leigh Schilling, PhD

University of Pittsburgh, 2021

Controlled-release drug delivery is a valuable strategy for providing long-acting treatment, especially to anatomical regions with limited access, such as the paranasal sinuses. Chronic inflammation of the sinuses associated with the prevalent condition, chronic rhinosinusitis (CRS), is routinely treated with topical corticosteroids. While numerous methods for daily intranasal administration exist, the anatomy and physiology of the nasal cavity and sinuses, along with maintaining patient adherence, can limit their efficacy. Controlled-release sinus stents are also available; however, their degradation or uneven contact can cause local adverse tissue reactions. Instead, a reversibly conformable system could improve mucosal compatibility while achieving sustained drug release. Accordingly, a thermoresponsive poly(N-isopropylacrylamide)-based hydrogel with poly(lactic-co-glycolic acid) microspheres (PLGA MS) was developed. This delivery system, called "TEMPS" (Thermogel, Extended-release Microsphere-based delivery to the Paranasal Sinuses), undergoes a reversible sol-gel transition at approximately 33°C such that it can be applied as a liquid at ambient temperature, conform to the sinonasal epithelium as it gels at body temperature, and localize controlled-release MSs. Following application in rabbit sinuses for 30 days, TEMPS engineered to steadily release the corticosteroid mometasone furoate significantly reduced sinonasal inflammation, as characterized by micro-computed tomography and histopathology analysis. As TEMPS is intended for apposition with ciliated epithelium, thermogel compatibility was demonstrated by *ex vivo* incubation with human nasal epithelium for 24 hours and showed that cilia motility was maintained. In CRS patients, enhancing cilia

regeneration would also help improve airway health. Thus, TEMPS was engineered to provide 30-day sustained release of retinoic acid, which promotes cilia differentiation. In terms of the formulation of TEMPS, the drug-loaded PLGA MSs are susceptible to hydrolysis, therefore the MSs and thermogel must be combined immediately prior to administration. Removing the water content of TEMPS through freeze drying resulted in a shelf-stable, ready-to-use form, mitigating aqueous instability. Freeze-dried TEMPS stored under ambient conditions for 6 weeks maintained its release kinetics and MS morphology. Additionally, when applied to a simulated mucosal surface, freeze-dried TEMPS rehydrated and gelled *in situ* without undergoing displacement. Ultimately, TEMPS is a versatile and clinically-translatable system that provides uniform distribution along the sinonasal epithelium for local drug delivery.

Table of Contents

Acknowledgements ..... **xv**

List of Equations ..... **xvii**

1.0 Introduction **1**

1.1 Sinonasal Anatomy and Physiology **2**

1.1.1 The Nose, Nasal Cavity, and Paranasal Sinuses **2**

1.1.2 Defense Mechanisms of the Upper Airways **3**

1.2 Nasal and Sinonasal Diseases: Rhinitis and Rhinosinusitis **5**

1.2.1 Allergic Rhinitis **5**

1.2.2 Acute Rhinosinusitis **6**

1.2.3 Chronic Rhinosinusitis **6**

1.3 Current Treatments for Rhinitis and Rhinosinusitis **8**

1.3.1 Medical Therapies **8**

1.3.2 Functional Endoscopic Sinus Surgery **10**

1.4 Challenges of Local Delivery to the Nasal and Sinus Cavities **11**

2.0 Controlled Drug Delivery to the Sinuses **13**

2.1 Biomaterials Used in the Context of Sinonasal Delivery Systems **14**

2.1.1 Naturally-Derived Biomaterials **14**

2.1.1.1 Polysaccharides **14**

2.1.1.2 Proteins **17**

2.1.2 Synthetic Biomaterials **18**

2.1.2.1 Polyesters **18**

2.1.2.2 Polyethers 19

2.1.2.3 Poly(N-isopropylacrylamide) 20

2.1.2.4 Polyurethane 21

2.1.2.5 Vinyl Polymers 21

2.1.2.6 Polyacrylic Acid 22

2.1.2.7 Silica 22

2.2 Systems for Controlled Sinonasal Drug Delivery 23

2.2.1 Nasal Packs, Dressings, and Spacers 23

2.2.2 Sinus Stents and Meshes 28

2.2.3 Nano- and Microparticles 35

2.2.4 *In situ* Hydrogels 42

2.2.5 Combination Systems 47

2.3 Discussion 55

3.0 TEMPS: A Thermoresponsive and Controlled Release System for Long-Acting Corticosteroid Delivery into the Paranasal Sinuses 58

3.1 Introduction 58

3.2 Materials & Methods 59

3.2.1 Microsphere Fabrication and Characterization 59

3.2.2 Thermogel Fabrication and Characterization 61

3.2.3 *In vitro* Drug Release and Bioactivity 62

3.2.4 Animal Model 63

3.2.5 Disease Induction and MicroCT Imaging 64

3.2.6 Treatment Application 65

3.2.7 *In vivo* Measurements 66

3.2.8 Histologic Preparation and Assessment 67

3.2.9 Statistical Analyses 68

3.3 Results 69

3.3.1 TEMPS Provides Extended Release of Bioactive Steroid in a Thermoresponsive and Cytocompatible System *in vitro* 69

3.3.2 Evaluating Inflammation in an Obstruction-Based CRS Rabbit Model 71

3.3.3 Sinonasal Inflammation was Reduced Following Treatment with Mometasone-TEMPS 74

3.3.4 Steroid was Safely Delivered from TEMPS Maintained in the Maxillary Sinuses for 4 Weeks 77

3.4 Discussion 79

4.0 Compatibility and Versatility of TEMPS for Promoting Sinonasal Cilia Regeneration 88

4.1 Introduction 88

4.2 Materials & Methods 90

4.2.1 Thermogel Fabrication: 90

4.2.2 Microsphere Fabrication 90

4.2.3 RA MS and RA-TEMPS Characterization 91

4.2.4 Gelation Temperature 91

4.2.5 Bioactivity Assay 92

4.2.6 Sinonasal Epithelial Cell Testing 92

4.2.7 Cilia Compatibility Testing 93

4.2.8 Statistical Analysis 94

4.3 Results 95

4.3.1 Development of Microspheres for Sustained Release of Bioactive RA 95

4.3.2 Drug Release and Gelation of RA-TEMPS 97

4.3.3 Cilia Maintain Motility after Incubation with Thermogel 98

4.3.4 *In vitro,* Preclinical, and Clinical Dosing Considerations for RA-TEMPS 100

4.4 Discussion 103

5.0 Shelf-Stable, Ready-to-Use TEMPS for Clinical Translation 108

5.1 Introduction 108

5.2 Materials & Methods 109

5.2.1 Preparation and Freeze Drying of TEMPS 109

5.2.2 Differential Scanning Calorimetry & Thermal Gravimetric Analysis 110

5.2.3 Scanning Electron Microscopy 111

5.2.4 Water Content & Swelling Ratio 111

5.2.5 Gelation Temperature & Kinetics 112

5.2.6 Drug Release & Bioactivity Characterization 112

5.2.7 'Drip Transfer' Assay 113

5.2.8 Statistical Analyses 113

5.3 Results 114

5.3.1 Determining the Thermogel Phase Transition Temperatures by DSC 114

5.3.2 Texture, Residual Moisture, and Gelation of Freeze-Dried Thermogel 116

5.3.3 Shelf-Stability and Mucoadhesion of FD-TEMPS 120

5.4 Discussion 124

6.0 Conclusions and Future Work 129

6.1 Rabbit Maxillary Antrostomy for TEMPS Application 130

6.2 TEMPS Integrity in the Presence of Respiratory Bacteria 133

6.3 Air-Liquid Interface Compatibility Studies 134

6.4 Stability and Sterilization of FD-TEMPS 136

6.5 Treg-TEMPS: An Immunoengineering Approach for CRS Treatment 139

Bibliography 144

List of Tables

Table 1. Steroid-Impregnated Nasal Packs, Dressings, and Spacers for Post-Operative CRS Treatment 26

Table 2. Controlled Release Systems for the Nasal Cavity and Sinuses 52

Table 3. Histopathology Scoring Criteria 68

Table 4. Properties of PLGA Used to Fabricate RA MSs 90

Table 5. RA MS Fabrication Parameters, Size, Loading, and Encapsulation Efficiency 96

Table 6. Prospective Preclinical and Clinical Dosing of RA-TEMPS 102

Table 7. Thermogel Transition Temperatures 116

List of Figures

Figure 1. Anatomy of the Nasal Cavity and Paranasal Sinuses..... 3

Figure 2. CT and Endoscopy Images of Healthy and Diseased Sinuses. 7

Figure 3. Overview of Biomaterials Used in Controlled Release Sinonasal Delivery Systems. 14

Figure 4. A Resorbable Nasal Pack in the Sphenoethmoidal Recess. 23

Figure 5. Degradable Sinus Stents for Local Corticosteroid Delivery to Specified Sinuses. 29

Figure 6. A Bioresorbable, Self-Expanding Polymeric Mesh for the Sinuses. 33

Figure 7. Nanoparticle Transport in CRS Mucus Samples. 37

Figure 8. PLGA/PEG Nanostructured Microspheres 39

Figure 9. Deposition of an *in situ* Gelling Suspension in a Nasal Cavity Model. 46

Figure 10. Biodegradable PLLA Stent with Drug-Loaded PLGA Nanoparticles. 48

Figure 11. Self-Healing Hydrogel with Anti-Bacterial and Anti-Inflammatory Liposomes.50

Figure 12. Schematic of the Single Emulsion Procedure for PLGA MS Fabrication. 60

Figure 13. Experimental Design for Evaluating TEMPS in Rabbits with Induced CRS. ... 64

Figure 14. Quanitifying Rabbit Sinus Opacification by Micro-Computed Tomography (MicroCT) Imaging..... 67

Figure 15. Bioactive Mometasone Furoate can be Released from TEMPS for 4 Weeks. 70

Figure 16. TEMPS Undergoes Reversible Apposition and is Compatible with SNECs..... 71

Figure 17. MicroCT Analysis of Rabbit Sinus Opacification at Baseline and After Disease Induction. 72

Figure 18. Successful Disease Induction in Rabbits Showed Evidence of Unilateral Disease by MicroCT, Endoscopy, and Histopathology. 73

Figure 19. MicroCT Imaging Showed Reduced Opacification of the Right Maxillary Sinus Following Application of m-TEMPS Compared to v-TEMPS. 75

Figure 20. Histopatholoy Sections Showed Evidence of Iatrogenic Trauma due to Application of TEMPS that was Reversed by Local Steroid Delivery. 76

Figure 21. IOP was Not Affected by 4 Weeks of Local Steroid Delivery from TEMPS. 78

Figure 22. Illustration of RA-TEMPS Delivery System and Compatibility Testing. 89

Figure 23. *In vitro* Characterization of RA MS Formulations..... 97

Figure 24. Release Kinetics and Gelation of RA-TEMPS are Consistent with RA MS and Thermogel Alone..... 98

Figure 25. Human Nasal Epithelium Incubated in Thermogel Maintained Cilia Motility. 99

Figure 26. Growth and Viability of SNECs Treated with Soluble RA or RA MSs. 101

Figure 27. Thermal Behavior of Gels as Measured by DSC Thermograms..... 115

Figure 28. Photographs Showing the Textures of Freeze-Dried Gels. 117

Figure 29. SEM Images of Freeze-Dried Gel Formulations. 118

Figure 30. Analysis of the Thermogel Water Content and Residual Moisture. 119

Figure 31. Rehydration, Swelling, and Gelation of Freeze-Dried Thermogels. 120

Figure 32. SEM of TEMPS and FD-TEMPS..... 121

Figure 33. Characterization of Mometasone MSs After 1st and 2nd Freeze-Drying Cycle. 122

Figure 34. Cumulative Release and Bioactivity of Mometasone from FD-TEMPS and TEMPS..... 123

Figure 35. Transfer Distance of Thermogel and TEMPS in Hydrated or Freeze-Dried Form. 124

Acknowledgements

First and foremost, I would like to express my gratitude to my mentor and dissertation advisor, Dr. Steve Little. Steve, thank you for welcoming me into your group, challenging me to grow as a researcher and a writer, and providing the delicate balance of guidance and independence throughout my time as a graduate student. I am grateful for the opportunity to complete my doctorate under your mentorship. I would also like thank my collaborators, Dr. Stella Lee and Dr. Eric Wang, who brought the need for a new sinonasal drug delivery system to our laboratory. Your expertise was critical to getting this project started as well as guiding me through the intricate details of the sinuses and sinonasal disease. To the additional members of my dissertation committee, Dr. Tagbo Niepa and Dr. Ipsita Banerjee, I am so appreciative of your insight through the dissertation process and encouragement through graduate school as a whole.

To the members of the Little Lab, I could not be more thankful to have worked alongside such an exceptional group. Dr. Abhinav Acharya and Dr. Riccardo Gottardi, thank you for your help while I got started in the lab. Dr. Ashlee Greene Anderson, I am grateful for the many questions your patiently answered and, in general, for being a constant friend and supporter. Dr. R. Warren Sands, thank you for your thoughtful recommendations, Dr. Stephen Balmert, for unwavering assistance in any number of experimental endeavors, and Dr. Yalcin Kulahci for your assistance with the rabbit studies. And to the current lab members, Dr. Nihan Yonet Tanyeri, Matthew Borrelli, Lizzy Bentley, and Julie Kobyra, your support these last few years, both virtually and in the lab, has made finishing graduate school during a pandemic so much more manageable. Finally, to the undergraduate students who I was fortunate to mentor, Sandra Walton,

Adam Carcella, and Erin Cannon, your questions and enthusiasm helped me grow, thank you for your time and energy in the lab.

There are numerous faculty, collaborators, and organizations at Pitt that supported me and my research over the last 5 years. My sincere gratitude to the CTSI program and Pitt Strive for their funding and training. Thank you to Dr. Lora Rigatti and the DLAR team for making the rabbit studies and analysis feasible. Dr. Maliha Zahid, your training and kindness were critical to completing the cilia testing. And thank you to John Moore for leading with the cilia collection. Dr. Susan Fullerton and Dr. Dan Lamont, the thermal analysis work would not have been possible without you. Finally, Dr. Sylvanus Wosu, Dr. Steve Abramowitch, Sussan Yetunde Olaore, and the Pitt Strive community, your support and energy made me feel welcome at Pitt and helped me grow in countless ways.

Finally, to my family, friends, and coworkers, I would not me here without your constant encouragement. Greg, Brian, and Keith, thank you for graciously supporting me as I left CCT to go back to school. To my friends, both those that have been with me for decades and those I've made at Pitt, I am so grateful for your presence in my life, especially during the trying times of getting a PhD. To my parents and sister, your unconditional love and support of learning is why I am here. To my dog, Berger, you joined us at exactly the right moment. Thank you for encouraging regular breaks. Finally, and most importantly, to my husband Ben, these last 5 years of graduate school were a roller coaster, thank you for being by my side through it all because I hate roller coasters. I can't wait to see what we take on next.

List of Equations

Equation 3-1: % Viability for Thermogel Cytocompatibility..... 62

Equation 3-2. Cumulative Standard Deviation (s)..... 69

Equation 5-1: Thermogel Water Content..... 111

Equation 5-2: Thermogel Swelling Ratio..... 111

Equation 5-3: Optical Transmittance for Gelation Kinetics 112

1.0 Introduction

Inflammatory diseases of the sinonasal mucosa, including rhinitis and rhinosinusitis, pose significant healthcare and socioeconomic burdens [1,2]. The prevalence of the most common form of rhinitis, allergic rhinitis ranges from 3% to 19% in the United States and 10% to 30% worldwide [1], while rhinosinusitis affects approximately 12% of adults in the US [3]. Domestically, the financial impact of these diseases results in annual expenditures exceeding $11.2 billion for allergic rhinitis treatments (as of 2005) [4] and $8.6 billion for chronic rhinosinusitis (as of 2007) [2]. This burden is not only associated with medical costs, but also diminished quality of life, reduced productivity, and multiple co-morbidities.

Treatments for rhinitis and rhinosinusitis can mitigate symptoms, however, effective delivery into the nasal cavity and paranasal sinuses remains a significant barrier to disease management. Numerous anatomical features and physiological mechanisms in the nose, nasal cavity, and sinuses exist to protect the upper respiratory tract from inhaled debris and microorganisms [5,6]. These same features, though, limit the deposition and retention of conventional topical nasal sprays, drops, and irrigation. Consequently, frequent dosing, specialized devices, and chemical modifications can be necessary for suspension and aerosolized therapeutics [7–9]. Alternatively, methods for controlled release delivery are an attractive solution to improve distribution while also avoiding the need for daily administration. To provide context for these delivery systems (which are discussed in detail in Chapter 2), in this chapter, the anatomy of the nose, nasal cavity, and sinuses is reviewed, as well as the presentation of rhinitis and rhinosinusitis. Current clinical standards for management of these diseases are discussed, as well as the challenges of efficient intranasal delivery.

1.1 Sinonasal Anatomy and Physiology

1.1.1 The Nose, Nasal Cavity, and Paranasal Sinuses

The intricate anatomy of the nose, nasal cavity, and paranasal sinuses is essential for processing the ~10,000 L of air that we inhale each day [10]. Air enters the external structure of the nose through the nares into the anterior nasal cavity, or nasal vestibule, which is divided into two compartments by the nasal septum (Figure 1). Posterior to the nasal vestibule is the nasal valve and three scroll-like projections, the inferior, middle, and superior turbinates (or conchae). The space between each turbinate and the lateral nasal wall is the inferior, middle, and superior meatus, respectively [5,6,11]. Within the middle and superior meatus are channels that connect to the paranasal sinuses, which are eight air-filled cavities symmetrically oriented across the mid-line of the face. The maxillary sinuses are the largest sinuses located in the cheeks along the upper jawbone (the maxilla) [6,12]. The frontal sinuses are situated in the forehead (behind the frontal bone) and the ethmoid sinuses comprise 8–15 air cells along the upper and lateral aspect of the nasal cavity [6]. The maxillary, anterior ethmoid, and frontal sinuses drain to the nose through the ostiomeatal complex in the middle meatus while the posterior ethmoid drains via the superior meatus [11]. Lastly, the sphenoid sinuses are positioned behind in the eyes surrounded by the skull base bone (the sphenoid) and drain to the nose via the sphenoethmoidal recess located posterior and medial to the superior turbinate [11,12].

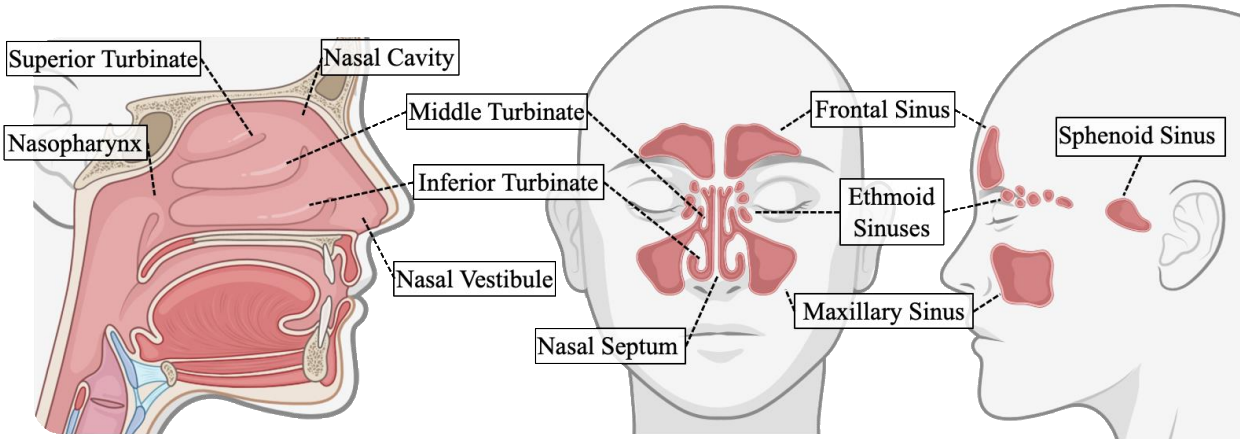

Figure 1. Anatomy of the Nasal Cavity and Paranasal Sinuses

The structures within the nasal cavity are responsible for several critical physiologic processes, including olfaction, sensation, barrier and immunologic defenses, and humidifying and warming inspired air. For example, inspired air undergoes logarithmic heating in the nasal cavity where the most rapid temperature increase occurs at the nasal valve so that the middle turbinate and nasopharynx are maintained at 32.2 ± 2.2°C and 33.9 ± 1.5°C, respectively [13]. Readers interested in in-depth analyses of each of the physiologic processes occurring in the nose, nasal cavity, and sinuses are referred to the following references [5,6,14].

1.1.2 Defense Mechanisms of the Upper Airways

Innate defenses of the upper airways, such as restricting particle entry from the air, can protect against inhaled pathogens or irritants, but also present challenges for effective intranasal drug delivery. In the nasal vestibule, particles >12 μm are filtered by air turbulence and thick hairs, or vibrissae, where the squamous epithelium also creates a protective barrier [5,6,10]. Posterior to the nasal vestibule, approximately 1.5 cm from the nares, is the nasal valve where respiratory

resistance and air flow velocity are at their maximum. The narrow dimensions of the nasal valve along with the airflow characteristics can restrict the entry of particles >3 μm [10,15].

Beyond the nasal valve, particles in the range of 0.5–3 μm are efficiently trapped by mucus overlaying the nasal mucosa and cleared [10]. Mucus is a viscoelastic mixture consisting primarily of water (~95% w/w), as well as mucin and globular proteins, salts, DNA, lipids, cells, and cellular debris. Mucins are high molecular weight proteins with a strong net-negative surface charge that are secreted by goblet cells and submucosal glands. Mucins protect the airway epithelium along with mucus as a whole, which forms a continuous barrier that is 5–15 μm in thickness and can trap microorganisms, cellular debris, and other potentially harmful material [16]. Below the viscoelastic mucus layer is an aqueous layer consisting of electrolytes called the periciliary fluid, which lies adjacent to the mucosal epithelium [9]. The nasal epithelium consists of pseudostratified columnar epithelial cells, goblet cells, ciliated cells, and non-ciliated columnar cells with microvilli [5]. Epithelial cells in the nasal cavity, sinuses, and many other regions of the body, have 50 to 200 specialized structures called cilia that extend 5–7 μm from the apical cell surface. Cilia are responsible for driving mucociliary clearance (MCC) whereby they extend into the mucus, perform a forward stroke, then bend and return to the starting position by traveling through the periciliary fluid [8,17]. MCC is a critical defense mechanism responsible for clearing mucus and entrapped debris to the digestive system via the nasopharynx. In healthy humans, cilia beat at a frequency of 9–15 Hz, resulting in turnover of the mucus blanket every 20–30 minutes [9].

Along with filtering and barrier defenses, there are several immunological defenses of the upper airways as well. Immunoglobulins, enzymes, and other protective proteins and gasses are secreted in the mucus [6]. Nitric oxide (NO), for example, is continuously produced in the upper respiratory tract and in the paranasal sinuses in particular [18,19]. NO has been shown to enhance

MCC as well as possess antimicrobial, antiviral, and antifungal effects [20,21]. Additionally, immune cells such as neutrophils and lymphocytes are present within the underlying mucosa [6].

In a healthy, homeostatic state, the upper airways are protected by these defense mechanisms, allowing other physiologic processes to proceed undisturbed. However, when these defenses are insufficient, bacteria, viruses, allergens, and environmental pollutants can lead to the development of a number of disease states.

1.2 Nasal and Sinonasal Diseases: Rhinitis and Rhinosinusitis

Rhinitis and rhinosinusitis are two common and related diseases of the nasal and sinonasal mucosa, respectively. While they share symptoms of nasal discharge and congestion, rhinitis is also associated with sneezing and nasal itching, and rhinosinusitis is more commonly accompanied by facial pain, pressure, and a loss or reduction in sense of smell [22–24]. Both conditions can significantly decrease quality of life (QoL) due to persistence of these symptoms as well as "extra-rhinologic" indications such as poor sleep and cognitive dysfunction [22,25,26]. Furthermore, as a result of the continuity of the nasal and sinus mucosa, rhinosinusitis is often preceded by rhinitis [24,25,27].

1.2.1 Allergic Rhinitis

There are several subclasses of rhinitis, including infectious, hormonal, occupational, and the most common, allergic rhinitis (AR) [23]. AR can develop as a result of an allergic response to dust mites, pollen, animal dander, small molecular weight chemicals, and many other triggers

[22,25]. Allergen exposure leads to cross-linking of IgE receptors on mast cells and the release of inflammatory mediators, such as histamine, prostaglandins, and leukotrienes. A late inflammatory response occurs with an influx of T helper type 2 (Th2) cells and the release of interleukin (IL)-3, IL-4, IL-5, and IL-13. These cytokines lead to a systemic overproduction of allergen-specific IgE antibodies from B cells with infiltration of eosinophils, basophils, and mast cells into the nasal mucosa and epithelium [23,25,28,29]. Additionally, the inflamed nasal mucosa is primed, or hyper-responsive, for future exposure to lesser amounts of allergen or nonspecific stimuli (such as cigarette smoke or pollutants) [25,29]. Proper management of rhinitis is essential because patients often have coexisting respiratory conditions including asthma, sleep apnea, and rhinosinusitis [30].

1.2.2 Acute Rhinosinusitis

Rhinosinusitis encompasses a broad spectrum of diseases characterized by inflammation or infection of the nasal and paranasal mucosa [27]. Rhinosinusitis is classified by the duration of symptoms, etiology, and the presentation of changes to the mucosa. Acute rhinosinusitis (ARS) is defined by the presence of symptoms for less than 4 weeks. It is typically caused by viral or bacterial infection, and therefore, it is further sub-classified as acute bacterial rhinosinusitis (ABRS) or viral rhinosinusitis (VRS).

1.2.3 Chronic Rhinosinusitis

When rhinosinusitis symptoms persist for longer than 12 weeks, it is classified as chronic rhinosinusitis (CRS) [24,31]. As mentioned previously, CRS can significantly diminish QoL. In fact, CRS patients report a rating of general health status (health utility score) worse than that of

patients with chronic obstructive pulmonary disorder or Parkinson's disease [32]. CRS is of multifactorial etiology in which environmental stressors, pathogens, or commensal flora can trigger a dysfunctional host-environment response and subsequent chronic mucosal inflammation [33,34]. As a result, structural changes to the nose and sinuses can occur with inflammatory mucosal tissue and secretions filling the sinuses (Figure 2A) [35]. Microbial biofilms have also been identified in some CRS patients and are generally associated with severe and recalcitrant disease. Whether biofilms have a role in CRS pathogenesis, though, remains unclear [36].

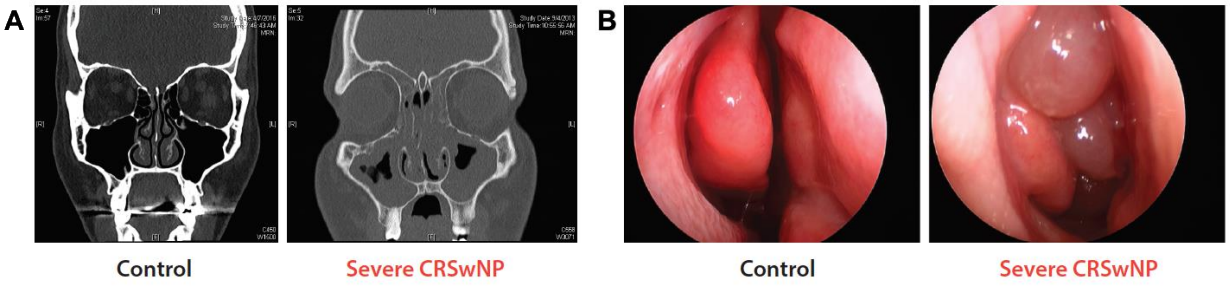

Figure 2. CT and Endoscopy Images of Healthy and Diseased Sinuses.

(A) CT scans and (B) endoscopic images of healthy individual (Control) and one with severe CRSwNP.

Reproduced with permission [35]. Copyright 2017, Annual Reviews, Inc.

A notable complexity of CRS is that there are two disease subgroups or phenotypes that are differentiated by the absence or presence of nasal polyps, CRSsNP and CRSwNP, respectively [33,37,38]. Like AR, CRSwNP is more often associated with inflammatory airway diseases and characterized by a Th2-biased profile with presence of nasal polyps, which are edematous teardrop-like growths along the mucosa (Figure 2B). In addition to nasal polyps, edema and an abundance of eosinophils, basophils, mast cells, B cells, and plasma cells are observed as well as elevated levels of IL-4, IL-5, and IL-13 [35]. CRSsNP, on the other hand, is associated with a

mixed or T helper type 1 (Th1)-biased inflammatory response. This disease phenotype is generally characterized by a neutrophilic response with observations of fibrosis, collagen deposition, glandular hyperplasia, and increased expression of TGF-β [35]. Interestingly, CRSwNP is more common in the US and Europe, while CRSsNP is more prevalent in Asia [37].

1.3 Current Treatments for Rhinitis and Rhinosinusitis

1.3.1 Medical Therapies

Following diagnosis of rhinitis or rhinosinusitis using doctors' questionnaires, nasal examination or endoscopy, hypersensitivity tests, or radiographic imaging, a range of medical therapies are prescribed for treatment. Both over-the-counter and prescription medications can be used that are administered by a variety of delivery methods.

The most conservative treatment available for sinonasal conditions is nasal saline irrigation, which can assist with the clearance of mucus, debris, and inflammatory mediators from the sinonasal cavities. Additionally, irrigation aids in keeping the mucosa moist which can promote MCC [34]. The best results are often achieved with high volume rinses, generally >100 mL and sometimes as much as 240 mL. Saline irrigation is a common adjunct treatment for CRS management that can improve QoL symptoms and reduce medication needs. Evidence for effectiveness for ARS management is less compelling but it can aid with symptom relief [24]. Overall, saline irrigation is a low cost and low risk treatment strategy that can be recommended along with other medical therapies.

Antibiotics are one class of medical therapies that can be used for treating rhinosinusitis, specifically if there is evidence of a bacterial infection. For ABRS, amoxicillin is typically a first line of therapy, sometimes prescribed with clavulanate, for 10 days at most. ABRS can resolve without treatment, however, and the associated cost and potential for adverse events following antibiotic treatment must be considered. Similar concerns exist with CRS. While antibiotic treatments can result in some improvement in CRS patients, the concerns of medication interactions, mild adverse events, and risk of developing bacterial resistance must be considered. As of 2016, no randomized control trials have shown a clear benefit of topical antibiotics for CRS management [24].

Corticosteroids, rather, are currently the clinical standard for CRS management and have demonstrated some level of efficacy for ARS and AR as well. Corticosteroids act by both activating anti-inflammatory genes and inhibiting proinflammatory genes, such as those expressed by epithelial cells [39]. Notably, second-generation intranasal corticosteroids (INC) have the benefit of very low systemic bioavailability. For example, mometasone furoate and fluticasone propionate nasal sprays have <0.1% and <1.0% systemic bioavailability, respectively. In comparison, oral steroids and older INCs, such as triamcinolone acetonide and budesonide, have much higher systemic bioavailability (46% and 34%, respectively). INCs are generally preferred over oral steroids for the reduced risk of systemic side effects such as growth inhibition, decreased bone mineral density, and glaucoma, among others [40]. Moderate efficacy of INCs for seasonal AR has been demonstrated [28] and second-generation INCs can help with symptom relief for ARS but are generally not recommended for uncomplicated disease [24]. Topical sprays are recommended for management of CRSsNP and CRSwNP as they can reduce symptoms and improve endoscopy scores. Steroids can also be added to nasal irrigation fluids, but this off-label

use can be associated with higher costs relative to sprays [24]. Oral corticosteroids have shown no clear beneficial evidence for CRSsNP. In contrast, for CRSwNP, oral corticosteroids can be prescribed for short durations and result in significant improvements, but this is generally not recommended more than once every 2 years [24].

Other medical therapies such as decongestants and antihistamines can also be used for nasal symptom relief. Intranasal decongestants can relieve congestion by causing vasoconstriction that reduces the volume of the nasal mucosa and improves nasal airflow [34]. There are noted benefits of decongestants for ARS and AR, but short-term use is recommended [24,28]. Similarly, their short-term use for management of CRS as an adjunct therapy can be advised [34]. Antihistamines can reduce sneezing and nasal discharge by competitive antagonism of H_1 receptors found on nerve endings, smooth muscle cells, and glandular cells. By preventing histamine binding, antihistamines can reduce AR symptoms, and have some anti-inflammatory effects as well. [29]. Second-generation oral antihistamines are preferred for AR treatment for their non-sedating effects, as well as intranasal antihistamines, and are generally prescribed on an as-needed basis [28,30]. Antihistamines can also reduce nasal secretions associated with ARS [24], but are not recommended for CRSsNP or CRSwNP treatment [34].

1.3.2 Functional Endoscopic Sinus Surgery

The medical therapies described above are generally effective for management of AR and ARS, however CRS can be refractory to these treatment methods and surgical intervention can be recommended. In such cases, functional endoscopic sinus surgery (FESS) is performed to reestablish sinus outflow tracts by removing inflamed tissue and bone. FESS is rather common with over 250,000 surgeries performed in the US each year [31]. In addition to removing diseased

tissue, surgery can improve the distribution of local maintenance therapy (daily corticosteroid nasal sprays or saline irrigation), which reduces the need for oral corticosteroids [24,33]. A study using CT scans compared the anatomy of the nasal passage and sinuses of a normal, healthy individual to a CRS patient before and after surgery. In the normal individual, the maxillary ostia were 62 mm^2 and 65 mm^2 in area on the left and right sides, respectively. In the CRS patient, the ostium area on both sides was reported to be 0 mm^2 pre-operatively, while post-operatively, it was dramatically increased to 270 mm^2 and 180 mm^2 on the left and right sides, respectively [41]. The surgically enlarged ostia are important to improving post-operative drug delivery via daily topical methods as well as enables the use of degradable sinus stents [42], which are discussed in greater detail in Section 2.2.2. FESS can be an effective strategy for mitigating CRS symptoms, though it does have shortcomings. As surgery does not address the underlying cause of chronic inflammation, continued use of post-operative medical therapies is necessary. Additionally, in a study of CRSwNP patients, polyp recurrence was significantly decreased 6 months post-operatively; however, at 18 months, 40% of patients showed signs of disease relapse despite the continued use of medical therapy [43]. Moreover, revision surgery is needed in an estimated 20–50% of patients, particularly those with comorbidities, such as asthma and frontal sinus disease [43,44].

1.4 Challenges of Local Delivery to the Nasal and Sinus Cavities

The efficacy of current medical therapies is often limited by the barriers that protect the nasal cavity and sinuses (both pre- and post-operatively). In particular, mucus indiscriminately traps harmful materials, debris, drug molecules, and drug carriers by size exclusion, hydrogen

bonding, and electrostatic, hydrophobic, and specific binding interactions [7]. While mucus restricts permeability, MCC clears mucus and trapped materials such that topical nasal sprays have a half-life of only ~20 minutes in the nasal cavity [9]. In addition to rapid clearance, INC sprays have been found to deposit only 30% of the applied dose in the nasal cavity with the remaining dose swallowed and metabolized in the liver [40]. Access to the sinuses via the nasal cavity is especially limited due to the narrow ostia and poor ventilation [45]. While FESS can improve access for topical maintenance therapy, delivery to the frontal sinuses remains limited even following surgery [46]. Alternative devices for enhancing delivery to the sinuses have been explored, such as pulsating aerosols [46] and breath-powered Bi-Directional technology [8] or by adjusting patient head position while applying irrigation, sprays, and nebulizers [34]. Each of these methods, though, still require daily administration for clinical efficacy.

The limitations of daily delivery methods and challenges with patient adherence have motivated a growing body of research for controlled release systems that can achieve local and sustained drug concentrations in sinonasal tissues. These delivery systems have been designed using a number of different biomaterials, which are discussed in the following chapter.

2.0 Controlled Drug Delivery to the Sinuses

There has been considerable development of biomaterial-based systems that can locally deliver anti-inflammatory, antibiotic, decongestant, or antihistamine medications to the sinonasal cavities over an extended duration. Various delivery vehicles including nasal packs, dressings, sinus stents, polymeric meshes, nanoparticles, microparticles, and *in situ* hydrogels have been designed that leverage properties of naturally-derived and synthetic biomaterials. A summary of these materials is presented in Figure 3. In this chapter, these materials are briefly introduced with an emphasis on features that are valuable for drug delivery in the nasal and sinus cavities, such as compatibility with mucosal tissue, properties of bioadhesion or mucoadhesion, and gel-forming capabilities. The design and performance of the resulting delivery systems for targeted treatment of rhinitis and rhinosinusitis are discussed, including their benefits and limitations, which, recently, has motivated the development of combination systems that leverage desirable properties of their individual components to enhance therapeutic delivery. In particular, combination delivery vehicles can provide greater control of the duration of therapeutic release, as well as the ability to encapsulate multiple therapies, provide mechanical support, or conform to the mucosa. The future clinical use of controlled release systems with these attributes could have a transformative impact on improving treatment of difficult-to-control chronic diseases of the sinonasal mucosa.

	Packs, Dressings & Spacers		Stents & Meshes		Nano & Microparticles		Hydrogels & *In situ* gels	
Naturally-derived	CMC Hyaluronic acid Fibrinogen	Gelatin Calcium alginate			NaCMC HPMC	Chitosan	HPMC Chitosan Gellan gum	Pectin Sodium hyaluronate
Synthetic	PU	PVAc	PLGA PLLA	PGCL PLCL	PLGA PEG-PLA	Poloxamers Silica	PVP Carbopol	Poloxamers pNIPAAm

Figure 3. Overview of Biomaterials Used in Controlled Release Sinonasal Delivery Systems. CMC, carboxymethyl cellulose; PU, polyurethane; PVAc, poly(vinyl acetate); PLGA, poly(lactic-co-glycolic acid); PLLA, poly(L, lactic acid); PGCL, poly(glycolide-co-caprolactone); PLCL, poly(lactide-co-caprolactone); NaCMC, sodium carboxymethyl cellulose; HPMC, hydroxypropyl methyl cellulose; PEG, poly(ethylene glycol); PLA, poly(lactic acid); PVP, poly(vinylpyrrolidone); pNIPAAm, poly(N-isopropylacrylamide).

2.1 Biomaterials Used in the Context of Sinonasal Delivery Systems

2.1.1 Naturally-Derived Biomaterials

2.1.1.1 Polysaccharides

Polysaccharides are the most abundant natural polymers, and their versatility and biodegradability make them prevalent raw materials in many industries, including biomedical and pharmaceutical applications. Polysaccharides consist of sugar units linked by glycosidic bonds that can be chemically modified to semi-synthetic materials or fabricated in numerous forms, such as gels, foams, and particles [47]. As such, sinonasal drug delivery systems have been designed with polysaccharides as the primary component or combined with other polymers to modify properties.

Cellulose is a hydrophilic macromolecule derived from plants that has been chemically modified to create numerous cellulose derivatives with wide-reaching applications. Through etherification, water-insoluble cellulose can also be modified to cellulose ethers that are water soluble [48]. Several semi-synthetic cellulose ethers that have been classified by FDA as Generally Regarded As Safe (GRAS) are heavily used in pharmaceutical dosage forms. In particular, cellulose ethers have been shown to increase the viscosity of aqueous solutions and have bioadhesive properties, making them useful for oral, transdermal, and transmucosal drug delivery. Carboxymethyl cellulose (CMC) is the most heavily used cellulose ether, which has been used in gel and foam nasal packs because it can activate the coagulation cascade [49]. Sodium carboxymethyl cellulose (NaCMC) is a polyanionic cellulose ether that is particularly suited for transmucosal delivery because of its enhanced bioadhesion to mucosal surfaces compared to other cellulose ethers. At certain concentrations and conditions, NaCMC can also be used as a release enhancer by increasing osmotic pressure. Hydroxypropyl methyl cellulose (HPMC) exhibits good water and solvent solubility, making it a useful film coating material. Depending upon how it is used in the formulation, it can also enhance drug release by increasing osmotic pressure or control release as a hydrophilic matrix material with bioadhesive properties [48,50].

Hyaluronic acid (HA) is an essential component in the extracellular matrix (ECM) with a high affinity for water due to its abundance of negative charges. It is composed of alternating units of D-glucuronic acid and *N*-acetyl-D-glucosamine. HA and its salt form, sodium hyaluronate, can be biocompatible, biodegradable, non-immunogenic, non-thrombogenic, and bioactive. Chemical modification, such as esterification, can improve the stability of HA in hydrogels [51]. HA is also a natural component of airway secretions that has been shown to stimulate cilia beat frequency and is involved in several inflammatory pathways. In fact, clinical studies in both CRS and AR patients

have demonstrated a therapeutic effect of including sodium hyaluronate in nasal irrigation fluids [52].

Alginate is another naturally occurring water-soluble polysaccharide that is derived from seaweed and can be non-toxic, biocompatible, biodegradable, and is GRAS. Alginate, which is composed of alternating blocks of α-L-guluronic acid and β-D-mannuronic acid, is a polyanionic polymer with carboxylic groups giving it inherent mucoadhesive properties. Alginate is also present in salt forms, such as calcium alginate. Notably, in the presence of divalent cations (such as Ca^{2+}) alginate forms gels and precipitates. Swelling and viscoelasticity of calcium alginate gels can be adjusted by changing the ratio of guluronic acid or mannuronic acid, also gel properties can be altered by crosslinking or combining alginate salts with other polymers [53,54].

One of the most widely used natural mucoadhesive polymers is chitosan, a cationic copolymer of N-acetyl-D-glucosamine and D-glucosamine. It is obtained from the deacetylation of chitin, which is prevalent in the outer skeletons of crustaceans. Chitosan can exhibit low toxicity, biodegradability, and biocompatibility, as well as antimicrobial, permeation enhancing, and hemostatic effects. The primary mechanism for chitosan's mucoadhesive properties are electrostatic interactions between its positively charged amino groups that undergo protonation in acidic conditions and negatively charged mucus. It is noteworthy that chitosan is a pH-sensitive biopolymer due to the high prevalence of amino groups and therefore it has limited mucoadhesion at pH > 6 and becomes insoluble at higher pH as well [53,55,56]. The pH of healthy nasal mucosal has been reported to be slightly acidic with a range of 5.3–7.0 (mean 6.3). In rhinitis patients it has been reported to increase to 7.2–8.3, while in post-operative CRS patients it has been shown to decreased to a mean value of 5.7 (range of 3.8–7.7) [57,58]. Thus, the pH-dependency of chitosan's mucoadhesive capabilities may pose as a limitation for its use in the nasal and sinus cavities.

Gellan gum is an exopolysaccharide produced by *Sphingomonas elodea* bacteria that is widely used as a gelling agent. The structure of gellan gum contains free carboxylate groups making it anionic in nature. In the presence of cations and water, it undergoes gelation by a coil-to-helix transition. The double helical segments then aggregate forming a three-dimensional gel, the strength and texture of which can be altered by the concentration of gellan gum and cations. In its native structure, acylated gellan gum can form non-brittle and elastic gels, while deacylated gellan gum, on the other hand, forms brittle gels [59]. Gellan gum hydrogels are relatively mechanically weak but can be modified at free hydroxyl and carboxyl groups or gellan gum can be combined with additional polymers to optimize gel properties [60].

Similarly, pectin, a high molecular weight polysaccharide extracted from plant cells, is another naturally occurring ion-responsive gelling agent. Pectin is an anionic biopolymer composed of a poly-(1-4)-α-D-galacturonic acid backbone that is widely utilized in the food and pharmaceutical industries for its gelation properties. Gelation occurs due to aggregation of polymer chains resulting from hydrogen bonding, divalent cation cross-bridging, and hydrophobic interactions [61]. The gelling mechanism is dependent on several factors, including the material source, the degree of methoxylation, pH, and the presence of solutes [62].

2.1.1.2 Proteins

In addition to polysaccharides, proteins, including fibrin and gelatin, are another class of natural polymers that can be formulated in mucosal drug delivery systems. The inactive form of fibrin, fibrinogen, is a soluble glycoprotein that is primarily sourced from the liver and composed of three pairs of polypeptide chains. It is involved in many biological functions including blood clotting, wound healing, and inflammation. Fibrinogen exhibits mucoadhesive properties and can provide a scaffold by integrating drugs and growth factors for local delivery [63,64]. Gelatin, on

the other hand, is obtained from denaturing collagen, an abundant component in ECM. Gelatin can have low immunogenicity, high degradability, and can be stable at high temperatures and over a wide range of pH. It has gel-forming and foaming properties and can be grafted with synthetic polymers [65]. The gelatin used in nasal packs is often derived from purified porcine or bovine tissue and these packs can dissolve within 5 days after placement [49].

2.1.2 Synthetic Biomaterials

The other main category of biomaterials used in the design of drug delivery systems for the nasal and sinus cavities are synthetically derived. Properties of these materials have been reviewed extensively and thus, the following is a brief summary of the synthetic polymers and silica that have been used in sinonasal delivery applications.

2.1.2.1 Polyesters

Poly(lactic acid) (PLA) and poly(glycolic acid) (PGA) are two ubiquitous polyesters used in controlled drug delivery, as well as other applications with FDA approval. PLA and PGA can be biocompatible and, by hydrolysis, bioresorbable (i.e., their degradation products are eliminated by natural pathways). Notably, PLA exists in two forms, poly-L-lactide (PLLA), which is semi-crystalline with a high tensile strength (45–70 MPa), and poly-DL-lactide (PDLLA), which is an amorphous polymer [66]. The copolymer poly(lactic-co-glycolic acid) (PLGA) is widely used in drug delivery application because its rate and extent of degradation can be controlled by its hydrophilicity and crystallinity, which in turn can control the release rate of encapsulated therapeutics. A number of parameters can be adapted to tune release rates, such as increasing the

ratio of slower degrading LA relative to GA to decrease the rate of biodegradation and extend the release profile of drug carriers [67–70].

Poly(ε-caprolactone) (PCL) is another versatile polyester that degrades over a period of months to years because of its surface hydrophobicity and crystallinity. Like PGA and PLA, it can be biocompatible and bioresorbable and is often used as an elastomer because of its low glass transition temperature (-60°C) and low melting point (60°C) [71,72]. Copolymers of PCL with glycolide or lactide (PGCL or PLCL) can also be employed to control mechanical properties and degradation rates. Due to the control of the properties of these polymers, PCL, PLGA, and PLA have been used to fabricate sinonasal stents, nanoparticle, and microparticle delivery systems.

2.1.2.2 Polyethers

Polyethylene glycol (PEG), also referred to as polyethylene oxide (PEO), and polypropylene oxide (PPO) are versatile polyethers with differing affinities for water that can also be biocompatible. PEG is a non-ionic and crystalline polymer that is highly soluble in water and available over a wide range of molecular weights (from 400 Da to over 50 kDa for medical applications). Furthermore, because of its high solubility in organic solvents, it can be functionalized or modified in forms such as mPEG, or monomethyl-ether terminated PEG [73,74]. PEG can be used in hydrogels, to suppress nonspecific interactions of charged materials, or to reduce particle aggregation [74,75]. Low molecular weight PEGs can have muco-inert properties when coated at a sufficiently high density on particle surfaces, also referred to as PEGylation [76]. In contrast to PEG, PPO is a non-crystalline, flexible polymer that is insoluble in water at room temperature, except at low molecular weights. PPO is often used in block copolymers, such as poloxamers [73].

Poloxamers are synthetic amphiphilic polymers composed of hydrophilic PEO (A) and hydrophobic PPO (B) in an ABA-triblock configuration. Poloxamers have gained FDA approval in a variety of pharmaceutical applications including oral, parenteral, and topical routes of delivery. In particular, they can be used to encapsulate hydrophobic compounds in micelles, as surface coatings on hydrophobic nanoparticles, and as thermoresponsive hydrogels. Poloxamer solutions can undergo thermo-reversible gelation above their critical micelle concentration, which is dependent on the ratio of PPO to PEO. Below their sol-gel transition temperature ($T_{sol\text{-}gel}$), poloxamer solutions are liquid and upon reaching the $T_{sol\text{-}gel}$, the PPO blocks become dehydrated resulting in aggregation of the co-polymer chains into a micellar structure. Two common poloxamers are poloxamer 407 (P407) and poloxamer 188 (P188). P407, also known by its tradename Pluronic® F127, is composed of 70% PEO and 30% PPO (4000 g/mol) and P188 is 80% PEO and 20% PPO (1800 g/mol). Both P407 on its own and combinations of P407 and P188 have been formulated in thermoresponsive gels because their $T_{sol\text{-}gel}$ is close to body temperature. These gel formulations also exhibit mucoadhesive properties and have been shown to be non-irritating to mucosal tissue [73,77,78].

2.1.2.3 Poly(N-isopropylacrylamide)

Poly(N-isopropylacrylamide) (pNIPAAm) is another synthetic thermoresponsive polymer that is formed by polymerization of N-isopropylacrylamide (NIPAAm) monomers. It is a non-biodegradable polymer that undergoes a phase transition from liquid to gel at a lower critical solution temperature (LCST) near body temperature. For this reason, it has broad applicability in biomedical applications. Furthermore, properties of pNIPAAm-based gels can be tuned by chemical and physical crosslinking with other natural or synthetic polymers, such as PEG [79]. The mechanism for gelation of pNIPAAm is a change in polymer chain conformation due to

altering interactions with water. Below the LCST, the polymer chains are soluble in water and present in a flexible extended coil. Once heated to the LCST, the polymer chains become hydrophobic leading to chain collapse into globular structures. Salts, pH, and the addition of hydrophilic or hydrophobic copolymers can influence the temperature at which this phrase transition occurs [80,81].

2.1.2.4 Polyurethane

Polyurethanes (PU) encompass a broad range of synthetic polymers whose physicochemical and mechanical properties are dependent on their constituent polymers. Generally, PUs have a urethane bond in their main chain and are comprised of a hard and soft segment, which provide mechanical strength and flexibility, respectively. The soft segment of a biodegradable PU is often a polyester or polyether, and the hard segment must consist of a nontoxic diisocyanate and degradable chain extender. For applications such as degradable foams, the rate of degradation is generally governed by the soft segment's susceptibility to hydrolysis [82,83].

2.1.2.5 Vinyl Polymers

Polyvinyl acetate (PVAc) and polyvinylpyrrolidone (PVP) are two versatile vinyl polymers that can be used to create many medical and pharmaceutical materials, such as hydrogels and sponges. PVAc can be fully or partially hydrolyzed to polyvinyl alcohol (PVA) where the amount of hydroxylation can control physical, chemical, and mechanical properties. Through chemical or physical crosslinking, PVA can be formed into hydrogels, or dehydrated to form a nasal pack sponge. As a biomaterial, it can be biocompatible, non-toxic, and bioadhesive [84]. PVP is a hydrophilic polymer that can be biocompatible, biodegradable, non-toxic, chemically inert, and temperature- and pH-resistant. It is GRAS by FDA and used in oral, topical, transdermal, and

ocular drug delivery systems. In addition to uses as polymeric microspheres and drug-loaded fibers, recent work has shown that incorporating PVP within hydrogel formulations can increase the gel strength [85].

2.1.2.6 Polyacrylic Acid

Carbomers, which are often referred to by their trade name Carbopol®, are polyacrylic acid polymers that exhibit pH-dependent properties. When hydrated in water, carbomers form acidic solutions with increasing viscosity and can form gels at pH 4–6. Carbopol 974P NF is an oral pharmaceutical grade carbomer that is highly crosslinked and can form viscous gels in aqueous solutions above its pKa of 5.5. It is a favorable candidate in controlled release applications due to its mucoadhesive and gel-strengthening properties. It is also used in many oral and mucosal delivery applications including tablets, bioadhesives, and extended-release formulations [86,87].

2.1.2.7 Silica

Silica (SiO_2) is another class of synthetic material that has been found to be generally safe, biocompatible, and biodegradable. To provide greater control of silica degradation *in vivo*, the addition of an organosilane unit to the silicon alkoxide precursor during synthesis can be performed to create organosilica. Pores in the material can be formed by adding a surfactant so that the organosilica units condense around the surfactant micelles to create a silica network. In particular, mesoporous silica-based particles are often used for drug delivery applications because of their high surface area, larger pore size (2–100 nm), and chemical and thermal stability [88,89].

2.2 Systems for Controlled Sinonasal Drug Delivery

The biomaterials introduced in the previous section have been utilized, both on their own and in combination, for creating a broad range of sinonasal drug delivery systems, which are discussed in detail in the following.

2.2.1 Nasal Packs, Dressings, and Spacers

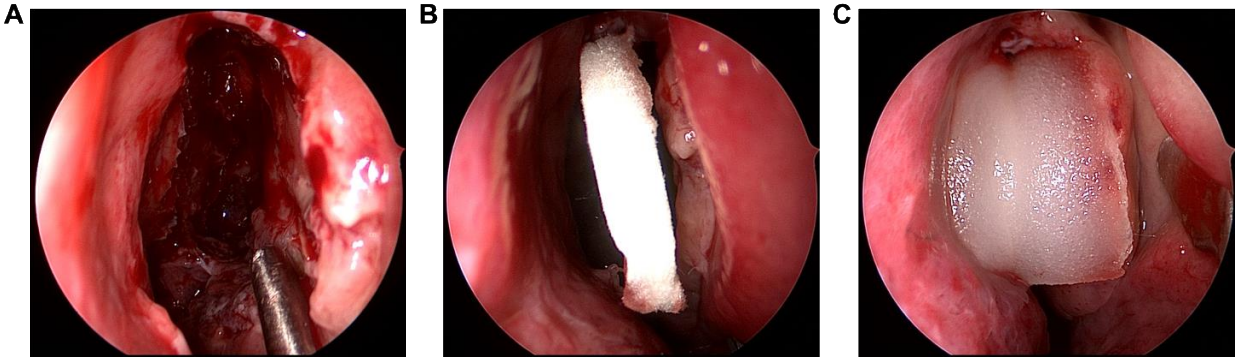

Figure 4. A Resorbable Nasal Pack in the Sphenoethmoidal Recess.

(A) A post-operative sphenoethmoidal recess (B) with placement of an unhydrated dressing and (C) hydration of the dressing, which causes the material to make contact with the mucosal surface and medialize the middle turbinate.

Nasal packs were initially developed for controlling bleeding, reducing adhesions, and maintaining patency following sinonasal surgeries (Figure 4), however these biomaterials have also been proposed as carriers for topical medication following FESS. These products, including nasal packs, dressings, and spacers, are composed of naturally-derived or synthetic materials and can be either absorbable or nonabsorbable [49,90]. In this section, focus will be placed on the

different types of biomaterials that have been evaluated for local corticosteroid delivery in clinical and preclinical studies (Table 1).

The semi-synthetic biomaterial, CMC, is an attractive nasal pack material because it can be biocompatible, biodegradable, and its mesh-like matrix can be loaded with a corticosteroid. One such product is SinuFoam™ (Smith & Nephew, London, UK), a CMC foam consisting of dry fibers that are hydrated immediately prior to placement to form a gel that dissolves within 1 week [91]. While SinuFoam is intended to promote healing and control minor bleeding, it has also been evaluated for off-label delivery of dexamethasone in CRSsNP patients. Following FESS, patients were randomized for bilateral placement of SinuFoam in the ethmoid sinuses that was hydrated with sterile water or a solution containing 16 mg dexamethasone. Over the 3-month follow-up, both groups exhibited improvement, and there were no statistically significant differences in endoscopy scores between those that received steroid-soaked or placebo nasal packs [92]. An important consideration in interpreting these results though, is that all patients received standard post-operative care, including saline irrigation and a short course of oral steroids. Thus, the benefits of the local dexamethasone release may have been obscured.

Similar to SinuFoam, SinuBand™ (BioInspire Technologies, Inc., Palo Alto, CA) is another bioabsorbable dressing that is composed of fibrinogen and has been evaluated for local delivery of fluticasone propionate (FP) in rabbits [93] and CRSwNP patients [94]. SinuBand is a pliable thin film that can adhere to the sinus mucosa without obstructing sinus drainage. In a preclinical study, the biocompatibility and pharmacokinetics of SinuBand loaded with FP (SinuBand FP) were compared to that without drug (SinuBand). Additionally, a synthetic sponge (Merocel, Medtronic Inc., Minneapolis, MN) that is traditionally used a hemostatic nasal tampon was evaluated for a nonabsorbable control. In New Zealand rabbits with healthy mucosa, SinuBand

was fully absorbed within 15 days and FP was detectable out to 44 days in the sinus mucosa (n = 1). The placement of SinuBand or SinuBand FP on surgically stripped mucosa (to simulate sinus surgery) was shown to initially slow down re-epithelization compared to Merocel, but the difference did not persist [93]. In a clinical study, the safety and efficacy of SinuBand FP was evaluated in CRSwNP patients, most with severe disease requiring revision surgery. Patients assigned to the SinuBand FP group received two 2x2 cm dressings loaded with 40 μg/cm^2 of corticosteroid. No significant changes in urine cortisol levels or intraocular pressure were detected, supporting systemic and ocular safety. The most notable sign of clinical efficacy was a significantly lower polyp score in ethmoid cavities receiving SinuBand FP compared to Merocel, although there was no significant difference in comparison to SinuBand without steroid. Other comparisons related to inflammation were not statistically different between groups, with the exception that patients receiving SinuBand FP reported significantly less nasal congestion [94].

Additional studies evaluating corticosteroid-soaked dressings have used other absorbable naturally-derived materials, including calcium alginate [95], porcine gelatin [96], and hyaluronic acid [97]. In an internally controlled trial, a calcium alginate pack soaked in 80 mg triamcinolone solution was compared to a saline-soaked pack inserted in the middle or superior meatus of CRSwNP patients during FESS. The packing was removed 1 week after surgery while standard post-operative care (a short course of oral antibiotics and low dose oral corticosteroid followed by longer duration of topical corticosteroids and saline irrigation) was maintained. After 8 weeks, evidence of significantly enhanced wound healing and reduced polyp recurrence (assessed using the Perioperative Sinus Endoscopy, or POSE, scale) was observed on the side receiving the corticosteroid packing [95]. Similar results of improved POSE scoring have been reported for a porcine-based gelatin sponge (GelFoam®, Pfizer, New York, NY) soaked in a hydrocortisone

solution [96]. In another study, the frequency of synechiae formation (post-operative adhesions that can block the sinus ostia) was compared in patients that received an absorbable esterified hyaluronic acid spacer (MeroGel, Medtronic, Inc.) soaked in triamcinolone (40 mg/mL) or the nonabsorbable Merocel sponge. While the number of patients in the corticosteroid spacer group presenting with synechiae was lower (5 of 252 patients), it was not statistically different from those in the nonabsorbable sponge group (13 of 233 patients) [97].

Table 1. Steroid-Impregnated Nasal Packs, Dressings, and Spacers for Post-Operative CRS Treatment

Material (Trade Name)	Corticosteroid	Study Participants	Reference
Naturally-derived biomaterials			
CMC (SinuFoam™)	Dexamethasone	CRSsNP patients	[92]
Fibrinogen (SinuBand™)	Fluticasone propionate	Rabbits with healthy or stripped mucosa	[93]
		CRSwNP patients	[94]
Calcium alginate	Triamcinolone acetonide	CRSwNP patients	[95]
Gelatin (Gelfoam®)	Hydrocortisone	CRSwNP patients	[96]
Hyaluronic acid (MeroGel)	Triamcinolone acetonide	CRSsNP and CRSwNP patients	[97]
Synthetic biomaterials			
Polyetherester urethane (NasoPore™)	Triamcinolone acetonide	CRSwNP patients	[98,99]
	Mometasone furoate	CRSwNP patients	[100]
Polyvinyl acetate (Merocel)	Triamcinolone acetonide	Bilateral refractory CRS patients	[101]

In contrast to naturally-derived biomaterials, several studies have evaluated a synthetic, absorbable co-polyetherester urethane foam, NasoPore™ (Stryker, Kalamazoo, MI), impregnated with triamcinolone [98,99] or mometasone furoate [100]. These studies in CRSwNP patients undergoing FESS were designed to compare the corticosteroid-eluting spacer inserted in one nasal cavity to a saline-soaked spacer on the other side [98,100], or to assess the efficacy of bilateral

triamcinolone-soaked spacers in patients receiving oral prednisone or placebo [99]. One key finding from this work was significant improvement evaluated by a 22-item QoL questionnaire (Sinonasal Outcome Test, SNOT-22) and by an endoscopy scoring system (Lund-Kennedy) in both groups treated with the bilateral triamcinolone-soaked spacers [99]. This suggests that the corticosteroid-eluting spacer could improve post-operative outcomes without the need for systemic corticosteroids, an important finding for reducing risks of adverse effects. In another study evaluating mometasone-soaked NasoPore, post-operative outcomes were significantly improved in patients that received a higher dose for longer duration (2800 μg for 14 days compared to 1400 μg for 7 days) [100].

Another synthetic packing material, Merocel, which has been used as a control in some of the previously discussed studies, has been evaluated for brief post-operative corticosteroid delivery as well. Because Merocel is a hydroxylated polyvinyl acetate sponge that it is nonabsorbable, it must be removed. Thus, a study in CRS patients with refractory disease evaluated the effects of packing Merocel soaked in triamcinolone (80 mg) to saline-soaked Merocel on the contralateral side for 2 days following FESS. Even with this short corticosteroid treatment, significant improvements in postoperative mucosal edema were observed throughout the 3-month follow-up on the side receiving the steroid-soaked material. Incidence of crusting was also significantly reduced at 1 week and 1 month post-operatively, however no other significant differences (such as changes in polyp scoring or nasal discharge) were observed [101].

The application of clinically-available biomaterials to localize corticosteroid delivery has demonstrated varied success. Multiple confounding factors in the study designs, such as the patient population, disease severity, use of post-operative medical therapies, and methods for interpreting efficacy, make comparing the studies challenging, though the clinical efficacy of these trials have

been discussed in detail in several reviews [102–104]. Notably, there are a number of contraindications for the use of nasal packs, dressings, and spacers following FESS. For example, experimentation in rabbit models has shown that if the biomaterial is left in contact with the healing mucosa for too long, it can be incorporated into the tissue and cause further inflammation [105]. Also, nasal packing can be associated with pain while the material is in place, as well as mucosal damage, pain, and bleeding during removal [103]. Thus, nasal packing for hemostasis following FESS is generally not advised [106]. These biomaterials are a convenient vehicle for concentrating corticosteroids to promote mucosal healing, however, they are limited in the ability to control the drug release profile. These studies, though, have helped motivate the design of local controlled release systems for the sinonasal mucosa, which are discussed in the following sections.

2.2.2 Sinus Stents and Meshes

In contrast to nasal packs and dressings, sinus stents and meshes are better able to provide mechanical support to maintain patency of the sinuses following FESS. Sinus stents are fabricated using biodegradable polymers so that they should not require removal and can be loaded with therapeutics for local delivery to the sinonasal mucosa as they degrade. Sinus stents and meshes are in all phases of development, ranging from preclinical evaluation to FDA-approved implants (Table 2).

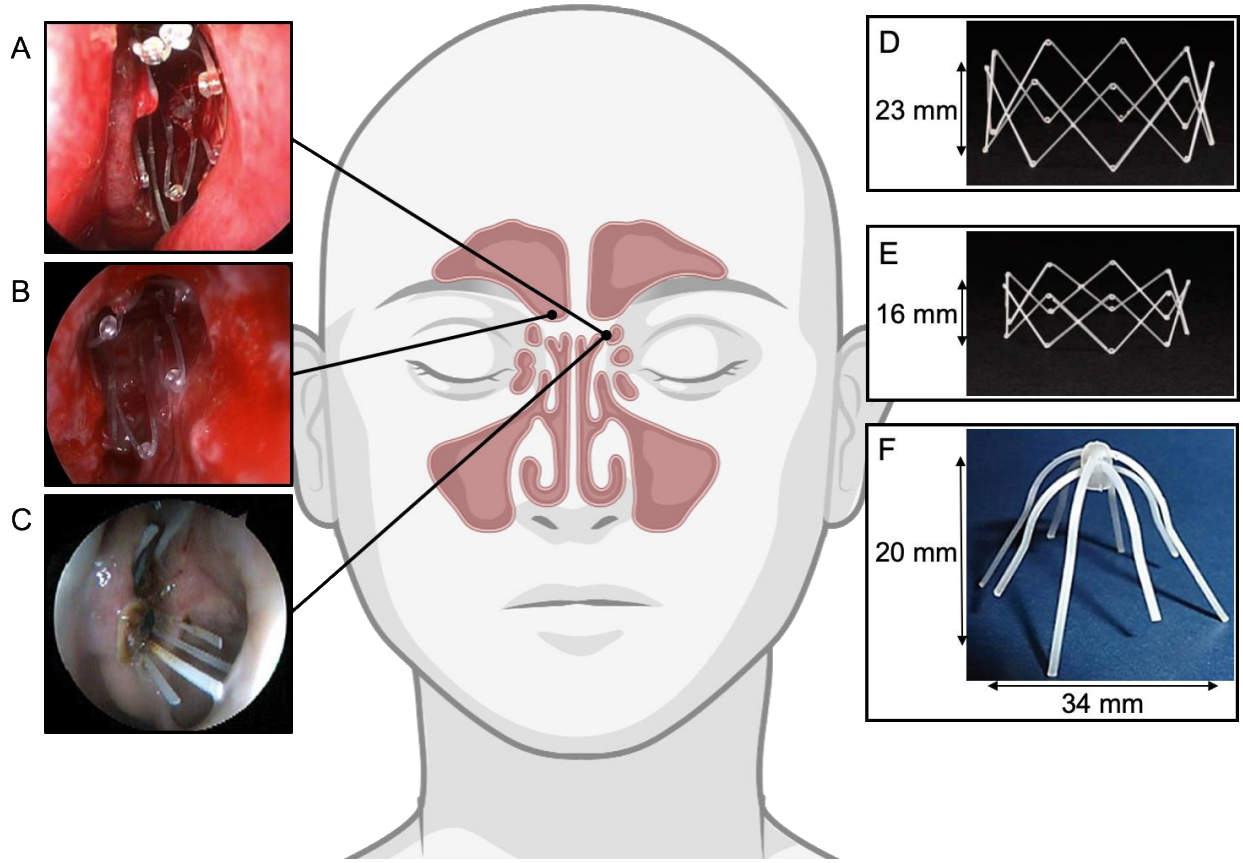

Figure 5. Degradable Sinus Stents for Local Corticosteroid Delivery to Specified Sinuses.

(A) Propel is designed for insertion in the ethmoid sinus and (B) Propel mini can be implanted in the frontal (shown in B) or ethmoid sinus. (D) Propel and its smaller version, (E) Propel mini, are cylindrical stents. (C) Sinuva is designed for in-office placement in the ethmoid sinus and (F) has a multi-pronged design. (A) Reproduced with permission [107]. Copyright 2011, John Wiley & Sons, Inc. (B) Reproduced with permission [108]. Copyright 2016, John Wiley & Sons, Inc. (D,E) Reproduced from [109]. (C,F) Reproduced with permission [110]. Copyright 2014, John Wiley & Sons, Inc. (D-F) Product dimensions were obtained from the Instructions for Use for each implant.

Currently, the only FDA-approved controlled release implants for the sinuses are the Propel® family and Sinuva® (Intersect ENT, Palo Alto, CA) [111–113]. These degradable stents are fabricated from PLGA with a self-expanding design for insertion into a specific sinus cavity

(Figure 5) [107,110]. Propel is a traditional radially-expanding cylindrical stent that is intended for placement in the ethmoid sinuses [111]. The Propel mini is a smaller version of this design for either the ethmoid or frontal sinuses [108,109]. The Propel contour is an hourglass-shaped implant designed for the frontal or maxillary sinuses [113,114]. Propel, Propel mini, and Propel contour are each loaded with 370 µg mometasone furoate for release over 30 days as the stent degrades. To extend the duration of drug release, Sinuva was designed to deliver 1350 µg mometasone over 90 days. In contrast to the Propel family, Sinuva has an 8-prong design and is indicated for in-office deployment in the ethmoid sinuses of post-operative patients [110,113]. While Propel was initially evaluated for perioperative insertion, it has also been successfully deployed in the ethmoid sinuses of post-operative patients in office settings [115]. The Propel and Sinuva stents are inserted by a physician under endoscopic visualization, as described in the products' Instructions for Use. A custom single-use delivery system is used for placement of the implant. The stent is manually crimped and inserted at the distal end of a custom single-use delivery system that consists of a ~12 cm long sheath. The delivery system is advanced into the sinus cavity and when the placement location is reached, the plunger at the proximal end is depressed while withdrawing the device so that the stent exits the distal end and expands to make contact with the sinus tissue.

The first clinical trials evaluating Propel in CRS patients undergoing primary or revision FESS began in 2008 [107], with trials for the other Propel and Sinuva stents conducted over the subsequent 8 years. The clinical results of these trials are discussed in depth in several reviews [111–113]. Briefly, safety and efficacy were compared following placement of a drug-eluting stent on one side and either a non-drug-eluting stent or no intervention on the contralateral side. Some studies also evaluated bilateral drug-eluting stents. Propel was shown to reduce inflammation and the formation of polyps and adhesions [111]. Additionally, endoscopic visualization confirmed the

bioresorbable nature of the stents, where about half of the material remained 21 days after insertion and no material was found after 60 days [116]. Following FDA-approval for Propel in 2011 [42] clinical trials evaluating Propel mini and Propel contour in the frontal sinus were initiated in 2014 and 2015, respectively [108,114]. From 2013 to 2016, Sinuva was evaluated in two randomized, sham-controlled, and blinded trials in patients that had undergone prior surgery and were deemed candidates for a revision surgery [110,117,118]. Overall, patients that received the bilateral Sinuva implants showed reduced nasal obstruction, congestion, polyps, and ethmoid sinus obstruction compared to those that received the sham implants [117,118]. Furthermore, at day 90, the number of patients that needed revision surgery reduced by 61% in the bilateral implant group and only 37% in the sham group [118].

In addition to PLGA stents (Propel and Sinuva), a PLLA stent for antibiotic delivery has also been evaluated in preclinical studies [119,120]. Cho *et al.* designed a 3D-printed sinus stent coated in ciprofloxacin (an antibiotic) for treating acute rhinosinusitis. *In vitro* characterization of the drug release profile revealed a burst release in the first 2 days and about half of the loaded drug (5 μg) was released in 2 weeks. For *in vivo* studies, the amount of ciprofloxacin was increased to 2 mg to achieve antibacterial efficacy, measured by the ratio of the area under the concentration-time curve to minimal inhibitory concentration (AUC:MIC). At 1 and 3 weeks after stent placement in healthy rabbits, the AUC:MIC in maxillary sinus tissue was 135 and 120, respectively, exceeding the target value of >100. These studies also demonstrated tolerance to the surgically implanted stent (via a dorsal incision) [119]. In a follow up study, the ability of the stent to inhibit biofilm formation was demonstrated *in vitro* and its therapeutic efficacy was evaluated in an ARS rabbit model. Stents were inserted 1 week after inoculating the sinuses with *Pseudomonas aeruginosa*. Over the subsequent 2 weeks, a significant reduction in bacterial load

was found in subjects that received the drug-eluting stent compared to sham controls. These results also corresponded to improvements in sinus opacification evaluated by microCT scoring and histological evidence of damage to the mucosa and submucosa [120].

Rather than a traditional stent design, another polymeric implant in the form of an expanding mesh scaffold has recently been proposed for biomedical applications, including rhinosinusitis treatment [72,121]. This implant consists of a PLGA base braid that is coated with an elastomeric co-polymer, poly(glycolide-co-caprolactone) (PGCL) or poly(lactide-co-caprolactone) (PLCL) and crosslinked (Figure 6A–D). The elastomeric coating was shown to significantly increase mechanical properties, such as radial stiffness and chronic outward force, even in comparison to metal alloy stents. Furthermore, controlling the crosslink density of the elastomer could optimize the elasticity achieving an elongation-to-break ratio of 300% while minimizing permanent deformation to less than 25%. Biocompatibility of implants with different resorption profiles was assessed in swine and ovine arteries. Notably, those fabricated with faster degrading polymers (10:90 LA:GA and PGCL) exhibited a significant inflammatory response in comparison to slower degrading polymers (75:25 LA:GA and PLCL). In sheep, an implant consisting of 85:15 PLGA with PLCL was fully resorbed after 18 months, though a mild to moderate inflammatory response was observed [72]. Although these biocompatibility studies were performed in arteries, the authors have patented a drug-eluting implant that was assigned to Lyra Therapeutics, Inc. (Watertown, MA) [122], who are currently conducting clinical trials for an intranasal polymeric implant. The implant, LYR-210, is a self-expanding tubular mesh comprising biodegradable and elastomeric polymers that can conform to the mucosal tissue and release 2500 µg mometasone furoate over 24 weeks. In an open-label Phase 1 clinical trial, 20 CRS patients that were potential candidates for surgery received the bilateral implants placed in intact middle

meatus (Figure 6F–H). The primary outcome for this study was to assess systemic safety by measuring serum cortisol, IOP, and plasma drug concentrations, all of which remained within normal ranges. Additionally, SNOT-22 scores were significantly improved relative to baseline. A 100% procedural success rate was also reported, although 7 of 40 implants had to be re-deployed. Another shortcoming that was noted was that 5 implants were dislodged spontaneously due to coughing or sneezing [121]. Despite these limitations, safety of LYR-210 was established and a larger randomized Phase II trial with a sham comparator is currently on-going (ClinicalTrials.gov Identifier: NCT04041609).

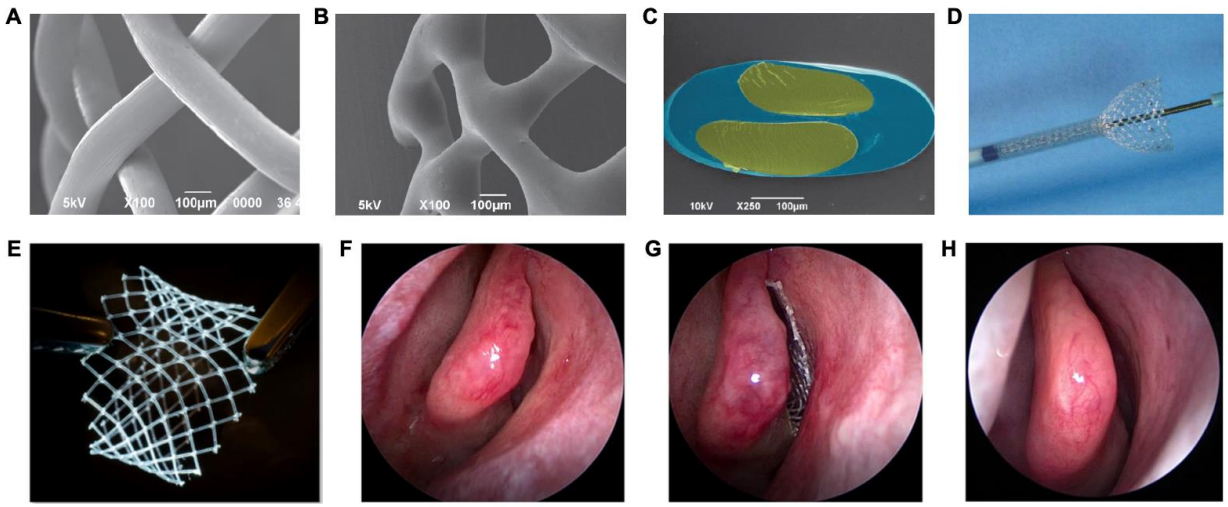

Figure 6. A Bioresorbable, Self-Expanding Polymeric Mesh for the Sinuses.

(A-C) SEM images of (A) the PLGA base braid (B) with elastomer coating and (C) false-colored cross-section showing the braid in yellow and elastomer in blue. Photographs showing (D) the self-expansion of the implant and (E) LYR-210. (F–H) Endoscopy images of the middle meatus (F) before placement, (G) after placement of LYR-210, and (H) at 1 week after its removal. (A–D) Repoduced with permission [72]. Copyright 2017, Springer Nature. (E–H) Reproduced with permission [121]. Copyright 2019, John Wiley & Sons, Inc.

A notable similarity between Propel, Sinuva, and LYR-210 is that the approximate concentration of daily mometasone release is much less than what is delivered by daily nasal sprays. If we estimate a linear release profile from bilateral stents to approximate the daily dose, then Propel and Sinuva deliver ~25–30 µg per day. Under the same assumptions, the daily release from bilateral LYR-210 is ~15 µg per day. In comparison, mometasone nasal sprays deliver 50 µg per actuation, and a typical dose is twice daily to each nostril (totaling 400 µg per day). It should be noted that only a fraction of the nasal spray dose is deposited in the nasal cavity (about 30% [40]), yet even a fraction of the applied nasal spray still equates to 4-fold more drug than what is released from these sinus implants. Of course, degradable implants are better able to localize the therapeutic to the sinus mucosa concentrating the released drug in a region of the sinuses rather than distributing it throughout.

In addition to limitations related to the corticosteroid dose, challenges can be encountered with the placement of sinus stents and meshes as well as the tissue response as the implant degrades. Propel and Sinuva can only be used in patients who have undergone FESS, whereas LYR-210 is restricted to surgically-naïve CRS patients. Each of these implants is also indicated for specific locations within the sinuses. Incorrect placement can result in the need for early removal, the implant becoming dislodged [121], crusting, granulation, and scarring [123], or nasal and ocular irritation [124]. While infrequent, adverse events noted during the clinical trials for Propel and Sinuva included sinus pressure and irritation, nasal discomfort, nose bleeds, and a distorted sense of smell [111,117,118]. A possible cause for these adverse reactions is an inflammatory response that is elicited by the degradation of the implant, which was observed during early development of the composite mesh scaffold [72].

Even with these limitations, Propel and Sinuva are the only FDA-approved implants for controlled release in the sinuses that have shown clinical efficacy and LYR-210 is progressing in clinical trials. Their success bolsters confidence that other controlled release systems in earlier phases of development may be able to address remaining clinical hurdles for local treatments of rhinitis and rhinosinusitis.

2.2.3 Nano- and Microparticles

Nanoparticles (NP) and microparticles (MP) can be fabricated from the same biodegradable polymers as sinus stents, along with numerous other natural and synthetic materials, but their small spherical morphology and surface properties play critical roles in their ability to be retained and to potentially penetrate mucus. As a result, nanoparticle-based strategies have been investigated for intranasal vaccination [125] and delivering treatments for central nervous system disorders. In fact, in just the last 3 years, nearly 20 journal articles have reviewed the development of nanoparticles for nose-to-brain drug delivery. As the field of intranasal applications for NPs and MPs is quite extensive, the following will not encompass all therapeutic targets, but will focus only on those designed for local treatment for diseases of the sinonasal mucosa (Table 2).

As long-term use of intranasal corticosteroids is prescribed for both allergic rhinitis and chronic rhinosinusitis treatment, their encapsulation in synthetic polymeric nanoparticles has been explored to reduce dosing frequency and improve drug retention. Mometasone furoate has been loaded in PLGA NPs using nanoprecipitation and solvent evaporation methods with 90% encapsulation efficiency (the final amount of drug loaded relative to the initial amount) and 7 days of sustained release. Further *in vitro* characterization also evaluated optimal storage conditions for the drug carriers. Specifically, the effect of cryoprotectant solutions on the ratio of mean particle

diameter after freeze drying relative to the initial diameter (S_f/S_i) was measured. Nearly all conditions formulated with 4–8% sucrose or mannitol achieved the target value of S_f/S_i close to 1, meaning the NP diameter remained close to its initial value of 117 ± 13 nm, with the exception of 6% mannitol, which doubled in size (S_f/S_i = 2.18) [126]. While this study did not evaluate the interaction of the NPs with mucus, mucoadhesion of triamcinolone-loaded poloxamer 188 nanocapsules (P188 NCs) was evaluated both *ex vivo* and *in vivo*. The ~128 nm triamcinolone/P188 NCs were formulated with a Eudragit RS100 polymeric coating, which created a positive surface charge. As a result, the amount of drug that was retained in and permeated through bovine mucosal samples after 24 h was higher for the P188 NCs compared to other carrier formulations and a commercial triamcinolone nasal spray (Nasacort®, Sanofi, Bridgewater, NJ). Enhanced mucoadhesion of the P188 NCs was also demonstrated in rat nasal cavities by quantifying the amount of drug that was washed out following intranasal dosing. Similar to the mometasone/PLGA NPs, the triamcinolone/P188 NCs were fabricated by nanoprecipitation and achieved ~97% encapsulation efficiency [127].

In addition to synthetic polymers, naturally-derived chitosan has been used for NP fabrication because of its mucoadhesive and temperature-responsive properties. Abruzzo *et al.* developed NPs that utilized the ionic interactions between positively charged chitosan and negatively charged cromolyn, a decongestant that inhibits mast cell degranulation and subsequent AR symptoms. By tuning the drug to polymer ratio, stable NPs that were 387 ± 7 nm in diameter with ~51% encapsulation efficiency and ~64% drug loading (the amount of drug relative to total amount of drug and polymer) were fabricated. Due to their positive surface charge, the NPs exhibited good mucoadhesion, which corresponded with sustained *in vitro* drug permeation for >12 h [128]. Another chitosan-based NP formulation has been designed for releasing a H_1-

antihistamine, cetirizine. The cetirizine-loaded deoxycholate-chitosan-hydroxybutyl nanoparticles (CDHBC-NP) were designed for stimuli-responsive drug release. Specifically, drug that was freely embedded in the NP was released in the first 6 h by temperature-induced shrinkage of the NPs. Additional drug that was covalently grafted to the polymer backbone was then slowly released over 72 h as the polymer degraded in the presence of lysozyme. The NPs were also shown to have a positive zeta potential promoting mucoadhesion, average particle diameters of 116–148 nm, and ~30% drug loading [129].

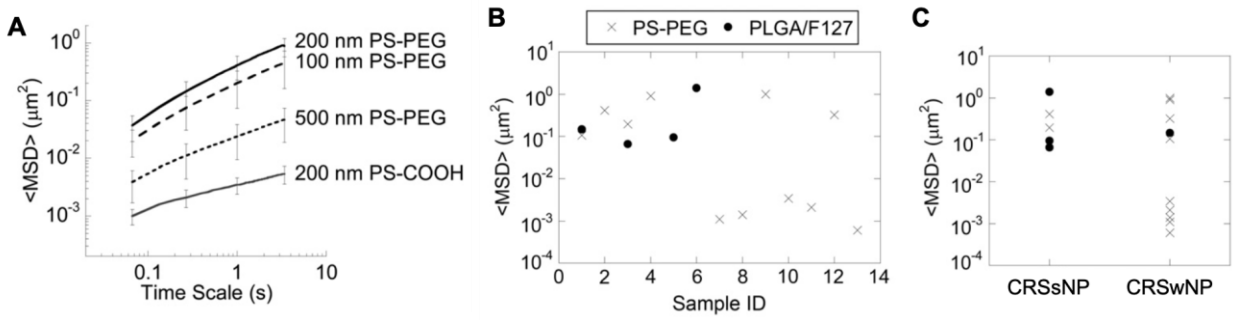

Figure 7. Nanoparticle Transport in CRS Mucus Samples.

(A) Ensemble-averaged geometric mean square displacement (<MSD>) as a function of time scale for uncoated (PS-COOH) and coated (PS-PEG) NPs of indicated diameters. (B) Transport of 200 nm PS-PEG and ~200 nm PLGA/F127 NPs for individual patient samples, (C) which showed a correlation to the CRS disease subtype, CRSsNP or CRSwNP. Modified with permission [130]. Copyright 2011, Elsevier.

Beyond tunable drug release mechanisms, nanoparticles have also shown the capability to penetrate mucus, which is of particular importance for local delivery to inflamed sinonasal mucosa. However, the subtype of CRS has been shown to have an effect on NP transport. Using CRS patient mucus samples, the *ex vivo* transport of PEGylated polystyrene particles (PS-PEG) with a diameter of 100 nm or 200 nm was significantly enhanced compared to both 200 nm uncoated PS NPs and

500 nm PS-PEG NPs (Figure 7A). These findings were confirmed using ~200 nm Pluronic F127-coated PLGA (PLGA/F127) NPs for future development of a biodegradable nanocarrier. A noteworthy finding from this study was that the transport of 200 nm PS-PEG NPs was uniform and rapid in samples obtained from CRSsNP patients (n = 4), which was attributed to the ability of the coating to minimize adhesive interactions with mucus. However, samples obtained from CRSwNP patients showed inconsistent results, where transport was rapid in only 4 of 9 samples (Figure 7B,C) [130]. This study highlights particular challenges of CRS management due to the existence of two disease subtypes that can alter the mucus barrier as well as consistent transport across the mucus barrier for therapeutic delivery.

Given the limitations of penetrating the mucus barrier, a particular focus for the development of microparticle-based delivery is enhancing mucoadhesion to increase residence time in the nasal cavity. Lee *et al.* reported a PLGA/PEG nanostructured microsphere (NM) formulation that was fabricated by electrospinning and milling. The PLGA/PEG NMs were 6.72–7.64 μm in diameter with 10x the surface area compared to controls. As a result, they showed significantly enhanced retention in murine sinonasal cavities 12 h after administration (Figure 8A,B). The PLGA/PEG NMs were loaded with resveratrol, a compound that can suppress mucosal remodeling and has been shown to reduce characteristics of CRSwNP in mice but has limited bioavailability. By encapsulating the drug, a 42-hour release profile was demonstrated *in vitro*. Furthermore, in a murine eosinophilic model of rhinosinusitis, the sustained release of resveratrol had a greater anti-inflammatory effect as indicated by reduced polyp formation and decreased inflammatory mediators compared to bolus treatment (Figure 8C–E) [131].

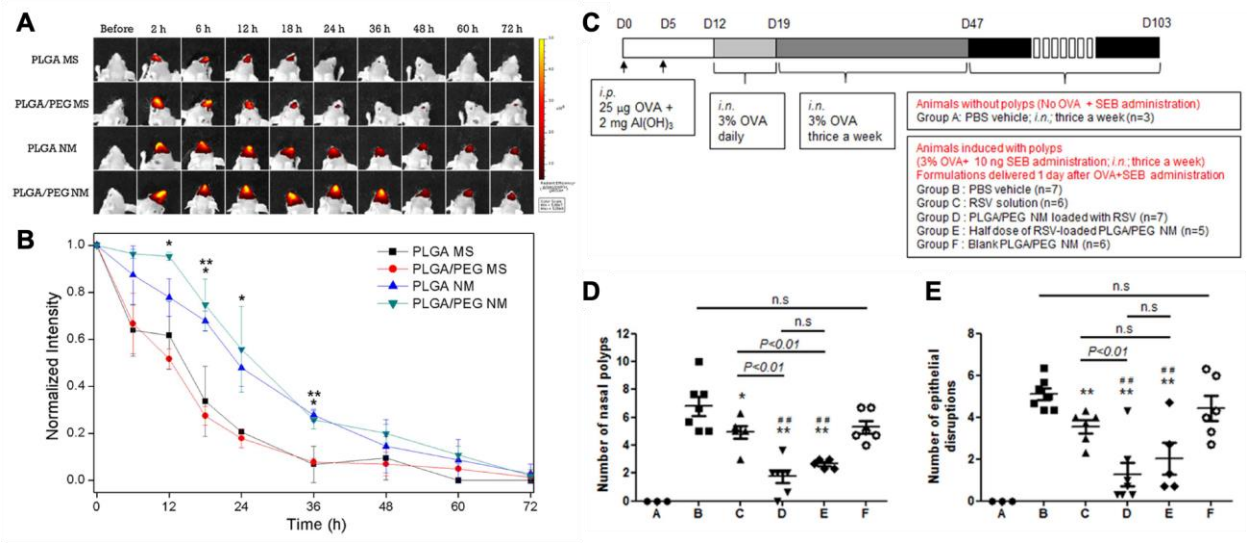

Figure 8. PLGA/PEG Nanostructured Microspheres

(A) Images of BALB/c mice after administration of fluorescent PLGA and PLGA/PEG microspheres without (MS) or with a nanostructured surface (NM). (B) Quantification of fluorescent intensity. *At 12, 18, 24 and 36 h, PLGA/PEG NM were significantly different from PLGA MS and PLGA/PEG MS ($p < 0.05$). **At 18 and 36 h, PLGA NM were significantly different from PLGA MS and PLGA/PEG MS ($p < 0.05$). (C) Murine model timeline and treatment groups. (D) Number of nasal polyps and (E) epithelial disruptions counted for each group. Significant differences are denoted relative to Group B (* $p < 0.05$, ** $p < 0.01$) or to Group F ($^{\#} p < 0.05$, $^{\#\#} p < 0.01$). Reproduced from reference [131].

Chitosan, which was previously discussed as a material used to formulate NPs, has also be used to create micron-sized drug carriers to increase retention in the nasal cavity. Chitosan-based microspheres (CTS MS) loaded with levocetirizine, an antihistamine, were fabricated by emulsification and crosslinking with glutaraldehyde and varying the ratio of drug to polymer. At a ratio of 1:3, the MSs exhibited the highest encapsulation efficiency (~87%) as well as good *ex vivo* mucoadhesion (~76% of MSs remained adhered to mucosal tissue using a "wash-off method"). These ~11 µm levocetirizine/CTS MSs also exhibited drug release for 8 h *in vitro* [132]. Another CTS MS formulation was fabricated by spray drying and loading a traditional Chinese

medicine, astragalus polysaccharide (APS) [133], which has several pharmacological effects including the ability to regulate immune function [134]. In this study, a design of experiments approach was used to evaluate four fabrication parameters (the inlet temperature, feeding rate, CTS molecular weight, and drug to polymer ratio). The maximum drug loading achieved was 21.5%, which was used as the output for optimization, and each of the APS/CTS MS formulations showed sustained release for ~24 h. In addition to *in vitro* characterization, delivery of APS from the MSs was evaluated in an OVA-induced AR rat model. Subjects treated with APS/CTS MSs showed a significant reduction in sneezing as well as reduced number of eosinophils and neutrophils in nasal lavage fluid compared to the disease control and an INC suspension control [133].

Microparticles have also been investigated as carriers for INCs. For example, budesonide is a poorly water-soluble corticosteroid that has been formulated in MPs composed of cellulose ethers (HPMC or NaCMC) and β-cyclodextrin. Cyclodextrins are cyclic oligosaccharides that can surround lipophilic drugs with an outer hydrophilic surface to increase aqueous solubility and stability. As a result of the MP formulation, the dissolution rate of budesonide was significantly improved compared to pure drug. *In vitro* characterization also demonstrated efficient encapsulation (81–99%) and drug loading (12–15%) in MPs with a mean diameter of 11–13 μm [135]. Others have produced longer release profiles of another INC, mometasone furoate (which is essentially insoluble in water according to the Nasonex® Product Monograph, Merck Canada, Inc., Canada). An amphiphilic copolymer of PLGA and mPEG was selected to enhance diffusion of acidic degradation products, thus protecting the drug cargo, and enhancing release. MPs that were fabricated with a range of polymer molecular weights and LA:GA exhibited a mean diameter of ~12 μm and sustained release of mometasone for over 35 days *in vitro* [136].

Yet another way in which microparticles-based systems have been proposed for treating sinonasal conditions is by providing controlled release of exogenous nitric oxide [137,138]. The objective of these studies was to provide a mechanism to increase NO levels, which have been shown to be low in CRS patients. Accordingly, organosilica MPs were synthesized with degradable nitrosylated thiol groups that created release of NO for 64 h. The MPs were fabricated by sol-gel synthesis, lyophilized, and pestled to create 5–10 μm MPs. The antimicrobial capabilities of the NO-releasing MPs were tested against 6 different bacterial isolates from CRS patients and a 4–10 log reduction in bacteria colony forming units (CFUs) was observed [137]. In a follow-up study, the investigators explored adding nitrate and manuka honey to the formulation of NO-releasing MPs to enhance NO release and for the broad-spectrum antimicrobial effects of manuka honey. The combination of the 3 components significantly increased biofilm volume reduction of a clinical isolate of *Pseudamonas aeuginoas* [138]. While these studies are in early phases of development, they pose a potential strategy for treating biofilm-positive patients who typically have poor clinical improvement following FESS.

Nano- and microparticle-based systems have been explored for delivering a number of different therapeutics for rhinitis and rhinosinusitis management, however maintaining the particles within the nasal cavity or sinuses is necessary for their ultimate success. Nanoparticles can be designed to penetrate mucus in a size- and surface chemistry-dependent manner. Alternatively, the surface of microparticles can be fabricated to achieve mucoadhesion through increased surface area or electrostatic interactions with mucus. While these studies have demonstrated encapsulation and release of therapeutics and some have shown *in vivo* efficacy, an area for continued development is the application method for particle-based systems, particularly characterizing their uniform distribution along the sinonasal mucosa.

2.2.4 *In situ* Hydrogels

In situ hydrogels can be applied as a liquid and undergo a phase transition to a gel under physiological conditions, such as temperature increase or the presence of ions. For intranasal drug delivery, *in situ* gels have many advantages over other delivery vehicles, the most noteworthy of which is their ability to uniformly conform to the mucosal tissue. In comparison to conventional daily systems, *in situ* gels can increase drug retention and bioavailability by reducing post-nasal drip and mucociliary clearance. Also, *in situ* gels can provide sustained release behavior that could improve patient adherence, reduce dosing frequency, and reduce systemic side effects [139–141]. As with nano- and microparticles, there is a broad range of intranasal applications for *in situ* hydrogels with recent reviews discussing their application for nose-to-brain or systemic delivery [142–144]. Herein, *in situ* hydrogels developed specifically for rhinitis and rhinosinusitis treatments are reviewed (and summarized in Table 2).

In situ hydrogels designed for the nasal and sinus cavities frequently use thermoresponsive polymers, such as poloxamer 407 (P407), so that gelation occurs in response to temperature increase. Altuntaş *et al*. showed that increasing the concentration of P407 from 16% to 18% decreased the $T_{sol\text{-}gel}$ from 50°C to 29.5°C [141], which is a suitable temperature for gelation in the posterior nasal cavity or sinuses [13]. Carbopol (CP) 974 NF and PEG (400 Da) were added to the formulation to increase mucoadhesive strength and enhance release, respectively. A formulation consisting of 18% P407, 0.25% CP 974P NF, and 5% PEG400 (w/v) was shown to continuously release mometasone furoate for 180 minutes [141]. The P407-based formulation was evaluated *in vivo* for delivering allergic rhinitis treatment [145] and promoting mucosal healing [146]. Daily treatment with the mometasone-loaded gel in rats with OVA-induced AR significantly reduced symptoms, including sneezing and nasal rubbing, as well as OVA-specific IgE serum antibodies

compared to controls [145]. A similar gel formulation was evaluated for delivering 3 active ingredients: mometasone furoate, levofloxacin hemihydrate (an antibiotic effective against gram-positive and gram-negative bacteria), and retinyl palmitate (a vitamin A derivative that has been shown to increase cilia regeneration). Due to the challenge of identifying a medium that met sink conditions for all three components, the release profiles for the three drugs were not measured. The gel was evaluated in a rabbit model simulating FESS by drilling a whole in the medial wall of the maxillary sinus. The ostial diameter was better maintained in subjects treated with gel containing the 3 active ingredients compared to blank vehicle, however the individual active ingredients and an aqueous suspension of the 3 drugs was not assessed. Preventing ostial stenosis is important to the success of FESS and these results suggests that the combination therapy was effective. Histopathological analysis also showed decreased evidence of chronic inflammation in the combination therapy group [146].

Another poloxamer-based hydrogel was designed to release dexamethasone for CRS treatment with a particular focus on optimizing the mechanical properties of the gel [147]. A formulation was selected that consisted of 15.5% P407 (w/v) with 0.3% HPMC and 0.1% chitosan (w/w) to enhance mechanical strength and mucoadhesion, respectively. Mechanical properties that would enable the thermoresponsive gel to be applied via a catheterized syringe or aerosolized nasal spray were targeted. These properties included low hardness (0.29 ± 0.64 N) to facilitate ease of transfer and spread on the mucosa along with strong adhesiveness (1.18 ± 0.06 N mm) and cohesiveness (0.76 ± 0.02) to maintain contact with the mucosa and to withstand shear stress during application, respectively. A moderate value of mucoadhesion (0.34 ± 0.51 N mm) to human nasal mucosa was desirable to prevent tissue damage. Low viscosity at storage temperature (0.115 ± 0.02 Pa·s at 8°C) and a rapid increase at body temperature (32.94 ± 0.95 Pa·s at 34°C) were

favored for ease of application. Additional *in vitro* characterization showed that the $T_{sol\text{-}gel}$ occurred at 34°C with sustained release of dexamethasone for 72 h, and steady *ex vivo* permeation of the drug across human nasal mucosa for 8 h without damaging the tissue integrity [147].

Rather than for corticosteroid delivery, thermoresponsive hydrogels have also been developed for intranasal application of alternative anti-inflammatory therapies. For example, a traditional Chinese medicine, paeonol, was complexed with β-cyclodextrin to enhance stability and formulated in a poloxamer-based hydrogel. A gel formulation consisting of 22% P407, 2% P188, and 2% PEG (6000 Da) was selected for its gelation temperature, melting temperature, and viscosity values of 33.5 ± 0.29°C, 55 ± 0.56°C, and 70 ± 0.67 Pa·s at >30°C, respectively. The formulation demonstrated continuous drug released for 24 hours *in vitro* as well as low cilia toxicity using a toad palate model. Its therapeutic efficacy was evaluated in an OVA-induced AR guinea pig model, in which the gel was applied 3 times daily for 11 days. Evidence of an anti-inflammatory effect was observed by reduced serum levels of IgE and leukotriene E4 [148]. While this study demonstrated efficacy using multiple doses each day, it seemingly contradicts the demonstration of 24-hour *in vitro* release and the efficacy of treatment applied once daily remains in question. As another treatment strategy, a thermoresponsive gel consisting of chitosan and sodium β-glycerophosphate (β-GP) was developed to deliver siRNA targeting vascular endothelial growth factor (VEGF) with the objective of preventing nasal epithelial cell growth that can lead to polyp formation in CRS. The formulation was shown to undergo gelation after incubation at body temperature for several minutes and to sustain *in vitro* siRNA release for over 2 weeks. *In vivo,* the siRNA hydrogel effectively reduced mucosal thickness in rats with CRS induced by staphylococcal enterotoxin B [149].

Instead of using temperature as the mechanism for gelation, physiological concentrations of ions have been utilized as a stimulus for applying ion-responsive gels to deliver therapies for nasal inflammatory disorders. A gellan gum-based ion-responsive hydrogel has been developed for delivering mometasone furoate and its therapeutic efficacy was demonstrated in an OVA-induced AR rat model [150]. Nižić *et al.* also used gellan gum to design an *in situ* gel and optimized the formulation by evaluating its deposition in a silicone nasal cavity model (Figure 9). Concentrations of the active ingredient (fluticasone propionate), gel components (pectin, gellan gum, sodium hyaluronate, and Tween 80) and administration parameters (administration angle and inspiratory flow rate) were screened, and then rheological properties and gelation time were measured for selected formulations. Targeted turbinate deposition was achieved by administering the spray at a smaller angle from the horizontal plane, increased inspiratory flow rate, and adding sodium hyaluronate to the formulation. The *in vitro* characterization indicated that the following values would have the highest therapeutic potential: 0.058% fluticasone, 0.031% Tween 80, 0.1% gellan gum, 0.05% sodium hyaluronate, 0.66% pectin (w/w), with an administration angle of 45° and inspiratory flow rate of 36 L/min (Figure 9C). The presence of pectin and gellan gum in this formulation, as well as all those that were tested, caused immediate gelation upon contact with simulated nasal fluid (containing NaCl, KCl, and $CaCl_2$). Furthermore, the presence of gellan gum was critical to achieving greater values of the gel storage modulus (G'), which is suggested to increase retention time in the nasal cavity, and to enhancing fluticasone release (~50% after 8 hours) [140].

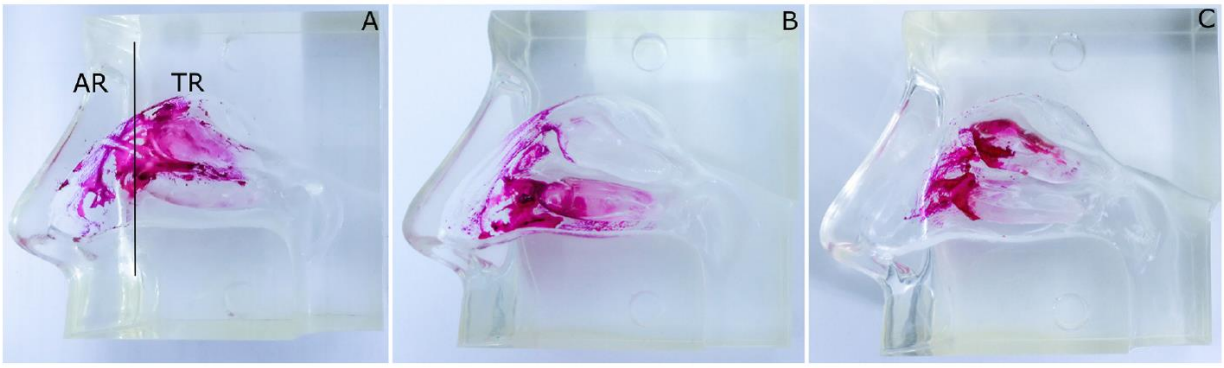

Figure 9. Deposition of an *in situ* Gelling Suspension in a Nasal Cavity Model.

Ion-responsive hydrogels were prepared with fluticasone, Tween 80 and (A) pectin and sodium hyaluronate, (B) pectin, or (C) pectin, sodium hyaluronate and gellan gum. The administration angle and inspiratory flow rate were evaluated at (A) 53° and 60 L/min, (B) 33° and 60 L/min, and (C) 45° and 36 L/min, respectively. AR = anterior region, TR = turbinate region. Reproduced with permission [140]. Copyright 2019, Elsevier.

Formulations based on thermo- or ion-responsive polymers have been designed to deliver corticosteroids, antibiotics, and other therapeutics for allergic rhinitis and chronic rhinosinusitis. Two of these studies have also considered properties of the gel that would enhance its intranasal application [140,147]. A notable advantage of *in situ* hydrogels in comparison to stents, meshes, and particle-based delivery systems is their ability to conform to the sinonasal mucosa as they gel. Given the intricate anatomies of the nasal cavity and sinuses, this is particularly beneficial. Furthermore, *in situ* gels can be applied to any region of the nasal or sinus cavities and do not require individual designs for specific sinuses as is the case with stents. However, a limitation of the *in situ* formulations described above is that the controlled release ranged from only 3 to 72 hours, and therefore, these would still require daily dosing or multiple times per week.

2.2.5 Combination Systems

A recent trend in the design of controlled release systems for the nasal cavity and sinuses is to employ the advantages of multiple biomaterials in combination systems (Table 2). Specifically, stents can provide mechanical support to maintain sinus patency, hydrogels can improve mucosal apposition and enhance intranasal retention, while nano- and microparticles can offer greater control and flexibility of drug release. Several groups have shown that this is a viable strategy to improve therapeutic delivery for rhinitis and rhinosinusitis in preclinical models.

A PLLA stent coated with a single antibiotic (introduced in Section 2.2.2) was modified by incorporating PLGA nanoparticles that released two therapeutics with bactericidal activity [151,152]. With this design, drug release could be extended by coating the stent with ciprofloxacin (a hydrophilic drug) in the inner layer and a combination of NPs loaded with ciprofloxacin or ivacaftor (a hydrophobic drug) in the outer layer (Figure 10A–C). A linear and sustained release profile for both drugs was exhibited for 3 weeks (Figure 10D) [151] in comparison to prior work in which stents coated with aqueous ciprofloxacin had a high burst release in the first 48 h [119]. Furthermore, *in vitro* anti-biofilm activity was demonstrated [151]. In a follow-up study, drug-coated or sham stents were implanted in rabbits with disease induced by *Pseudomonas aeruginosa* inoculation. After 3 weeks, subjects treated with the drug-loaded stent exhibited reduced sinus opacification by microCT, 2-log reduction in bacterial counts, and reduced thickness of the epithelium and subepithelium compared to controls (Figure 10E–G) [152]. The extended release of 2 synergistic antibacterial treatments from an implanted stent with nanoparticle coating is proposed as an effective treatment for recalcitrant CRS, although uniform contact with the entire mucosal surface remains a limitation of stent-based systems.

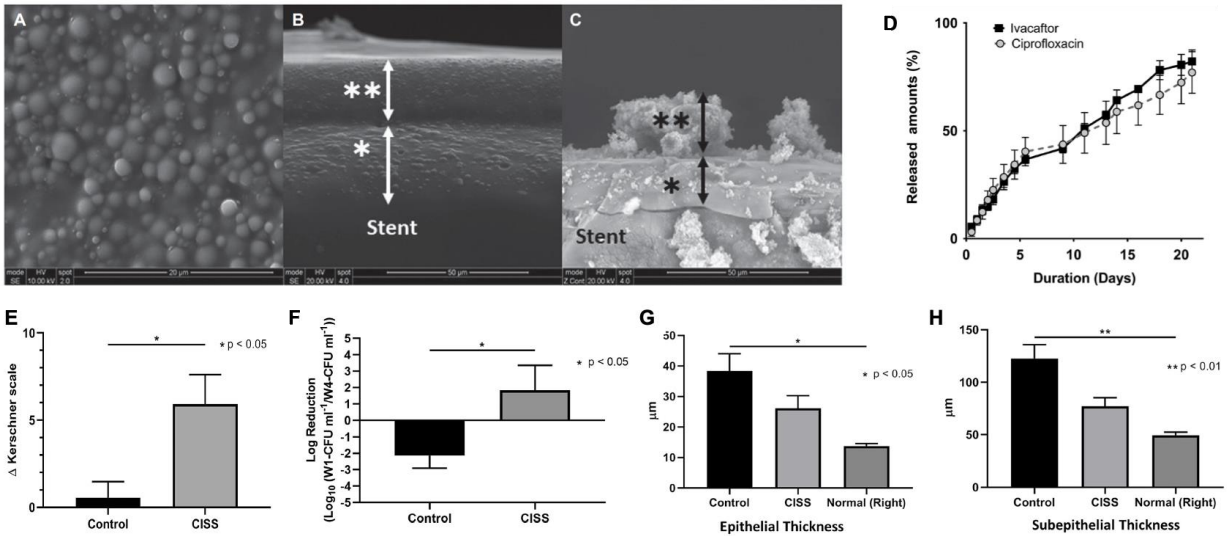

Figure 10. Biodegradable PLLA Stent with Drug-Loaded PLGA Nanoparticles.

(A–C) SEM images of the ciprofloxacin and ivacaftor-coated sinus stent (CISS) showing (A) top-down and (B) cross-section view before use, and (C) after 21 days *in vitro* release. (D) CISS *in vitro* release profiles. (E–H) Rabbit study results showing (E) significant improvement by CT, (F) significantly reduced bacterial load, and (G) significant reduction in epithelial and (H) subepithelial thickness following treatment with CISS. (A–D) Reproduced with permission [151]. Copyright 2019, John Wiley & Sons, Inc. (E–H) Reproduced with permission [152]. Copyright 2019, John Wiley & Sons, Inc.

Rather than utilizing stents, others have investigated the combination of hydrogels with lipid-based or polymeric drug carriers to enhance distribution, retention, and local controlled release. Chen *et al.* designed a degradable PEG hydrogel in combination with liposomes loaded with two therapeutics to provide anti-bacterial and anti-inflammatory ABRS therapies. Clarithromycin (CAM), a 2nd generation macrolide, and budesonide (BUD) were loaded into separate batches of lecithin and cholesterol liposomes using solvent evaporation and sonication. A 4-arm-PEG-thiol was then dissolved in the liposome solution and silver ions were added to form the hydrogel. As a result of the dynamic metal coordination bonds between the silver ions and the thiol groups, the gel possessed a self-healing capability such that it could pass through a 0.45 mm

injection needle for application (Figure 11A,B). Release of both drugs was sustained over 7 days *in vitro*, which was similar to the system's degradation rate. To evaluate efficacy, the liposome and hydrogel system was injected into rabbit maxillary sinuses with induced ABRS using *Streptococcus pneumoniae* inoculation. After 2 weeks, the local release of both drugs was shown to improve the appearance of the sinuses in CT imaging, eliminate purulent secretions, and reduce edema of the sinus tissue. Additional evidence of efficacy was demonstrated by reduced bacterial detection rates and lower levels of inflammatory cells and cytokines (Figure 11C) [153]. Alternatively, degradable chitosan-based hydrogels have also been used to increase the retention of PLGA microparticles. Chitosan and PVP were combined at an equal weight percentage to enhance mechanical properties of the gel while maintaining mucoadhesion and biocompatibility. The hydrogel was chemically crosslinked with glutaraldehyde and PLGA MPs encapsulating dexamethasone were added at 12.5% (wt %). The complete formulation exhibited room temperature gelation within ~30 minutes and extended drug release for >30 days [154].

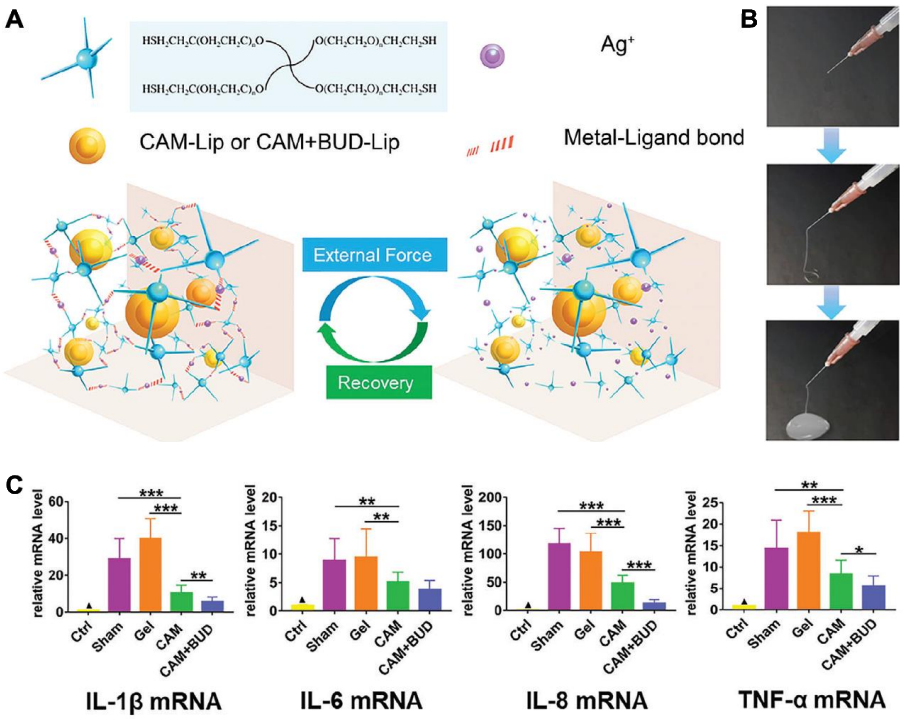

Figure 11. Self-Healing Hydrogel with Anti-Bacterial and Anti-Inflammatory Liposomes.

(A) Schematic of the self-healing process of the PEG hydrogel with clarithromycin (CAM)- and budesonide (BUD)-loaded liposomes (Lip). (B) Extrusion of the hydrogel through a 0.45 mm syringe needle. (C) RT-PCR data for inflammatory cytokines measured in rabbit maxillary sinus mucosa following ABRS induction and 2 weeks of local drug administration. * p < 0.05, ** p < 0.01, *** p < 0.00, ▲: VS any other group, p < 0.001. Reproduced with permission [153]. Copyright 2020, John Wiley & Sons, Inc.

Chitosan can also be fabricated with β-GP to create a thermoresponsive hydrogel, which has been investigated in combination with PEG-PLA NPs. The PEG-PLA NPs were loaded with microRNA (miRNA)-146a as a strategy for treating allergic rhinitis because miRNA-146a can suppress inflammation, and allergic inflammation in particular. The miRNA-146a-loaded NPs had a mean diameter of ~550 nm and demonstrated sustained release for 2 days. The NPs were combined with hydrogel, consisting of 4.5% chitosan and 12% β-GP (w/v), and the system was shown to gel in under 4 minutes at 34 °C and possess a mucoadhesion strength of 30 ± 1.61 g/cm^2.

Furthermore, a pharmacologic effect was demonstrated after intranasal dosing in rats with OVA-induced AR [155].

Table 2. Controlled Release Systems for the Nasal Cavity and Sinuses

Delivery System	Material(s)	Drug(s)	Duration of Release	Development Status	Reference
Stents & mesh scaffolds	PLGA			FDA-approval for use in	
	Propel®	Mometasone furoate	30 d	ethmoid	[107,116,156]
	Propel mini®		30 d	frontal & ethmoid	[108]
	Propel contour®		30 d	ethmoid & maxillary	[114]
	Sinuva®		90 d	ethmoid	[110,117,118]
	PLLA	Ciprofloxacin	2 wk (50%)	Rabbit ABRS model	[119,120]
	PLGA, PLCL or PGCL; LYR-210	Mometasone furoate	24 wk	Phase I open-label trial, Phase II trial in progress	[72,121,122]
Nano- & microparticles	PLGA (50:50, i.v. 1 dL/g) NPs	Mometasone furoate	7 d	*In vitro*	[126]
	Poloxamer 188 and Eudragit RS100 NPs	Triamcinolone acetonide	24 h	Drug deposition in rat nasal cavity	[127]
	Chitosan NPs	Cromolyn	12 h	*In vitro*	[128]
	Deoxycholate-chitosan-hydroxybutyl NPs	Cetirizine	72 h	*In vitro*	[129]
	PLGA (50:50, 11,000 Da) NPs with Pluronic F127 coating	N/A	Not evaluated	*In vitro*	[130]

Table 2. (continued)

Delivery System	Material(s)	Drug(s)	Duration of Release	Development Status	Reference
Nano- & microparticles (ctd.)	PLGA (1:1, i.v. 0.43 dL/g)-PEG MPs with nanostructured surface	Resveratrol	42 h	Murine eosinophilic rhinosinusitis model	[131]
	Chitosan MSs	Levocetirizine	8 h	*In vitro*	[132]
		Astragalus polysaccharide	24 h	Rat AR model	[133]
	HP-β-CP and HPMC or NaCMC MPs	Budesonide	120 min	*In vitro*	[135]
	Porous organosilica MPs	Nitric oxide	100 min	*In vitro*	[137]
		Nitric oxide, nitrate, manuka honey	280 min	*In vitro*	[138]
In situ hydrogels	Poloxamer 407, Carbopol 974 NF, PEG (400 Da)	Mometasone furoate	180 min	Murine AR model	[141,145]
	Poloxamer 407, Carbopol 974 NF	Mometasone furoate, Levofloxacin, Retinyl palmitate	Not measured	Rabbit maxillary sinus antrostomy model	[146]
	Poloxamer 407, HPMC, chitosan	Dexamethasone	72 h	*In vitro*	[147]
	Poloxamers 407 and 188, PEG (6 kDa)	Paeonol	24 h	Guinea pig AR model	[148]

Table 2. (continued)

Delivery System	Material(s)	Drug(s)	Duration of Release	Development Status	Reference
In situ hydrogels (ctd.)	Chitosan (100-300 kDa), β-GP	siRNA targeting VEGF	2 wk	Rat CRS model	[149]
	Gellan gum	Mometasone furoate	Not measured	Rat AR model	[150]
	Gellan gum, Pectin, Sodium hyaluronate, Tween 80	Fluticasone propionate	8 h (50%)	*In vitro*	[140]
Combination systems	PLLA stent + PLGA NPs	Ciprofloxacin, Ivacaftor	21 d	Rabbit ABRS model	[151,152]
	4-arm-thiol-PEG and Ag^+ hydrogel + lecithin and cholesterol liposomes	Clarithromycin, Budesonide	7 d	Rabbit ABRS model	[153]
	Chitosan-PVP hydrogel + PLGA (50:50, 0.45-0.60 dL/g) MPs	Dexamethasone	>30 d	*In vitro*	[154]
	Chitosan-β-GP *in situ* gel + PEG-PLA NPs	miRNA-146a	2 d	Rat AR model	[155]
	pNIPAAm-PEG (200 Da) *in situ* gel + PLGA (50:50, 0.32-0.44 dL/g) MPs	Mometasone furoate	30 d	Rabbit CRS model	[157]

2.3 Discussion

Local, controlled release delivery to the nasal and sinus cavities is a promising strategy for maintaining therapeutic concentrations over time to improve management of rhinitis and rhinosinusitis. As these are two prevalent conditions are associated with several co-morbidities, significantly diminished quality of life, and high healthcare costs, effective treatment delivery is imperative. However, traditional daily delivery methods (i.e., nasal sprays, drops, and irrigation) require repeat dosing and their access to the sinuses is limited. As a result, there has been considerable development over the past two decades of biomaterial-based systems that can concentrate medical therapies and promote mucosal healing of infected or inflamed sinonasal tissue.

For localized corticosteroid delivery, nasal packs, sinus stents, and polymeric meshes have each been used in patients with CRS. Inconsistent, and often insignificant, improvements have been reported in trials evaluating corticosteroid-soaked nasal packs, dressings, or spacers fabricated from naturally-derived or synthetic polymers. In contrast, PLGA sinus stents (the Propel family and Sinuva) have demonstrated safety and clinical improvement in post-operative outcomes, supporting their FDA approval. As a result, use of Propel has increased dramatically since its approval, with estimates in 2016 of annual sales exceeding 100,000 units and annual revenue close to $100 million [158]. Notably, the use of stents after sinus surgery contributes to an overall higher procedural cost as each of the Propel stents are approximately $750. Their use has been supported by an economic assessment, though, because of the reduced incidence of post-operative interventions. However, this economic assessment was based on the clinical trials

comparing Propel to a nonsteroid-eluting stent at 60 days after surgery and is therefore limited in both the comparison to other treatment strategies and in the duration of the follow-up period [159].

Along with the expense of the implants, there are challenges associated with the placement of degrading polymeric implants in the sinuses. As discussed earlier, Propel, Propel mini, Propel contour, Sinuva, and the composite scaffold, LYR-210, are each intended for specific locations in the sinuses and thus may not provide wide-spread distribution of corticosteroids, or multiple devices may be necessary, further increasing procedural costs. Furthermore, maintaining contact of a more rigid implant with the complex sinonasal anatomy can lead to patient discomfort caused by tissue damage. In fact, biodegradable implants can elicit host immune reactions as a result of degradation kinetics and degradation products, mismatch in mechanical properties between the implant and tissue, and micromotion of the implant [160]. This is a particular concern in the case of CRS as the target tissue is already the site of chronic inflammation.

On the other hand, nanoparticle-, microparticle-, and *in situ* hydrogel-based strategies that are still in early characterization or preclinical testing have the potential to offer greater flexibility in patient care through uniform distribution of a broad range, or even multiple, therapeutics, though there are remaining challenges that must be addressed. These drug delivery systems must be able to overcome the mucus barrier of the sinonasal epithelium to effectively deliver the drug payload. Consequently, there has been extensive research designing mucopenetrating nanoparticles and microparticles, which demonstrate the size advantage of nanoparticles for transport through mucus and the ability to modify their surface chemistry using muco-inert PEG or neutral polymers, such as Pluronic F127 [7,76,130]. Alternatively, mucoadhesive polymers or coatings can enhance particle retention in mucus, however the particles or drugs may become trapped within the mucus layer and unable to adequately penetrate to the underlying epithelium. *In situ* hydrogels, rather,

have the unique advantage of increasing residence time due to their temperature- or ion-responsive gelation in the nasal and sinus cavities, yet their drug release capabilities are more restricted. The studies reviewed here demonstrated sustained release for 3 days at most [147].

Taking into consideration some of the limitations of individual delivery vehicles, another strategy is to combine multiple biomaterials to leverage beneficial features of the distinct components. Thus, investigators have proposed coating stents with nanoparticles [151,152], combining liposome or PLGA drug carriers with hydrogels [153,154], and embedding polymeric microparticles in *in situ* hydrogels [155]. We have developed a combination system consisting of a thermoresponsive hydrogel with controlled release PLGA microspheres that is described in detail in Chapter 3, with additional characterization and modifications in Chapters 4. Finally, in Chapter 5, we consider the form of the delivery system that would be best suited for clinical translation.

3.0 TEMPS: A Thermoresponsive and Controlled Release System for Long-Acting Corticosteroid Delivery into the Paranasal Sinuses

3.1 Introduction

As introduced in the previous chapters, currently prescribed intranasal corticosteroids, such as mometasone furoate, are beneficial for CRS symptom relief [31,34], however their local delivery to the sinuses is challenging. Nasal irrigation utilizing pots and squeeze bottles outperforms sprays in the ability to access to the sinus cavities, but requires high volumes, practiced technique, and daily dosing [34]. The only FDA-approved local, controlled release devices for the paranasal sinuses are dissolvable stents (Propel and Sinuva), which are coated with mometasone furoate and implanted in one of the sinus cavities after surgery. Because the stents are designed to gradually degrade, local epithelial attenuation and cilia loss have been noted in the early response to stent placement [161]. This inflammatory response can lead to clinical adverse events including crusting, granulation, and scarring [123] as well as nasal and ocular irritation [124]. In one severe case, a stent was found to be extending through the skull base into the brain with significant cognitive consequences [162]. In this instance, the patient had undergone extensive surgery and 8 stents were placed throughout the sinus cavities [162]. Because of the varying anatomy of the ethmoid, maxillary, frontal, and sphenoid sinuses, specifically designed stents are necessary for each cavity and incorrect placement can lead to complications.

If a system could conform to the sinonasal mucosa, mimicking the native mucus layer, such a device would address the issues with existing delivery methods and be much better suited for long-term application. One such method is a combination system composed of a thermoresponsive

hydrogel (thermogel) with polymeric microspheres. Previously, we have demonstrated that degradable poly(lactic-co-glycolic acid) microspheres (PLGA MSs) embedded in poly(N-isopropylacrylamide) (pNIPAAm)-based hydrogel safely and effectively deliver long-term glaucoma treatment in rabbits [163]. The sol-gel transition allowed the gel to comfortably conform within the lower fornix of the eye creating a depot for several weeks of sustained drug delivery. Accordingly, we sought to explore the suitability of a combined microsphere-thermogel system for localized drug delivery in complex spaces, such as the sinus cavities, that require a conforming system to maintain long term apposition and retention. Furthermore, this technology, called "TEMPS" (**T**hermogel, **E**xtended-release **M**icrosphere-based-delivery to the **P**aranasal **S**inuses), offers the flexibility of encapsulating different drugs in the polymeric microspheres and broader implications for treatments of various inflammatory or allergic sinonasal conditions. In the following chapter, we discuss the development and characterization of TEMPS, as well as proof-of-principle testing in an obstruction-based rabbit model of CRS.

3.2 Materials & Methods

3.2.1 Microsphere Fabrication and Characterization

Mometasone-loaded PLGA MSs were fabricated using a standard single emulsion procedure (Figure 12). 200 mg PLGA (0.32-0.44 dL/g, 50:50 LA:GA, ester-terminated, RG503, Sigma, St. Louis, MO) and 10 mg mometasone furoate (AcrosOrganics, Thermo Fisher Scientific, Waltham, MA) were mixed with 4 mL dichloromethane. The drug/polymer solution was homogenized (Silverson L4RT-A, East Longmeadow, MA) in 60 mL 2% poly(vinyl alcohol)

(PVA, MW ~25 kDa, 98% hydrolyzed, PolySciences, Warrington, PA) at 5000 rpm for 1 min. The emulsion was then mixed with 80 mL 1% PVA and stirred at 600 rpm for 3 h for solvent evaporation. Microspheres were collected, washed 4x with MilliQ water, flash-frozen with liquid nitrogen, and lyophilized (VirTis Benchtop K freeze dryer, Gardiner, NY operated at 100 mTorr) for 48 h before storage at -20 °C. Samples of MSs were visualized by scanning electron microscopy (SEM) (JEOL JSM-6510LV/LGS SEM, Japan) following gold-palladium sputter coating (Denton Sputter Coater, Moorestown, NJ). Size distribution of MSs was determined by volume impedance measurements (Multisizer 3 Coulter Counter, Beckman Coulter, Indianapolis, IN).

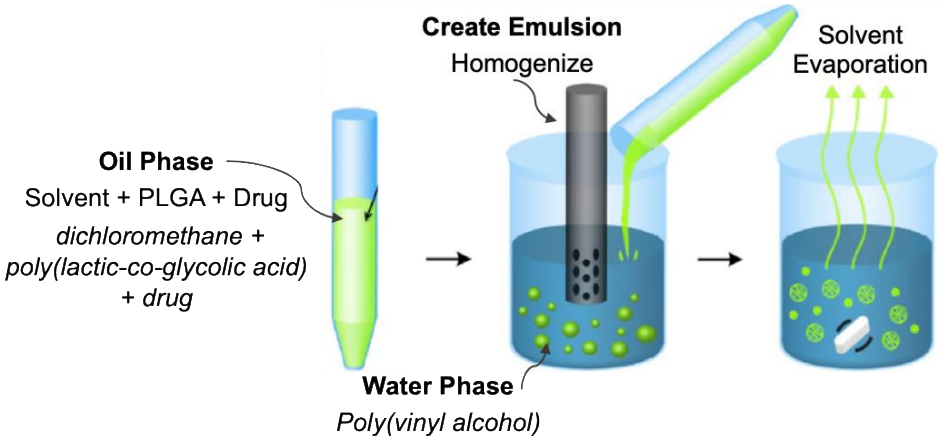

Figure 12. Schematic of the Single Emulsion Procedure for PLGA MS Fabrication.

Drug encapsulation was evaluated by dissolving 5 mg mometasone-loaded or blank MSs in 2 mL dimethyl sulfoxide (DMSO). The drug concentration was quantified by absorbance measurements at 262 nm using a UV-Vis spectrophotometer (Molecular Devices, Sunnyvale, CA). Encapsulation efficiency was calculated as the ratio of mometasone measured in the dissolved MSs relative to the amount that was initially added during fabrication and normalized based on MS yield.

3.2.2 Thermogel Fabrication and Characterization

Thermoresponsive hydrogel was prepared using reagents from Sigma-Aldrich (St. Louis, MO) and methods described by Bellotti *et al.* [79]. Briefly, 100 µL of 200 Da poly(ethylene glycol) (PEG) was added to 100 mg of N-isopropylacrylamide (NIPAAm) in a 15 mL conical tube. The aqueous free radical polymerization reaction was initiated by the addition of 2 mL of 0.5 mg/mL ammonium persulfate (APS) in water and 5 µL tetramethylethylenediamine (TEMED). Following overnight polymerization at 4 °C, the gel was washed 10x with warm MilliQ water (maintained at 40–50 °C) to remove unreacted monomer. The gels were collected in 20 mL glass vials and stored at ambient temperature.

The lower critical solution temperature (LCST) of TEMPS was characterized using absorbance measurements as a function of increasing temperature, as previously described [79]. Briefly, ~75 µL of gel was added to a clear bottom 96-well plate and absorbance at 415 nm was measured via a UV-Vis spectrophotometer. The temperature was gradually increased from 22 °C to 37 °C with 20 min intervals between each reading to allow the temperature to equilibrate. Additionally, reversibility of the sol-gel transition was demonstrated *in vitro*, whereby TEMPS and its individual components (gel and MSs alone) were incubated in a clear bottom, 96-well plate in an aqueous salt solution of simulated nasal fluid (SNF). SNF was formulated with 8.8 mg/mL NaCl, 0.6 mg/mL $CaCl_2$, and 3 mg/mL KCl in distilled water and the pH was adjusted to 6.4 [164]. At weekly intervals, absorbance was measured at 37 °C and 415 nm. Then the plate was cooled to room temperature and absorbance was measured again. The aqueous solution was replenished as needed and the plate was sealed during incubation to prevent evaporation.

Cytocompatibility of the pNIPAAm gel was evaluated using methods adapted from [79]. A sinonasal epithelial cell line (SNEC), RPMI 2650 (ATCC® CCL30™) was cultured in Eagle's Minimum Essential Medium (American Type Culture Collection, Manassas, VA) supplemented with 10% fetal bovine serum (FBS). SNECs were seeded at 20,000 cells per well in a 96-well plate. Thermogel samples (50 μL) were pre-incubated in medium overnight. The following day, the thermogel samples were transferred to wells containing cells, the medium was replaced, and plates were incubated for 24 hours. Positive controls consisted of cells incubated in medium alone and negative controls consisted of cells lysed for 20 minutes with 2.5% Triton X immediately before measuring metabolic activity as follows. Media and thermogel samples were removed from all wells and replaced with 10% PrestoBlue® viability reagent (ThermoFisher Scientific, Waltham, MA). After 3 hours incubation, reduction of PrestoBlue reagent was measured by fluorescence readings using a 540/580 nm for excitation/emission filters. The mean and standard deviation of fluorescence values (F) were determined (n = 6) and viability was calculated using Equation 3-1.

Equation 3-1: % Viability for Thermogel Cytocompatibility

$$\%\, Viability = 100 \times \left[1 - \frac{(F_{positive\ control} - F_{gel\ sample})}{(F_{positive\ control} - F_{negative\ control})}\right] \quad \text{(Equation 3-1)}$$

3.2.3 *In vitro* Drug Release and Bioactivity

In vitro release kinetics of mometasone furoate were evaluated using methods adapted from Ammar *et al.* [165]. To quantify release from MSs only, 10 mg MSs were incubated in 1 mL 2% sodium deoxycholate (NaDC) in water on a roto-shaker at 37 °C (n = 3). At regular time intervals, MS suspensions were centrifuged, the supernatant was collected and diluted 1:3 in methanol, and

the absorbance was measured at 248 nm [165]. The average absorbance value of release samples from blank MSs (n = 3) was subtracted at each timepoint. Drug release from TEMPS was determined using a similar procedure, with the exception that 10 mg MSs were suspended in 100 µL pNIPAAm gel (n = 5).

Throughout the *in vitro* release assay, release samples were diluted with DMSO and stored at -20 °C for bioactivity measurements. Following the vendor protocol for the Human Glucocorticoid Receptor (NR3C1, GR) Reporter Assay (Indigo Biosciences, State College, PA), the bioactivity of drug released between day 25 and 28 of TEMPS incubation was tested for its ability to bind to the engineered cells and induce luciferase expression. As a control, drug was solvated in DMSO the day of the assay to compare the bioactivity of fresh and released drug (n = 3 per dilution).

3.2.4 Animal Model

This study evaluating TEMPS in male and female New Zealand rabbits (2-4 kg) was approved by the Institutional Animal Care and Use Committee (IACUC) at the University of Pittsburgh. When necessary, animals were anesthetized with ketamine (10-50 mg/kg IM) and xylazine (2-5 mg/kg SQ). Lidocaine hydrochloride was applied to the nares to provide topical analgesia for endoscopy. Following all procedures, antisedan (5 mg/kg IV) was dosed for xylazine reversal and rabbits were given SQ saline (10 mL/kg) for higher anesthesia doses. If pain management following procedures was necessary, meloxicam was dosed for 1-3 days (0.2 mg/kg PO or SQ).

3.2.5 Disease Induction and MicroCT Imaging

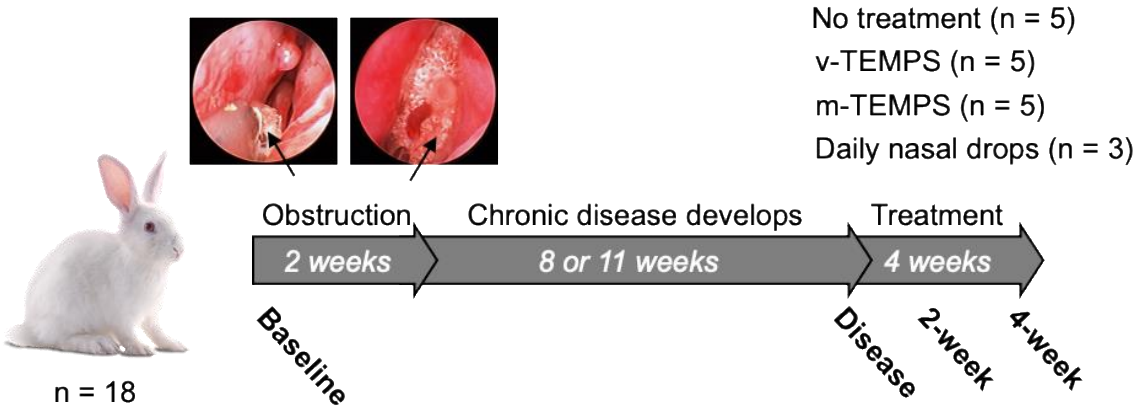

Figure 13. Experimental Design for Evaluating TEMPS in Rabbits with Induced CRS.

A sterile sponge was inserted in the sinus ostia (arrows) to obstruct drainage of the left maxillary sinuse for 2 weeks. Over the next 8 or 11 weeks, chronic disease developed. At the established disease state, rabbits were divided into 4 groups for bilateral treatment. m-TEMPs and v-TEMPS refer to mometasone-loaded and vehicle-only TEMPS, respectively.

A reversible obstruction of the left ostiomeatal complex was created to induce disease, simulating CRS in the maxillary sinus. Animals were anesthetized (ketamine, 35 mg/kg IM and xylazine, 5 mg/kg SQ) and the nasal cavity was visualized with a 1.9 mm 0° endoscope (Karl Storz, Tuttlinggen, Germany). A sterile polyvinyl alcohol sponge (aseptically trimmed to approximately 12 x 3 x 1 mm) was inserted through the left naris and packed in the opening of the sinus ostia, lateral to the middle turbinate as shown in Figure 13 and previously described [166]. Two weeks later, the sponge was removed under endoscopic visualization. Over the subsequent 11 weeks, disease phenotype progressed towards a chronic inflammatory pathology, as previously characterized by Cho *et al.* [166].

Opacification of the sinus cavities was monitored by skull micro-computed tomography (microCT) imaging using a Fidex system (Animage, Pleasanton, CA). For subjects that did not show evidence of opacification after the initial chronic disease induction, disease was re-induced as follows. Three sponges were inserted to ensure full blockage of the left sinus ostia for 2 weeks. Eight weeks after the sponge removal, microCT imaging was performed to assess disease re-induction.

3.2.6 Treatment Application

Following chronic disease induction, animals were divided into 4 groups for bilateral treatment: no treatment, blank vehicle TEMPS (v-TEMPS), mometasone-loaded TEMPS (m-TEMPS), and daily nasal drops. A one-time application of TEMPS was performed by percutaneously injecting the material into the maxillary sinus through the canine fossa using an 18 G needle. Approximately 20 mg of blank MSs or mometasone-loaded MSs were suspended in 0.4 mL of thermogel and injected into the left and right maxillary sinus cavities for the v-TEMPS or m-TEMPS groups, respectively. A no treatment group served as a negative control that also received the one-time percutaneous punctures without material injection. Similarly, a positive control treatment group received the one-time bilateral punctures without injection and daily nasal drops were applied for 4 weeks consisting of 31.25 µg of steroid in 100 µL (Mometasone Furoate Nasal Spray, Apotex Inc., Toronto, Ontario, diluted with PBS) to the left and right nares via a 0.5-inch 22 G flexible PTFE dispensing needle.

3.2.7 *In vivo* Measurements

Bilateral intraocular pressure (IOP) was measured at 4 timepoints: baseline, established disease state, 2-weeks, and 4-weeks after treatment application. To control for diurnal variations [167], IOP measurements were performed in the morning by the same technician on unrestrained, alert animals using a TonoVet rebound tonometer (Icare, Finland).

Additionally, at these 4 timepoints, bilateral sinus opacification was analyzed using microCT imaging (Figure 14). Using OsiriX Lite (Pixmeo SARL, Switzerland), the left and right maxillary sinuses were identified in a coronal view on three consecutive 155.79 μm thickness scans near the mid-point of the middle turbinate. The image contrast and brightness were adjusted so that only calcified tissue was visible (window level ~800, window width ~1400) and a region of interest was defined by tracing a polygon along the inner edge of the maxillary sinus wall, excluding calcified bone. The median CT # of this defined region, as calculated by the software, was recorded by an investigator blinded to the subject ID and the treatment group for measurements at the 2-week and 4-week timepoints.

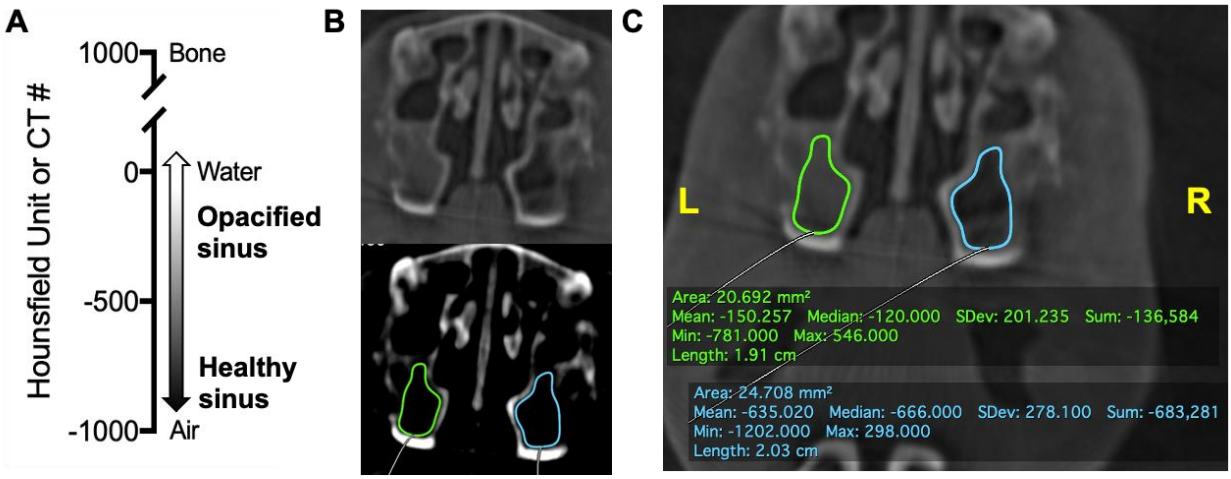

Figure 14. Quanitifying Rabbit Sinus Opacification by Micro-Computed Tomography (MicroCT) Imaging. (A) CT #, or Hounsfield unit, scale indicating the range of radiodensity measurements for healthy and opacified rabbit sinuses. (B, C) Representative image of rabbit sinuses with disease induced in the left sinus. (B, top) Tissue view and (bottom) bone view showing polygonal regions. (C) CT imaging software calculated parameters for the two regions, including the median CT # of -150 for the disease-induced side (green outline) and -635 for the control side (blue outline).

3.2.8 Histologic Preparation and Assessment

At the conclusion of the study, anesthetized animals were euthanized with pentobarbitol (100 mg/kg IV), and tissue was prepared for histological evaluation. The maxillary bones of 14 rabbits were harvested and fixed by immersion in 10% neutral buffered formalin for 1 week. Following fixation, the specimens were transferred to 10% formic acid for decalcification. After 1 week, the decalcification solution was tested every other day for end-point determination using 5 mL of the used decalcification solution combined with 5 mL ammonium hydroxide and 5 mL ammonium oxalate. If the test solution was cloudy, the tissue was placed in new formic acid until the next test day. Once the test solution yielded a clear solution, sections were cut, placed in cassettes, dehydrated in a graded series of alcohol, and embedded in paraffin blocks. Paraffin-

embedded sections were cut to 4 µm using a microtome, mounted on glass slides, and stained with routine hematoxylin and eosin (H&E).

Table 3. Histopathology Scoring Criteria

Criteria	Score	Categories
Epithelial cell damage†	0-3	None, mild degeneration, moderate degeneration, loss of epithelium
Cilia damage†	0-2	Normal, disrupted, loss
Subepithelial edema†	0-3	None, mild, moderate, severe
Inflammation of submucosal glands†	0-3	None, mild, moderate, severe
Epithelial hyperplasia	0-3	None, mild, moderate, severe
Basement membrane	0, 1	Intact, disrupted
Granulocyte tissue infiltrate	0, 1	Absent, present
Granulocytes in lumen	0, 1	Absent, present
†Involvement	0-3	None, up to 1/3, 1/3 to 2/3, 2/3 to diffuse

Inflammatory scoring criteria (Table 3) were developed for analysis of the maxillary sinus sections. Epithelial cell damage, cilia damage, subepithelial edema, and inflammation of the submucosal glands was scored for severity (0–3) and involvement (0–3) and the two scores were multiplied for analysis. The remaining criteria were scored for severity or absence/presence only. The scoring was performed in a blinded manner by a board-certified veterinary pathologist.

3.2.9 Statistical Analyses

Statistical analyses were performed with GraphPad Prism v7 (San Diego, CA) and SAS JMP® Pro 14 (Cary, NC). Descriptive statistics were used to describe the mean and standard deviations (S.D.) and values are reported as the mean ± S.D., unless specified otherwise. The

cumulative standard deviation (s) (Equation 3-2) was used for cumulative release calculations. For the *in vitro* bioactivity assay, the half maximal effective concentration (EC50), 95% confidence intervals (CI), and R^2 were determined by nonlinear 3-parameter logistic regression using GraphPad. Using JMP, comparisons among groups with continuous data were performed by one-way ANOVA. After assessing the variances by Levene's test, Wilcoxon Method (unequal variance) or Tukey (equal variance) post-hoc testing was performed. For nominal data, comparisons among groups were performed by Chi-square testing using Pearson's p-values. For all analyses, $p < 0.050$ was considered as significant.

Equation 3-2. Cumulative Standard Deviation (s)

$$s = \sqrt{\frac{\Sigma(x_i - \bar{x})^2}{n-1}} \quad \text{(Equation 3-2)}$$

3.3 Results

3.3.1 TEMPS Provides Extended Release of Bioactive Steroid in a Thermoresponsive and Cytocompatible System *in vitro*

The combined thermogel and polymer microsphere system, or TEMPS, was engineered to provide extended release of bioactive steroid for 4 weeks. The steroid, mometasone furoate, was encapsulated in PLGA MSs that had a spherical morphology with mean diameter of 7.8 ± 2.9 µm, which was measured by volume impedance (Figure 15A) and confirmed by SEM imaging. In Figure 15A, the second peak near 28 µm was likely aggregates of MSs. Approximately 44 µg of

mometasone per mg MS was encapsulated, with a loading efficiency of 88%. The sustained release of mometasone for 4 weeks was demonstrated *in vitro* from both MSs (Figure 15B) and TEMPS (Figure 15C). Additionally, the bioactivity of released mometasone from TEMPS was similar to fresh drug. TEMPS release samples that were collected between day 25 and 28 had an EC50 of 0.33 pM (95% CI [0.17, 0.61] and $R^2 = 0.92$) measured by a glucocorticoid receptor reporter cell line assay, while that of fresh drug was 0.31 pM (95% CI [0.13, 0.65] and $R^2 = 0.90$) (Figure 15D).

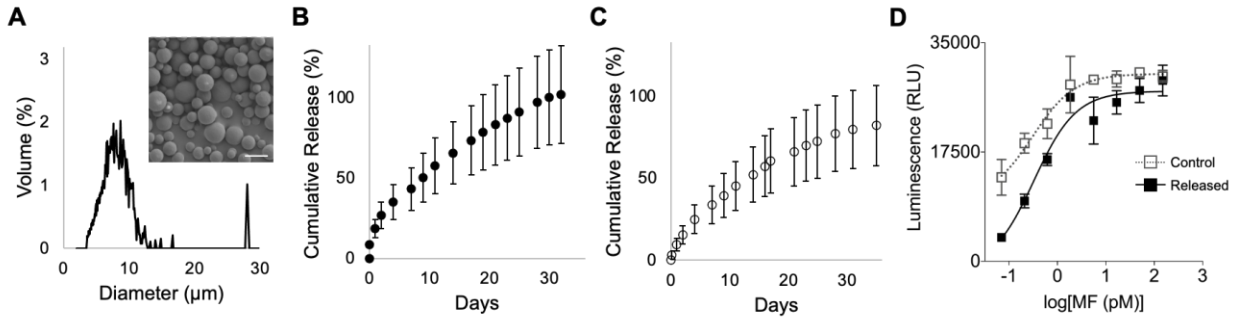

Figure 15. Bioactive Mometasone Furoate can be Released from TEMPS for 4 Weeks.

(A) Size distribution and (inset) representative SEM, scale bar = 10 µm, of drug-loaded MSs showing a smooth, spherical morphology with mean diameter of 7.8 µm. (B) Cumulative release of mometasone from MSs (n = 3) and (C) TEMPS (n = 5). Error bars represent mean ± cumulative standard deviation. (D) Drug released from TEMPS after 28 days of aqueous incubation at 37 °C displays activity (EC50 = 0.33 pM) similar to a control, drug prepared the day of the assay (EC50 = 0.31 pM). Error bars represent mean ± S.D.

This bioactive steroid is intended for localized delivery to the paranasal sinuses via a biocompatible and reversible thermoresponsive hydrogel. Accordingly, a PEG-pNIPAAm gel formulation with an LCST of 34-35 °C (characterized in previous work [79]) was selected for the thermoresponsive matrix. The presence of drug-loaded MSs did not alter the LCST, as shown in Figure 16A, although MSs caused a higher baseline absorbance value in the clear gel. Importantly,

the reversible phase change of TEMPS, as compared to MSs alone, was demonstrated by repeat absorbance measurements while the temperature was fluctuated between ambient and body temperature over 28 days (Figure 16B). Additionally, cytocompatibility of the PEG-pNIPAAm gel with SNECs was tested. After incubating for 24 hours with the gel, cellular viability was comparable to that of control cells (Figure 16C).

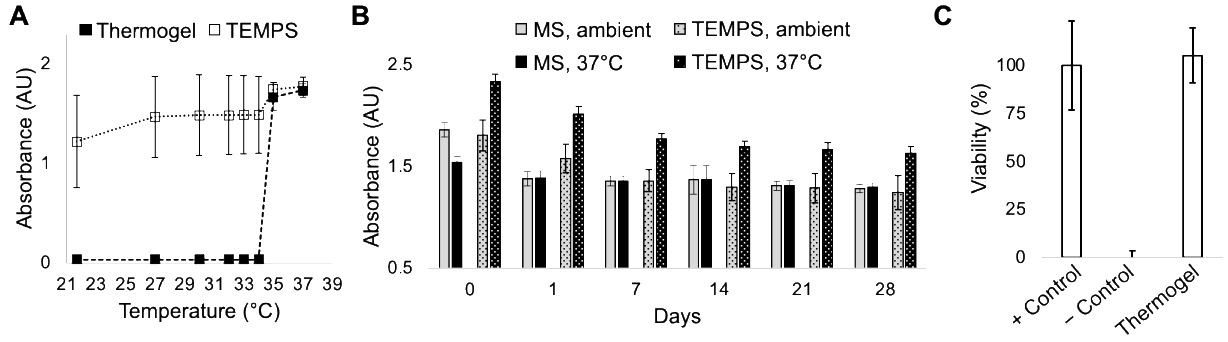

Figure 16. TEMPS Undergoes Reversible Apposition and is Compatible with SNECs

(A) Absorbance (415 nm) as a function of increasing temperature for samples (n = 4) of thermogel and TEMPS showing that both undergo a phase transition at 34-35 °C. (B) The reversible temperature-responsive phase change of TEMPS demonstrated by repeated absorbance measurements at ambient temperature and 37 °C over 28 days. (C) Thermogel cytocompatibility with SNECs showing that viability is maintained after 24-hour incubation with gel. Cell viability was measured using PrestoBlue reduction and % viability was calculated relative to positive (+) and negative (–) controls. Error bars represented mean ± S.D.

3.3.2 Evaluating Inflammation in an Obstruction-Based CRS Rabbit Model

Following *in vitro* characterization of TEMPS, it was evaluated *in vivo* in rabbits with induced sinonasal inflammation, however we found that recreating this heterogenous disease and

interpreting the extent of inflammation were not straightforward. At the disease state (8-11 weeks after removal of the obstructing sinus sponge), sinonasal inflammation was evaluated by nasal endoscopy and microCT. Purulent secretions were observed in 14 of 18 subjects on the disease-induced side, while no mucus or clear secretions were observed on the control side in the majority of subjects (16 of 18). Additionally, CT # was significantly higher relative to baseline, bilaterally, with a larger effect size on the disease-induced side (Figure 17A). Notably, the range in CT # reflects that robust sinonasal inflammation was not induced in all subjects. Following disease re-induction (n = 6), the CT # was significantly increased relative to baseline and the initial disease state, bilaterally (Figure 17B).

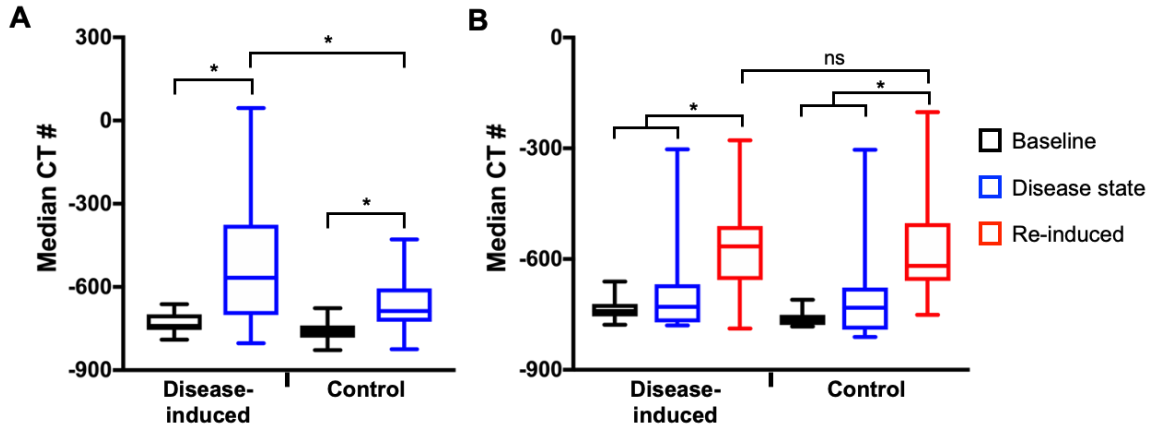

Figure 17. MicroCT Analysis of Rabbit Sinus Opacification at Baseline and After Disease Induction. (A,B) MicroCT results for the disease-induced and control sides including the group mean (line), 95% CI (box) and range (whiskers) at (A) baseline and the disease state (n = 18) and (B) baseline, the disease state, and re-induced disease (n = 6). Statistical significance was determined by repeated measures ANOVA with post hoc testing by Tukey method, *p < 0.05, ns = not significant.

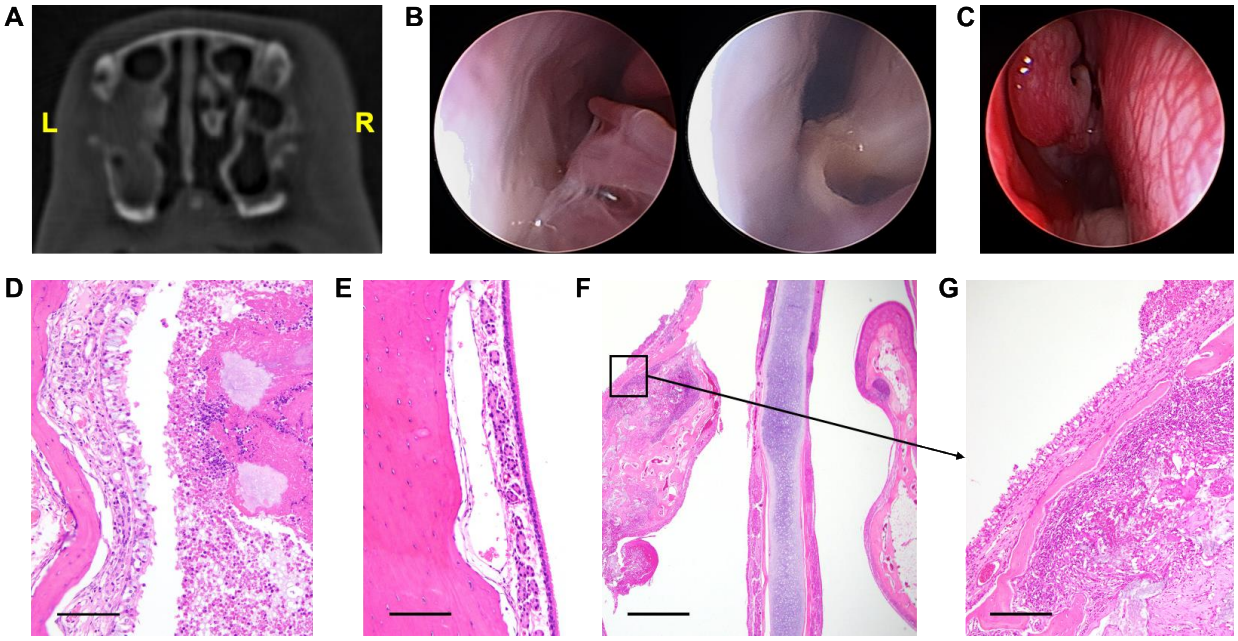

Figure 18. Successful Disease Induction in Rabbits Showed Evidence of Unilateral Disease by MicroCT, Endoscopy, and Histopathology.

(A) MicroCT and (B,C) endoscopy imaging showed evidence of opacification and mucus on the left side (B) but not the right side (C). (D,E) H&E staining of the sinuses at 20x magnification (scale bar = 1 mm) showing (D) diffuse damage of the ciliated epithelium and aggregates of granulocytes in the lumen on the left compared to a (E) healthy right side. (F) In the left nasal cavity, regionally extensive bone necrosis, resorption, and chronic active osteomyelitis at 2x (scale bar = 200 µm) and (G) 10x (scale bar = 100 µm).

At the study endpoint, microCT results as well as histopathology scoring were analyzed. Comparisons of the histopathology scores between the disease-induced and control sides showed no significant differences, however, when histopathology scores were compared to CT #, correlations between the two methods were identified. A significant moderate correlation of epithelial cell damage and cilia damage with CT # on the disease-induced side ($p < 0.020$, adjusted-$R^2 > 0.330$) was identified. Presence of granulocytes in the lumen also had a significant mild correlation with CT # ($p < 0.045$, adjusted-$R^2 > 0.236$). As an example of comparing multiple

analysis methods for one subject, evidence of disease was observed as sinus opacification (microCT), thick white mucus (endoscopy), diffuse damage to the ciliated epithelium, granulocytes, regionally extensive ulceration, bone necrosis/remodeling, and chronic active osteomyelitis (histopathology) (Figure 18).

3.3.3 Sinonasal Inflammation was Reduced Following Treatment with Mometasone-TEMPS

The efficacy of extended steroid release from TEMPS was assessed by comparing the change in CT # from the disease state to the 2- or 4-weeks treatment timepoints. On the control (right) side, change in CT # of the v-TEMPS group was significantly increased compared to no treatment ($p < 0.001$) and m-TEMPS ($p < 0.020$) at 2-weeks after treatment application. Similarly, at 4-weeks post-treatment, the change in CT # of the v-TEMPS group remained significantly increased compared to the no treatment, m-TEMPS, and daily nasal drop groups ($p < 0.001$, Figure 19A). In contrast, the change in CT # at 2- and 4-weeks after treatment on the disease-induced (left) side showed no significant differences between groups ($p > 0.050$, Figure 19B).

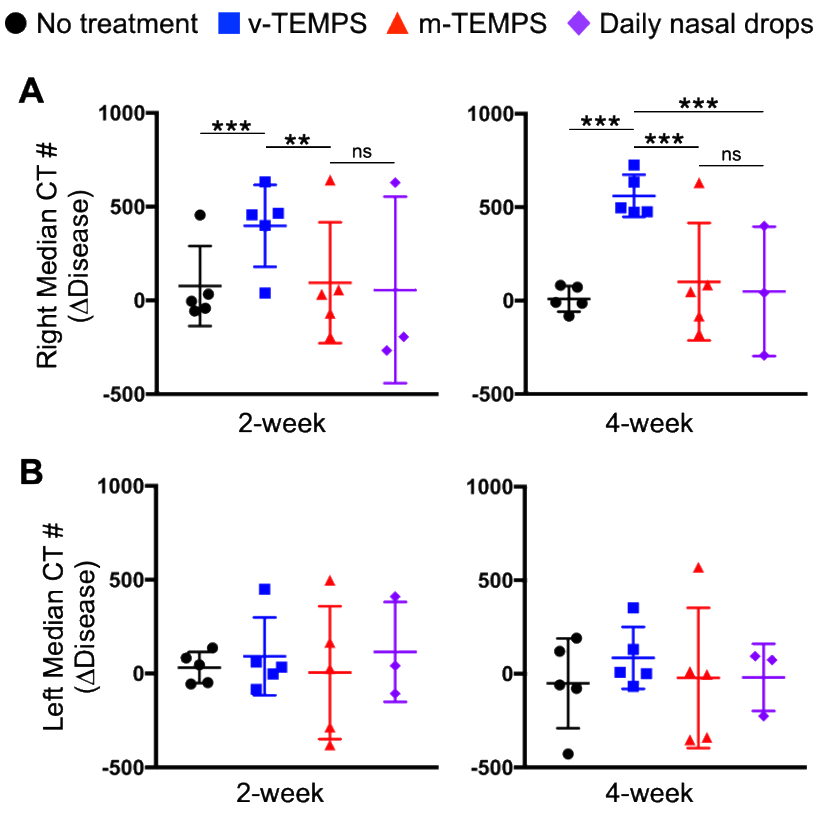

Figure 19. MicroCT Imaging Showed Reduced Opacification of the Right Maxillary Sinus Following Application of m-TEMPS Compared to v-TEMPS.

(A) Change in CT # between the disease state and treatment timepoints on the right and (B) left sides. Error bars represent the mean ± S.D. for each group: no treatment (n = 5), v-TEMPS (n = 5), m-TEMPS (n = 5), and daily nasal drops (n = 3). Statistical significance was determined by one-way ANOVA with post hoc Wilcoxon Method testing, *** $p < 0.001$, ** $p < 0.020$, ns = not significant.

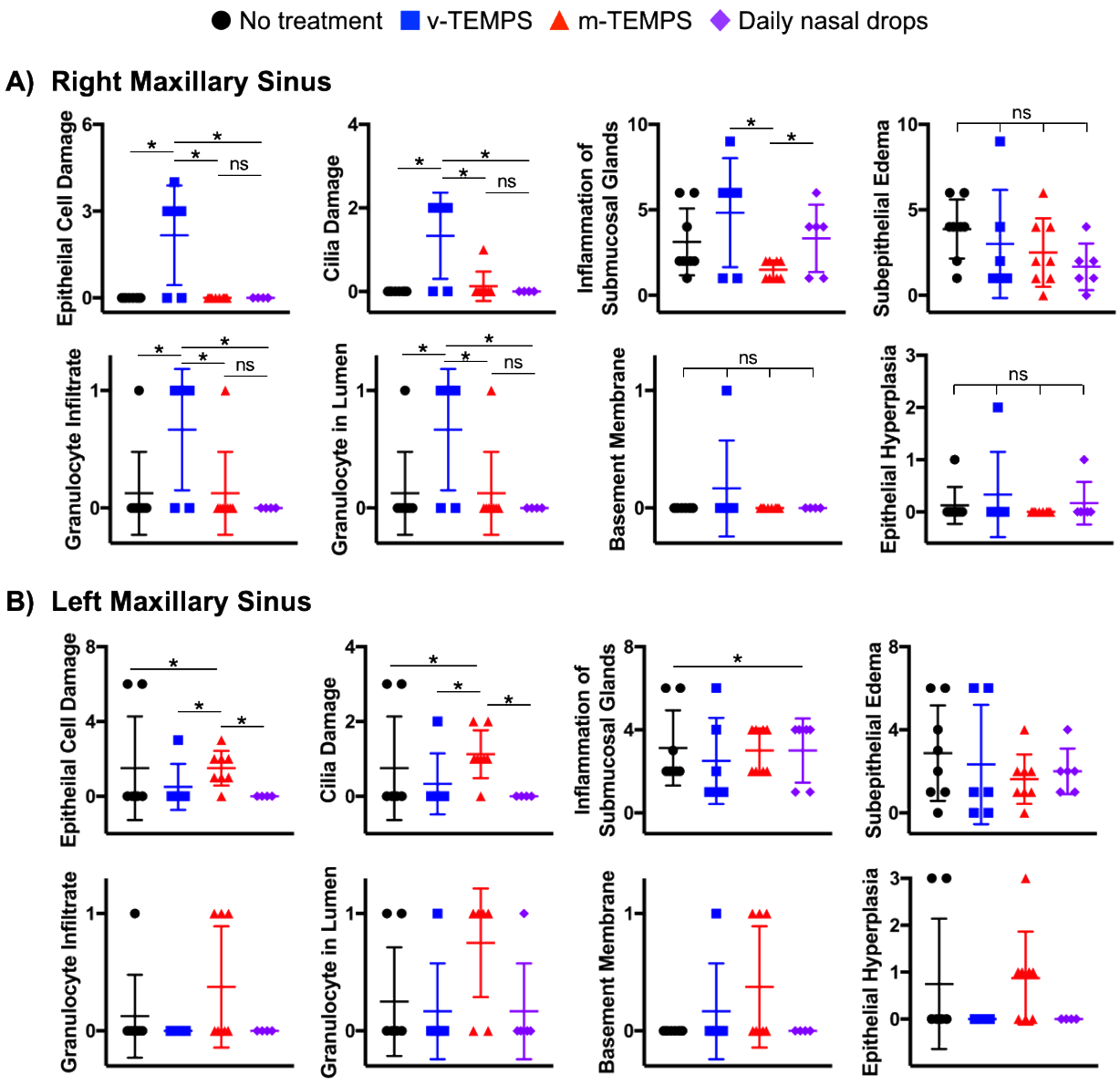

Figure 20. Histopatholoy Sections Showed Evidence of Iatrogenic Trauma due to Application of TEMPS that was Reversed by Local Steroid Delivery.

Two sections from each subject were stained with H&E and the (A) right and (B) left sides were scored by a blinded veterinary pathologist. Individual symbols represent the score for each section and error bars represent the mean ± S.D. for treatment groups: no treatment (n = 4), v-TEMPS (n = 3), m-TEMPS (n = 4), and daily nasal drops (n = 3). Statistical significance was determined by Chi-square test using Pearson's p-value, * $p < 0.050$, ns = not significant.

Further evaluation of the tissue response to treatments was performed using histopathology to score inflammation criteria at the study endpoint. On the right side, epithelial cell damage, cilia damage, granulocyte infiltrate and granulocytes in the lumen were significantly increased in the v-TEMPS group compared to all other groups ($p < 0.050$). Additionally, inflammation of the submucosal glands was reduced in the m-TEMPS group compared to the v-TEMPS and daily nasal drop groups ($p < 0.050$, Figure 20A). On the left side, epithelial cell damage and cilia damage were elevated in the m-TEMPS group relative to other groups ($p < 0.050$), but also exhibited more variability among subjects (Figure 20B).

3.3.4 Steroid was Safely Delivered from TEMPS Maintained in the Maxillary Sinuses for 4 Weeks

Throughout the study, bilateral IOP was measured to assess for ocular effects related to localized steroid delivery. Two weeks after treatment application, IOP was not elevated in any group. At 4 weeks, mean IOP of the daily nasal drop group was statistically elevated in comparison with baseline ($p < 0.050$). Importantly, the m-TEMPS group did not show elevated IOP at any timepoint (Figure 21A). Additionally, the IOP values reported here are within the range previously reported for healthy New Zealand rabbits, which over a 2-year period was 16.9 mmHg (range: 11.2-25.0, CV: 16.6%, n = 125) [167]. Similarly, the overall mean IOP in this study was 16.7 mmHg (range: 12.0-25.0, CV: 15.3%, n = 72).

The ability of TEMPS to be maintained in the maxillary sinuses for 4 weeks was evaluated post-mortem. Within the sinuses of one of the subjects treated with TEMPS, a foreign material was identified (Figure 21B). This sample was visualized using SEM and microspheres were identified (Figure 21C). In H&E sections of animals treated with TEMPS, material in the lumen

was observed that displayed spherical holes, which were likely the locations of polymer microspheres that dissolved during processing (Figure 21D). The presence of this material in histological sections was noted on the left and right sides of many subjects in both TEMPS-treated groups (Figure 21E).

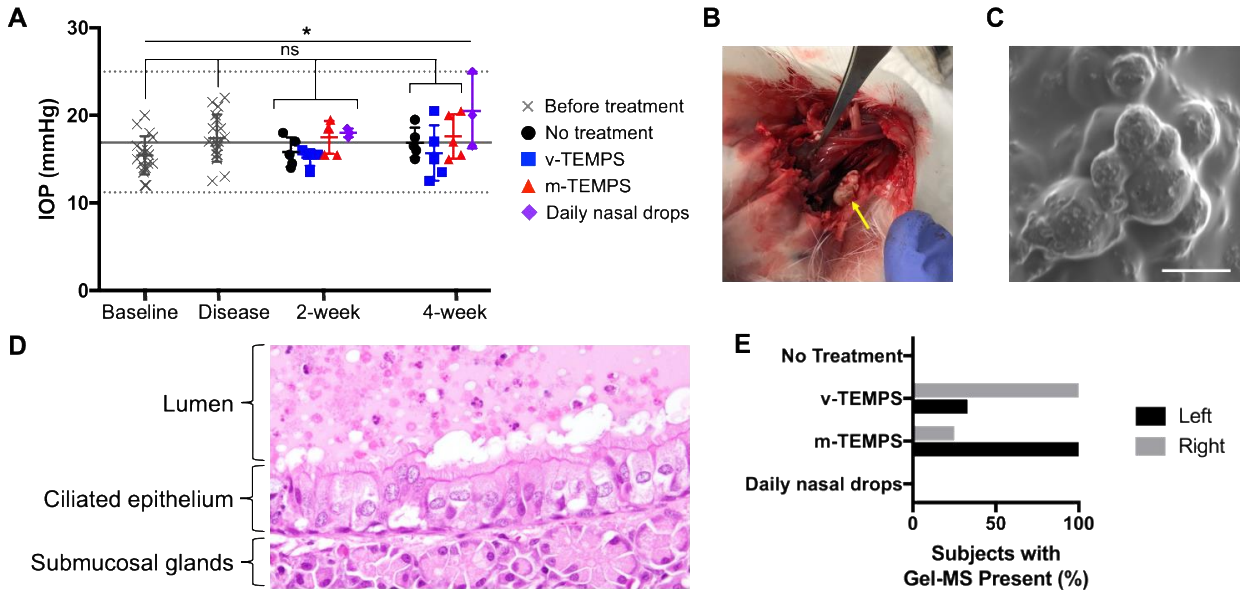

Figure 21. IOP was Not Affected by 4 Weeks of Local Steroid Delivery from TEMPS.(A) Mean bilateral IOP measurements for each subject are represented as individual symbols and error bars represent the group mean ± S.D. for: before treatment (n = 18), no treatment (n = 5), v-TEMPS (n = 5), m-TEMPS (n = 5), and daily nasal drops (n = 3). Solid and dotted lines denote the mean and range, respectively, of healthy New Zealand rabbit IOP values [167]. (B) A foreign material (yellow arrow) was recovered during post-mortem analysis from a subject treated with TEMPS. (C) The recovered material was visualized by SEM and spherical MSs were observed, scale bar = 10 µm. (D) Representative H&E section of a subject treated with TEMPS showed a foreign material in the lumen and apposed to the epithelium that contains spherical holes, which are consistent with the expected appearance of TEMPS (40x magnification). (E) Percentage of subjects in each treatment group where TEMPS material was observed in H&E sections by a blinded investigator. Statistical significance was determined by repeated measures ANOVA with Tukey post-hoc testing, * p < 0.050, ns = not significant.

3.4 Discussion

The sinonasal inflammation that is characteristic of CRS can be reduced by treatment with steroids [31]. Use of oral steroids, however, can increase risks of adverse effects, such as growth inhibition and decreased bone mineral density [40], and consequently topical methods are preferable if possible. While nasal steroid sprays are convenient, only 30% of the applied dose is deposited in the nasal cavity [40] with very little, if any, reaching the sinus cavities [31,45]. Nasal irrigation is more effective; however, it requires large volumes and daily dosing [34]. CRS patients whose symptoms are not improved by medical therapy can also undergo functional endoscopic sinus surgery to remove inflamed tissue and bone, but challenges of intra-sinus drug delivery still remain in these patients.

In this study, we have presented a potential solution that addresses many existing clinical hurdles with TEMPS. This system provided 4 weeks of sustained release of bioactive steroid, mometasone furoate, using a combination of thermogel and polymer microspheres. Importantly, the thermoresponsive nature of the non-biodegradable gel allows its application into the paranasal sinuses as a liquid at ambient temperature, conforming to the sinonasal epithelium as it gels. Within the nasal cavity, inspired air is quickly warmed from 25.3 ± 2.1 °C in the nasal vestibule to 33.9 ± 1.5 °C in the nasopharynx [13] and the paranasal sinuses lie along this temperature transition. Thus, TEMPS can be tuned to reversibly undergo a phase transition at a LCST of 34-35 °C . We propose that ambient temperature saline irrigation can return the gel to a liquid state for its removal. While demonstrating removal of the system *in vivo* was not feasible in the present study, TEMPS that was incubated *in vitro* at 37 °C for 4 weeks did reversibly undergo a phase change when cooled to ambient temperature at weekly intervals, as expected.

To our knowledge, this is the first hydrogel-based system for the paranasal sinuses that is designed for multiple weeks of sustained, localized steroid release. The advantage of using a gel to adhere topical treatment to the sinonasal mucosa has been previously recognized [168]. In an uncontrolled clinical study, physicians applied a hydrophilic mometasone furoate gel to the sinuses of CRS patients up to 3 times. Drug release kinetics were not specified, and likely not sustained, which is supported by the report of modest, but temporary improvement of the diseased mucosa [168]. Others have designed a thermoresponsive and bioadhesive gel for 4 hours of mometasone release [141]. This gel was composed of Pluronic® F-127 and Carbopol® 974P NF and tested for relieving allergic rhinitis in rats and promoting repair of a mucosal injury in rabbits [141,145,146]. Another mucoadhesive *in situ* gel designed for the nasal and sinus cavities was synthesized from poloxamer-407, hydroxypropyl methyl cellulose, and chitosan salt and demonstrated the gradual release of steroid, dexamethasone 21-phosphate disodium, for 3 days *in vitro* [169]. In each of these systems, the shorter duration of drug delivery is dictated by the gel component being the rate limiting step for release. In contrast, release kinetics of TEMPS are intended to be controlled by diffusion and bulk erosion of PLGA MS, which can be tuned to release drugs for days, weeks, months, or even years [170]. While *in vitro* characterization revealed that the pNIPAAm matrix (which surrounds the extended-release MS) caused a small reduction of the initial burst release from 18.5% (MSs alone) to 11.3% (TEMPS) after 24 hours aqueous incubation, the complete 4-week release profile was largely unchanged. It is likely that hydrophobic interactions between mometasone furoate, a lipophilic small molecule [40], and the pNIPAAm chains reduced the rate of initial release but did not limit the ultimate diffusion of drug from the system. Instead, the gel component primarily serves to retain the extended-release MSs and conform within the sinuses.

To measure mometasone release kinetics *in vitro,* a medium that maintained the lipophilic drug in solution was required. Others have measured the release of mometasone from PLGA endotracheal tubes in 1% sodium dodecyl sulfate (SDS) [165]. While an SDS solution was suitable for measuring mometasone release from PLGA MS alone, release from TEMPS could not be performed because SDS is also a detergent and quickly degraded the thermogel. Thus, other surfactants including sodium deoxycholate and tween-80 were evaluated. A solution of 2% sodium deoxycholate demonstrated both compatibility with the thermogel and the ability to maintain mometasone in solution that could be detected by spectrophotometry for *in vitro* quantification.

A benefit of the lipophilic nature of mometasone is that it can be efficiently encapsulated in polymeric microspheres at concentrations sufficient for clinical use. The PLGA MS formulation described herein encapsulated 44 µg mometasone per mg MS for an overall loading efficiency of 88% and loading content of 4.4%. In contrast, a recent PLGA nanoparticle formulation reported a mometasone loading content of 22.4% [171]. Despite the lower drug content, the MS formulation met the objectives for this study, including sustained release for 4 weeks (in comparison to 7 days from the nanoparticle formulation [171]) and drug loading that was sufficient for a clinical dose. Specifically, ~250 mg MSs would provide a sufficient quantity of drug to locally release ~400 µg mometasone per day for 4 weeks. This dosage is equivalent to that achieved by bilateral, twice daily applications of a mometasone furoate nasal spray. Furthermore, currently available degradable sinus stents have a total loaded dose of 370 µg or 1350 µg mometasone per implant and are designed for gradual release over 30 or 90 days, respectively [42,118]. In patients with severe inflammation, increased steroid dosing with sustained delivery may be warranted and provide more effective symptom relief [172]. Importantly, the PLGA MS component of TEMPS

enables sufficient surface area-to-volume loading of mometasone, as well as flexible dosing by adjusting the amount of MSs in the system [173].

The dosing flexibility provided by TEMPS is a product of both the amount of embedded MSs as well as the total volume for application. The system is intended to be applied as a thin coating along the sinus epithelium, either targeted to specific areas of inflammation or distributed throughout the sinuses for widespread treatment. Reported volumes of the maxillary and frontal sinuses of post-operative CRS patients and healthy individuals range from 37 cm^3 to 57 cm^3 [41]. At the MS concentration tested in this pilot study (50 mg/mL), a patient dose of TEMPS would equate to 5 mL, or just 9-14% of reported sinus volumes. Additionally, this dosing volume is comparable to the clinical study previously mentioned in which 2-10 mL of a mometasone gel was applied in post-operative CRS patients and no adverse effects related to this treatment were reported [168].

The anticipated human dose was scaled for the pilot rabbit study using FDA guidance for Human Equivalent Dose, which specify that a rabbit dose should be 3.1 times a human dose (in mg/kg). Using the assumptions of dosing 400 µg/day to a 60 kg human, the equivalent dose for a 3 kg rabbit is 62 µg/day. To achieve this dosing, 0.4 mL of TEMPS was injected bilaterally. This dosing volume was compared to a model of the rabbit nasal passage, which described the sinuses as a "lateral recess" with a volume of 1029 mm^3 on each side [174]. Therefore, the scaled dose was less than half of the rabbit sinus volume.

Another safety consideration for applying TEMPS is the material's cytocompatibility, which was evaluated using human SNECs derived from a squamous cell carcinoma of the nasal septum (RPMI 2650). While characterization of this cell line has reported several biologic differences from the primary nasal epithelium, it is the only alternative to human nasal epithelial

cells (hNECs) [175]. In previous work, RPMI 2650 cells and hNECs were both used for compatibility testing of mucoadhesive and nanostructured microparticles that were developed for experimental treatment of nasal polyps. The delivery vehicle was shown to be compatible with similar trends in viability between the two cell types [131]. Likewise, RPMI 2650 cells that were incubated with PEG-pNIPAAm gel for 24 hours showed comparable viability to control cells. Furthermore, these results are consistent with reported cytocompatibility of pNIPAAm gels with human conjunctival epithelial cells [79,163], as well as the numerous biomedical applications that have safely applied PEG-pNIPAAm hydrogels for *in vivo* testing [163,176].

The *in vivo* safety and retention of TEMPS was evaluated in a CRS disease model in rabbits [166]. Rabbits are frequently used for sinusitis studies because their sinus anatomy and immune response are more similar to humans than rodents [177]. However, as is the case in humans, rabbit sinuses are not accessible through the nares without surgically removing bone. For this pilot study, blank vehicle TEMPS (v-TEMPS) and mometasone-loaded TEMPS (m-TEMPS) were percutaneously injected into the left and right maxillary sinuses because the material is flowable at ambient temperatures. Recovery of the gelled material was demonstrated in one subject post-mortem, showing that the system was maintained for at least 4 weeks. During those 4 weeks, IOP was monitored, and subjects treated with sustained, local steroid from m-TEMPS did not show elevated pressures compared to baseline or the control groups. Additionally, pressures across treatment groups and time remained within the range previously reported for healthy New Zealand rabbits [167]. This is relevant to the safety of high-dose and long-term steroid use, which can pose the risk of elevated IOP and adverse ocular effects, particularly for oral or inhaled corticosteroids [40]. Treatment with the intranasal corticosteroid mometasone furoate, however, has shown no

significant differences in IOP following topical delivery via nasal sprays [178,179], stents [123], and as shown in this study, TEMPS.

Delivery of intranasal corticosteroids is intended to reduce inflammation, which can be non-invasively monitored by CT imaging. In clinical settings, CT is the gold standard imaging modality for the diagnosis of CRS and for pre-operative assessment of the extent and location of disease [24,31]. Paranasal sinus inflammation will present on CT imaging as opacification, which is then scored using various staging systems [180]. While scoring systems have been adapted for microCT imaging of disease in rabbit models [166,181,182], we reported opacification as the CT # instead, which is a measurement of the attenuation number of the x-ray beams through the tissue of interest [183,184]. To our knowledge, the presented method for assessing rabbit sinus opacification by reporting the median CT # of a region encompassing the sinuses is new to the field. The advantage of this method is that it allows for objective, blinded measurements that can be performed without prior training on assessing rabbit microCT scans and could be reproducible across investigators and institutions.

In this study, the efficacy of TEMPS was measured by microCT imaging at 4 timepoints and by histopathology analysis at the conclusion of the study. Comparison of the CT # between the TEMPS groups revealed that treatment with m-TEMPS resulted in significantly lower sinus opacification compared to v-TEMPS at 2- and 4-weeks after application. This trend of the presence of inflammation in the v-TEMPS but not the m-TEMPS group was also observed in histopathology analyses, specifically in damage to the ciliated epithelium, submucosal gland inflammation, and presence of granulocytes. Taken together, these results suggest that m-TEMPS was able to provide sustained, local release of mometasone *in vivo*, particularly because without a sustained release mechanism, the half-life of mometasone furoate is just 5.8 hours [185]. Furthermore, evidence that

TEMPS could be maintained in the rabbit maxillary sinus was observed 4 weeks after a single application. For comparison, in the clinical study that was previously mentioned, application of a mometasone gel that did not provide sustained release resulted in only temporary improvement of the diseased mucosa [168]. Notably, these observations of the efficacy of m-TEMPS were made on the control (right) sinus, rather than the disease-induced (left) sinus. The differences between the two sides are likely caused by the variability of disease induction, which is a limitation of this study. While this obstruction-based CRS disease model has been shown to induce persistent unilateral inflammation [166], in this study, changes in CT # from baseline to the disease state were inconsistent. Due to this variability and the small sample size, the effect of m-TEMPS to reduce inflammation caused by sinus obstruction could not be evaluated. In our published correspondence and replies with colleagues [186–188], we have gained further insight for this model, specifically to perform microCT measurements at the acute disease state to screen for successful disease induction, as well as carefully removing the obstructing sponge without clearing all purulent mucus in order to maintain the sinuses in hypoxic conditions. These modifications to the experimental design for inducing CRS are expected to increase the success rate in future studies.

Another limitation of the pilot rabbit study is that the application of TEMPS by percutaneous injection may have caused iatrogenic trauma. Notably, on the control side, this inflammatory trauma was reduced by the sustained release of mometasone from m-TEMPS compared to the blank vehicle, v-TEMPS. However, on the disease-induced side, there may have been an interacting effect of the ostial obstruction and TEMPS injection that limited the anti-inflammatory efficacy of m-TEMPS. In future studies, a different method for TEMPS application will be investigated to confirm safety and efficacy in preclinical studies. Although external

approaches for surgically disrupting rabbit sinonasal mucosa or implanting devices exist, these methods likely cause damage that is not representative of sinusitis [177]. Notably, in a clinical setting, TEMPS is intended to be applied transnasally following endoscopic surgery, which we propose would be a more suitable method for application in rabbits as well and is discussed as future work in Section 6.1.

Another consideration for the efficacy of *in vivo* drug delivery is the pharmacokinetics (PK), however, in the case of local delivery of mometasone furoate, a PK study for TEMPS would be particularly non-trivial given the tissue microenvironment and the drug stability. Traditionally, drug concentration can be measured non-invasively by collecting blood samples. However, plasma concentrations of mometasone are expected to be near or below limits of quantification because mometasone has <0.1% systemic bioavailability [40] due to its degradation at pH > 0.4 [189], which remains a notable benefit of the safety of this intranasal corticosteroid. As TEMPS is intended to locally deliver mometasone to the sinuses, a PK study would require serial sacrifice and tissue harvest in order to measure drug concentration in the sinus tissue or recovering the material from rabbit sinuses to measure the drug content that is remaining as a function of time. Although several studies suggest that release into surrounding tissue from implanted or injected PLGA MSs can be considerably faster than what is measured *in vitro* (likely due to accelerated hydrolysis caused by a dramatic increase in water content *in vivo* compared to *in vitro* [190]), this is not expected for TEMPS. With TEMPS, rather, the MSs are surrounded by the non-biodegradable pNIPAAm gel, which above the LCST, is in a collapsed, hydrophobic configuration both when applied to the sinus epithelium *in vivo* and when the material is incubated *in vitro*. Accordingly, the rate of hydrolysis (and therefore drug release kinetics) is expected to be similar

in vivo as to what has been demonstrated *in vitro* because the surrounding pNIPAAm gel is controlling the water content accessible to the PLGA MSs.

This pilot rabbit study established that TEMPS is a viable sinonasal delivery system that provides local and sustained release of a corticosteroid. *In vitro* characterization has demonstrated 30 days of drug release, cytocompatibility, and reversible gelation at the temperature of the sinuses. The *in vivo* study has demonstrated preliminary safety and efficacy. A patent application for TEMPS was filed on June 8, 2021 (PCT/US2021/036428), titled "Thermogel Sustained-Release Microparticle-Based Delivery to a Paranasal and/or Nasal Cavity". In the following chapter, the delivery capabilities of TEMPS are explored further as well as its tissue compatibility.

4.0 Compatibility and Versatility of TEMPS for Promoting Sinonasal Cilia Regeneration

4.1 Introduction

Inflammation that is characteristic of CRS can result in barrier dysfunction with loss of sinonasal epithelium integrity. In particular, this damage can disrupt critical innate defenses of the upper airways, such as mucociliary clearance (MCC). CRS patients often present with dysfunctional or missing cilia. As a result, inflammatory stimuli are ineffectively cleared [17,191,192]. As described previously in Section 1.1.2, in a homeostatic state, cilia drive the removal of mucus with trapped debris and microbes. Healthy human nasal cilia have a cilia beat frequency (CBF) of 9–15 Hz, resulting in mucus turnover approximately every 20 minutes [9,17]. However, in CRS patients, cilia loss and the resulting impaired MCC can result in longer residence times of potentially inflammatory triggers that can perpetuate the diseased state.

While the current clinical goal for the management of CRS is to control inflammation using broad and non-specific anti-inflammatory regimens, methods to promote mucosal healing, especially following FESS, would be beneficial. Post-operative success is contingent on the long-term maintenance of sinus patency and healing of the ciliated epithelium, for which vitamin A (VA) and its active metabolites, retinoids, have been investigated. Several studies have shown that the retinoid, retinoic acid (RA), can promote the regeneration of healthy cilia in rabbits [193–196]; however, the effects appeared to be temporary following a single topical application of aqueous RA gel [196]. In a clinical study, weekly application of a topical VA gel in post-operative CRS patients resulted in improved sinonasal wound healing [197]. Although these studies have shown

promising efficacy of RA or VA, the results have either been transient or required repetitive dosing.

In this chapter, the development of TEMPS for the sustained release of RA is presented (Figure 22A). Additionally, *ex vivo* compatibility of TEMPS with ciliated epithelial cells is evaluated (Figure 22B) as TEMPS is intended to be maintained in apposition with the sinonasal epithelium for extended durations.

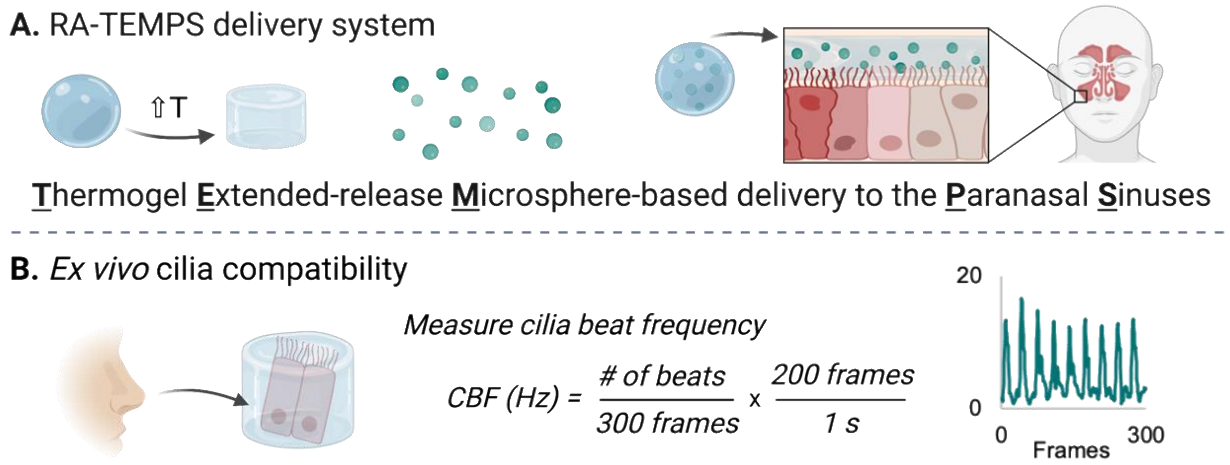

Figure 22. Illustration of RA-TEMPS Delivery System and Compatibility Testing. (A) RA-TEMPS is composed of a thermoresponsive hydrogel and RA-loaded PLGA microspheres for application along the sinonasal epithelium. (B) *Ex vivo* cilia testing consisted of collecting human nasal epithelium from the inferior turbinate, incubating the tissue samples in media or thermogel, and measuring CBF.

4.2 Materials & Methods

4.2.1 Thermogel Fabrication:

The thermoresponsive hydrogel was prepared as described in Section 3.2.2. Briefly, PEG, (200 Da) and NIPAAm were combined, and aqueous free radical polymerization was initiated by the addition of APS and TEMED. The resulting thermogel was washed with warm water and stored at room temperature.

4.2.2 Microsphere Fabrication

Table 4. Properties of PLGA Used to Fabricate RA MSs

PLGA	Molecular weight (Da)	Viscosity (dL/g)	LA:GA	End-group
RG 504H	38,000 – 54,000	0.45 – 0.60	50:50	acid
RG 505	54,000 – 69,000	0.61 – 0.74	50:50	ester
RG 755	50,000 – 75,000	0.50 – 0.70	75:25	ester

PLGA MSs were fabricated using a single emulsion-solvent evaporation procedure (depicted in Figure 12) with various PLGA (Sigma-Aldrich) listed in Table 4. PLGA (200 mg) was dissolved in dichloromethane (4 mL) creating the oil phase. All-trans-Retinoic Acid (RA) solubilized in dimethyl sulfoxide (DMSO) was added to the oil phase at 0.2%–5.0% (w/w). The oil phase was homogenized (Silverson L4RT-A, East Longmeadow, MA) in 2% poly(vinyl alcohol) (PVA, MW ~25 kDa, 98% hydrolyzed, PolySciences, Warrington, PA) (60 mL) at 3000–6000 rpm for 1 min. The emulsion was then mixed with 1% PVA (80 mL) and stirred at 600 rpm for 3 h for solvent evaporation. Microspheres were collected, washed 4x with MilliQ water, flash-frozen with liquid nitrogen, and lyophilized (VirTis Benchtop K freeze dryer, Gardiner, NY

operated at 100 mTorr) for 48 h before storage at -20 °C. During MS fabrication, exposure to UV light was minimized.

4.2.3 RA MS and RA-TEMPS Characterization

Microspheres were characterized for size, morphology, drug loading, and release kinetics. The size distribution of RA MSs was measured by volume impedance using a Beckman Coulter Counter (Multisizer-3, Beckman Coulter, Fullerton, CA). Microsphere shape and surface morphology were examined using scanning electronic microscopy (SEM) (JEOL, JSM-6330F, Peabody, MA). The encapsulation efficiency and drug loading were determined by dissolving MSs (5 mg) in DMSO (4 mL) and measuring the absorbance via UV-Vis spectrophotometry at 358 nm. *In vitro* release kinetics of the RA-loaded MSs were evaluated using methods adapted from previous work [157]. Briefly, MSs (10 mg) were incubated in 2% sodium deoxycholate (1 mL) on a roto-shaker at 37 °C in opaque microcentrifuge tubes. At regular time intervals, the supernatant was collected, diluted in methanol (3:1 v/v of methanol/supernatant), and the absorbance was analyzed via UV-Vis spectrophotometry at 338 nm. Release assays of RA-TEMPS were preformed using the same procedure with the exception that the MSs were suspended in thermogel (100 μL).

4.2.4 Gelation Temperature

The sol-gel transition of the thermogel and RA-TEMPS were evaluated using a heated water bath. Samples in glass vials were submerged in water that was gradually warmed from

ambient temperature to 37 °C. The temperature at which the clear liquid became an opaque gel was recorded as the gelation temperature.

4.2.5 Bioactivity Assay

Bioactivity of RA released from MSs after 7 days of *in vitro* incubation was measured using a Human Retinoic Acid Receptor Alpha (RARα) Reporter Assay (Indigo Biosciences, State College, PA). Release samples and a RA solution prepared the day of the assay (n = 3 per dilution) were incubated with the engineered cells following the vendor protocol and the induced luciferase expression was quantified to indicate the presence of bioactive drug.

4.2.6 Sinonasal Epithelial Cell Testing

RA concentrations were screened using SNECs, RPMI 2650. The cells were cultured in 96-well plates at 20,000 cells per well in EMEM supplemented with 10% FBS. On days 0–5, the medium was exchanged with fresh medium containing 0–10^{-5} mg/mL RA (n = 6–8). On the first, fourth, and sixth day after RA treatment, the relative cell concentration/cellular viability was measured using 10% PrestoBlue® viability reagent (ThermoFisher Scientific, Waltham, MA). After ~3 h incubation, reduction of the PrestoBlue reagent was measured by fluorescence readings at 540 nm/580 nm excitation/emission filters. The fluorescence values were normalized to the positive control, and a negative control (cells lysed with 2.5% TritonX) was included for comparison.

The growth and viability of SNECs treated with control medium (with 0.01% DMSO (v/v)), medium with blank MS (3 mg/mL), RA MS (3 mg/mL), or soluble RA (10^{-3} mg/mL, 0.01%

DMSO) was measured. Cells were seeded in 12-well plates at 200,000 cells per well in EMEM with 10% FBS. The next day, media were replaced with the 4 conditions (n = 3 per condition) and on the subsequent days, half of the medium volume was exchanged (control medium was used for the blank and RA MS conditions). On the first, fourth and seventh day, cells were harvested with trypsin and counted using trypan blue exclusion for viability assessment.

4.2.7 Cilia Compatibility Testing

The study protocol for collecting healthy nasal epithelial tissue was approved by the University of Pittsburgh Institutional Review Board (STUDY19080087 Healthy Control Comparator Biobank). Following informed consent, samples were collected as described by Zahid *et al* [198]. Briefly, the inferior turbinate on the left and right sides were brushed with a nasal curette to obtain ciliated nasal epithelial samples, which were stored in Leibovitz's L15 medium (ThermoFisher Scientific, Waltham, MA). Each sample was divided, such that half was incubated in medium for a paired control and half was incubated in the thermogel (Figure 22B). Samples were added to tubes containing thermogel so that the tissue would sink and become submerged within the thermogel (which was visually confirmed) while being incubated at 37 °C for the specified duration. Cilia motility of the control and thermogel-exposed cells were evaluated by high-speed video-microscopy using an inverted, high-speed microscope with 100x oil objective. Video-microscopy was performed at room temperature, so the thermogel was in a clear, liquid state and did not obstruct the imaging. Movies were recorded at 200 frames/s at room temperature using a Phantom x4.2 camera (Vision Research, NJ) or Pixelink M5 camera (Pixelink, Ontario, Canada). Analysis of CBF was performed on 9 ciliated cells per condition using an ImageJ macro [198].

The nasal epithelial samples were expanded and re-ciliated *in vitro* for further compatibility testing using previously described methods [198]. Cells were seeded on 6-well plates coated with 1.5 mL of 0.7 mg/mL rat-tail collagen I (Corning, Corning, NY). Media for the stationary culture phase consisted of Dulbecco's Modified Eagle Medium/Nutrient Mixture F-12 (DMEM/F12, ThermoFisher Scientific) supplemented with 2% UltroserG (Pall Life Sciences, Port Washington, NY) and 2% antibiotic-antimycotic (ThermoFisher Scientific). Media was exchanged three times each week and after 3 weeks, confluent epithelial cells were harvested with 200 IU/mL collagenase type IV (Worthington Biochemical Corporation, Lakewood, NJ). The collected cells were washed by centrifugation three times and seeded in 5 mL non-vented culture flasks in suspension media. Suspension media consisted of DMEM/F12 medium supplemented with 10% Nu-Serum™ IV (Corning) and 2% antibiotic-antimycotic. Cells were cultured for 8 days in continuous rotation at 80 rpm and 37 °C without changing the media. The re-ciliated cells were divided such that half was incubated in medium and half in thermogel for 24 hours and CBF was measured.

4.2.8 Statistical Analysis

SAS JMP® Pro 14 (Cary, NC) and GraphPad Prism v7 (San Diego, CA) were used to perform statistical analyses. Descriptive statistics were used to describe the mean and standard deviations (S.D.) and values are reported as the mean ± S.D., unless specified otherwise. For the *in vitro* bioactivity assay, EC50 values and 95% confidence intervals (CI) were determined by nonlinear 3- or 4-parameter logistic regression using GraphPad. Using JMP, comparisons among groups with continuous data were performed by one-way ANOVA. After assessing the variances by Levene's test, Wilcoxon Method (unequal variance) or Tukey (equal variance) post-hoc testing was performed. For all analyses, $p < 0.050$ was considered as significant.

4.3 Results

4.3.1 Development of Microspheres for Sustained Release of Bioactive RA

Microsphere fabrication parameters, including the weight of retinoic acid, properties of PLGA, and homogenization speed (Table 5), were varied to engineer RA-loaded MSs that produced sustained *in vitro* release for at least 30 days. The release kinetics and MS morphology were found to be influenced by the weight of RA added during fabrication. MSs with 5.0% (w/w) RA had a non-spherical morphology (Figure 23A) and exhibited a burst release of 70% of the encapsulated drug in the first 24 h (Figure 23D). In contrast, MSs loaded with 1.0% or 0.2% RA had a smooth, spherical morphology (Figure 23B,C), smaller average diameter (Table 5), and a reduced burst release of 60% or 45% after 24 h, respectively (Figure 23D). Release of RA from MSs fabricated with RG 504H PLGA was sustained for <14 days and, therefore, PLGA with higher lactic acid content (RG 755) or larger molecular weight (RG 505) was investigated to extend the release duration. (PLGA properties are summarized in Table 4.) It was found that RG 755 MSs released RA for at least 30 days (Figure 23E). When fabricated at a greater homogenization speed (4500 rpm or 6000 rpm), the resulting smaller MSs exhibited a faster release rate due to the higher surface area-to-volume ratio, while larger MSs (homogenized at 3000 rpm) released more slowly with a lag phase that began in the 2nd week and continued for >2 weeks. Because this extended lag phase was not desired, the remaining release profile was not measured. In contrast, RG 505 MSs with 0.5% RA exhibited a triphasic release profile over 35 days. In the first 7 days, 40% of the encapsulated drug was released, followed by a lag phase for 14 days, and a final release from day 27–35 (Figure 23F). Notably, when the loading of RG 505 MSs was increased to 1.0% RA, a large burst release (~95%) occurred in the first 24 h, which was not observed in RG 755 MSs loaded

with 1.0% RA (Figure 23E). These results suggest an interaction between the weight of RA and the PLGA properties, which, along with the homogenization speed, are critical parameters that can be adjusted to tune the release profile of retinoic acid.

Table 5. RA MS Fabrication Parameters, Size, Loading, and Encapsulation Efficiency

PLGA	RA weight (w/w)	Homogenization Speed (rpm)	MS Diameter (μm)	RA Loading (μg/mg)	Encapsulation Efficiency (%)
RG 504H	5.0%	5000	11.2 ± 5.1	53.7	107
	1.0%	5000	7.3 ± 2.3	9.4	94
	0.2%	5000	6.6 ± 2.1	1.5	76
RG 755	0.5%	3000	24.3 ± 7.0	4.0	79
	1.0%	3000	18.5 ± 5.4	7.4	74
	1.0%	4500	9.5 ± 3.1	8.8	78
	1.0%	6000	9.1 ± 5.0	5.9	59
RG 505	0.5%	3000	20.0 ± 6.2	3.4	68
	1.0%	3000	20.4 ± 7.7	8.3	83

In addition to sustaining release, the RA MSs should release drug that maintains its bioactivity. Using an engineered RARα reporter cell line, the bioactivity of cumulative RA released from MSs (RG 755, 1.0% RA, 6000 rpm) after 7 days of aqueous incubation had an EC50 of 0.7 nM with 95% CI of 0.2 nM and 1.7 nM (Figure 23G). Bioactivity of the released RA was similar to RA that was reconstituted the day of the assay (“Drug Control”; EC50 = 1.4 nM with 95% CI of 0.7 nM and 2.7 nM).

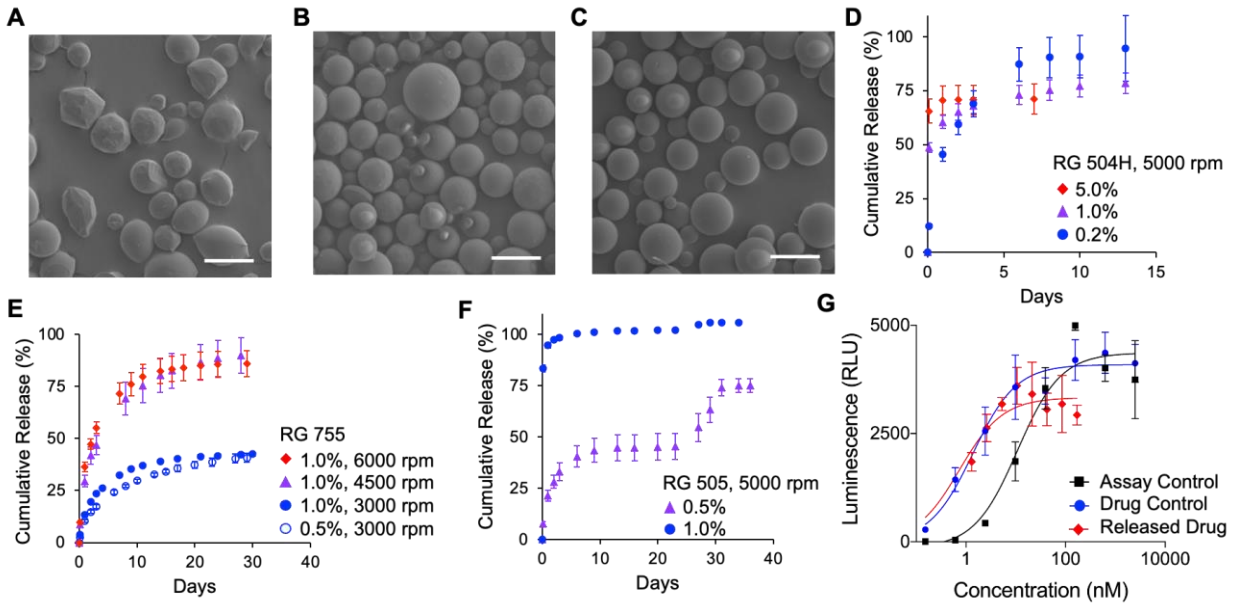

Figure 23. *In vitro* Characterization of RA MS Formulations.(A–D) MS morphology and release kinetics were affected by the weight of RA. (A–C) SEM images of MSs fabricated with RG 504H PLGA and loaded with (A) 5.0%, (B) 1.0%, and (C) 0.2% (w/w) RA (scale bar = 10 μm) and (D) the corresponding cumulative release profiles. (E) Using PLGA with a higher lactic acid content (RG 755) or (F) larger molecular weight (RG 505) extended the release profile with kinetics further controlled by the weight of RA or homogenization speed. (G) Bioactivity of cumulative RA released from MSs (RG 755, 1.0% RA, 6000 rpm) after 7 days was comparable to RA reconstituted the day of the assay ("Drug Control") (D–G) Error bars represent the mean ± S.D. (n = 3).

4.3.2 Drug Release and Gelation of RA-TEMPS

Microspheres formulated with RG 505 PLGA and 0.5% RA were selected for further characterization in combination with thermogel, creating RA-TEMPS. The cumulative release profile of RA from TEMPS (Figure 24A) was similar to the profile for MSs alone (Figure 23F, "0.5%") with ~1.1 μg RA per mg MS (35%) released in the first 8 days and ~2.3 μg RA per mg MS (68%) after 36 days. RA-TEMPS was also shown to undergo a reversible sol-gel transition at

33 °C, which was consistent with the thermogel alone (Figure 24B) as well as prior characterization of this thermogel formulation with and without microspheres [79,163]. Furthermore, this sol-gel transition temperature is consistent the approximate temperature of the sinuses [13].

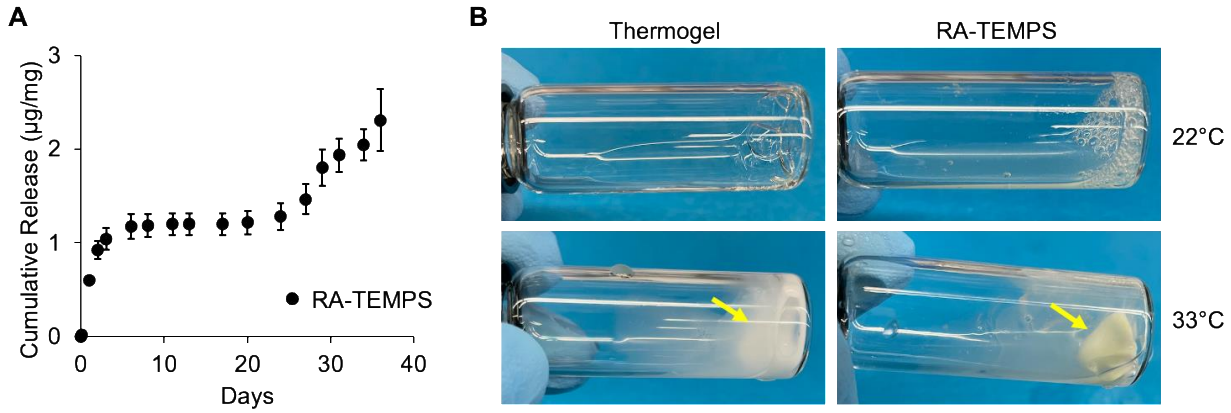

Figure 24. Release Kinetics and Gelation of RA-TEMPS are Consistent with RA MS and Thermogel Alone

(A) Cumulative release of RA (error bars represent mean ± S.D., n = 3) and (B) gelation of the thermogel alone and RA-TEMPS at 33 °C, indicated by the yellow arrows.

4.3.3 Cilia Maintain Motility after Incubation with Thermogel

Along with designing the sustained release of RA to promote cilia regeneration, the delivery system should be compatible with ciliated tissue. Accordingly, ciliated nasal epithelium collected from healthy volunteers was incubated *ex vivo* in thermogel or medium (control) and assessed by measuring changes in CBF (Figure 25A). CBF results were normalized to the paired control (Figure 25B) and it was observed that a short duration of incubation in thermogel (18–25 min) did not significantly affect CBF while incubation for 40–50 min or 2 h did demonstrate a significant change in CBF ($p < 0.05$). Notably, 2 re-ciliated samples that were incubated in

thermogel for 24 h showed no significant differences in CBF from the control. Overall, the *ex vivo* cilia samples remained motile after direct incubation in thermogel.

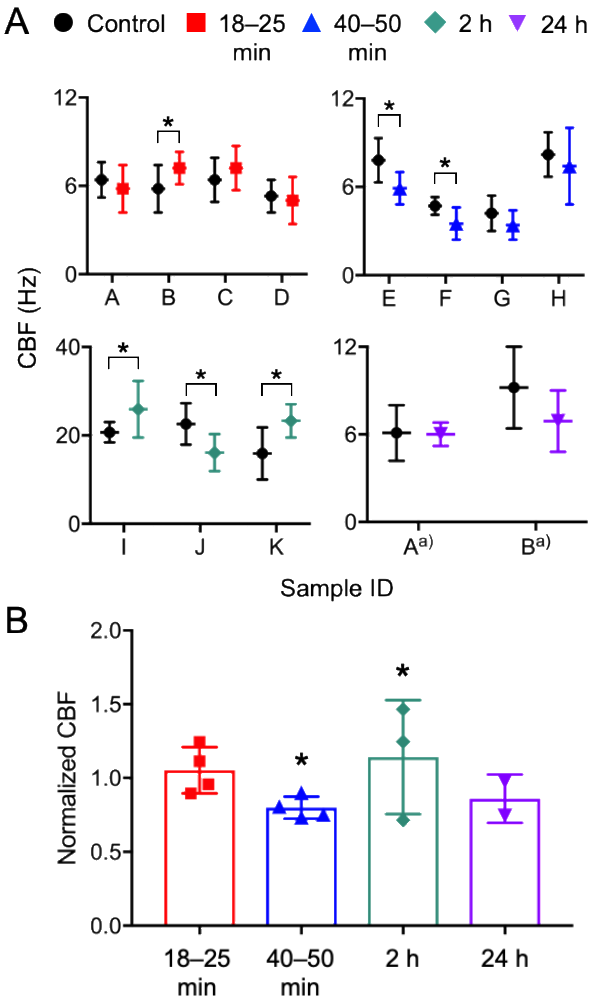

Figure 25. Human Nasal Epithelium Incubated in Thermogel Maintained Cilia Motility.

(A) CBF measurements (mean ± S.D., n = 9) for paired nasal epithelial samples incubated in medium (control) or thermogel. Statistical significance was determined by Student's t-test or Wilcoxon/Kruskal-Wallis test, *p < 0.05. a) Samples were expanded and re-ciliated before thermogel incubation. (B) Normalized CBF results (to paired control). Error bars represent the mean ± S.D. for samples incubated for 18–25 min (n = 4), 40–50 min (n = 4), 2 h (n = 3), and 24 h (n = 2). Statistical significance was determined by one-way ANOVA with post-hoc comparison to control conditions, *p < 0.05.

4.3.4 *In vitro,* Preclinical, and Clinical Dosing Considerations for RA-TEMPS

In addition to evaluating compatibility of the thermogel component of RA-TEMPS, the effects of dosing soluble RA or RA MSs were explored using SNECs. Treating SNECs with soluble RA revealed a concentration- and time-dependent effect. At the highest dose tested (10^{-1} mg/mL, which was 10-fold higher than the gel tested in rabbits [195]), cytotoxicity was observed after the first day of treatment (Figure 26A). When the dose was decreased to 10^{-2} mg/mL (consistent with the rabbit study), cellular toxicity was observed by the 6th consecutive day of treatment. Daily dosing of RA at 10^{-3} to 10^{-5} mg/mL did not exhibit cytotoxicity, although a decrease in PrestoBlue reduction (which measures metabolic activity) was observed over time. The decrease in PrestoBlue reduction does not appear to be caused by a change in proliferation as SNEC growth was comparable when cells were treated daily with media containing 10^{-3} mg/mL soluble RA in 0.01% (v/v) DMSO or control medium (containing 0.01% DMSO) (Figure 26B). Additionally, the presence of RA-loaded or blank MSs at 3 mg/mL did not affect SNEC proliferation. At this MS concentration, the daily concentration of released RA (based on the release profile in Figure 23F, "0.5%") is anticipated to be ~10^{-3} mg/mL RA per day (or ~10^{-4} mg RA per mg MSs per day). Along with comparable growth between the control, soluble RA, blank MS, and RA MS conditions, SNEC viability remained >94% (Figure 26C).

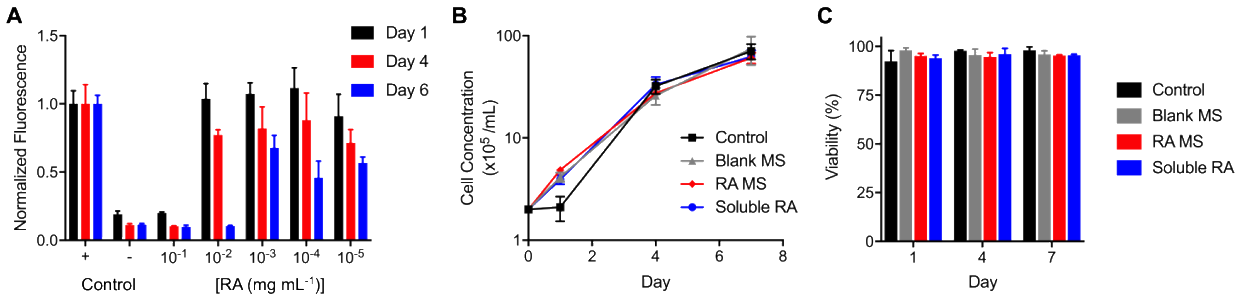

Figure 26. Growth and Viability of SNECs Treated with Soluble RA or RA MSs.

(A) Soluble RA treatment caused concentration- and time-dependent cytotoxicity to SNECs (n = 6–8). (B) Growth curve and (C) viability of SNECs treated with control media (0.01% DMSO (v/v)), Blank MS (3 mg/mL), RA-MS (3 mg/mL), or daily soluble RA (10^{-3} mg/mL, 0.01% DMSO) (n = 3).

The observed SNEC toxicity could be helpful in determining suitable concentrations for further *in vitro* testing of RA-TEMPS, as well as the prospective dosing for preclinical and clinical studies, which were estimated from studies evaluating aqueous gels. In the study evaluating a VA gel in CRS patients, 5000 IU/g was applied weekly [197]. The concentration of VA can be converted to retinol activity equivalents (RAE), where 1 IU VA is equal to 0.3 μg RAE. If it is assumed that ~2 g of gel was applied for each dose (to a 60 kg patient), the corresponding estimated daily amount of RA should be 0.050 mg/kg. This clinical dose could be achieved with RA-TEMPS by administering ~10^3 mg MS formulated with RG 505 PLGA and 0.5% RA (Table 6). The RA MSs would then be mixed in 5–10 mL of thermogel, the recommended volume of TEMPS for clinical studies [157]. To convert from a clinical to a preclinical dose appropriate for rabbits, the FDA guidance for a Human Equivalent Dose (HED) is to multiply the human dose (in mg/kg) by a factor of 3.1. Therefore, the amount of RA administered to a 3 kg rabbit would be 0.155 mg/kg, which would be achieved by administering TEMPS containing ~10^2 mg RA MS in ~0.4 mL thermogel [157]. Alternatively, a preclinical dose of RA-TEMPS could be inferred from the rabbit

studies in which a bolus of 0.01% RA gel was administered [195]. Assuming ~1 mL of gel was instilled in the rabbit sinuses, the corresponding dose of RA would be 0.033 mg/kg, which would be achieved with ~10 mg RA MS in TEMPS. The converted HED for a clinical study would be ~10^2 mg RA MS in thermogel (Table 6). The 10-fold range in these prospective preclinical and clinical doses of RA-TEMPS is a result of the differences in study designs, specifically that the VA gel was applied weekly while the RA gel was a single bolus that demonstrated efficacy 2 weeks later. Further *in vitro* functional testing followed by *in vivo* dosing studies should be performed to determine the optimal RA dosing and timeframe to promote robust regeneration of the ciliated epithelium. Importantly, both the concentration and duration of RA treatment can be finely tuned using RA-TEMPS by adjusting the amount of MSs embedded in thermogel as well as the MS release profile.

Table 6. Prospective Preclinical and Clinical Dosing of RA-TEMPS

Reference Dose	Amount of RA (mg/kg)		Corresponding dose of RA-TEMPS		Comments
	Human	Rabbit	Human	Rabbit	
5000 IU/g VA gel, weekly [197]	0.050	0.155	~103 mg MS in 5–10 mL thermogel	~102 mg MS in 0.4 mL thermogel	1 IU VA = 0.3 μg RAE Assumed patients were administered 2 g of VA gel Assumed a 60 kg human and 3 kg rabbit
0.01% RA gel, bolus [195]	0.011	0.033	~102 mg MS in 5–10 mL thermogel	~10 mg MS in 0.4 mL thermogel	Assumed rabbits were administered 1 mL RA gel Assumed a 60 kg human and 3 kg rabbit

RA = retinoic acid, VA = vitamin A, RAE = retinol activity equivalents

4.4 Discussion

TEMPS was engineered to provide sustained release of RA, which has been shown to promote regeneration of ciliated sinonasal mucosa [193–197]. Retinoids, which are derivatives of VA, along with VA, are in fact necessary for the maintenance of normal airway epithelium. Studies from the 1980's in VA-deficient hamsters revealed squamous metaplasia of the airway epithelium as a result of the vitamin deficiency, which could be reversed to normal pseudostratified ciliated epithelium by supplemental VA [199,200]. While VA was orally administered in these early models, more recent work has investigated the application of topical aqueous RA or VA gels for promoting sinonasal mucosal regeneration. Following a single application of RA gel to surgically stripped rabbit mucosa, qualitative improvements in mucosal and ciliary regeneration were observed 14 days later [193], as well as significantly improved cilia density, alignment, and uniformity [195]. Temporary functional improvement of the regenerated cilia was also observed [196]. At 2 weeks post-application, the *ex vivo* CBF of stripped and treated tissue was consistent with unoperated controls, however, the normalizing effect did not persist out to 4 weeks. In a clinical study evaluating the weekly application of topical VA gel for 2 months, post-operative scarring and adhesions were significantly reduced with evidence of healthy cilia and maintenance of the antrostomy size out to 12 months [197]. These preclinical and clinical studies suggest that while RA or VA can promote healing and regeneration of healthy sinonasal mucosa, they must be applied over an extended duration for a robust therapeutic effect. Thus, a controlled release formulation would be beneficial for both efficacy and patient adherence. As a result, we designed RA-TEMPS to release RA for at least 30 days in a delivery system that is compatible for direct contact with the sinonasal epithelium.

Herein, various PLGA MS formulations demonstrated controlled release of RA varying from less than 7 days to greater than 5 weeks. Notably, increasing the weight of RA was found to increase the burst release, which has been observed for other small molecules and protein drugs [173]. Furthermore, the magnitude of the initial burst varied with the properties of PLGA. These findings suggest that there is a limitation to the amount of RA that can be effectively dispersed throughout the polymeric matrix where the burst release could be a result of drug accumulation at the outer surface or that the percolation threshold was exceeded [201]. Others have observed a similar burst release of greater than 50% of the encapsulated RA in the first 24 h [202], as well as irregular MS morphology with higher amounts of RA [203]. In order to achieve release extending beyond 2 weeks, we found that formulating MSs with 50,000–75,000 MW, 75:25 (lactic acid to glycolic acid) PLGA (75:25 PLGA) or 54,000–69,000 MW, 50:50 PLGA (50:50 PLGA) was necessary. The release profiles for these two formulations were extended to at least 30 days, but with varied kinetics. Approximately 70% of the encapsulated drug was released in the first week from 75:25 PLGA MSs with an additional 10% releasing over the subsequent 3 weeks. This formulation, which was fabricated with 1.0% RA, did not exhibit a significant burst release in comparison to loading the same amount of RA in 50:50 PLGA MSs. By decreasing the amount of RA to 0.5%, the resulting 50:50 PLGA MSs exhibited a triphasic release profile in which ~40% of the encapsulated drug was released in the first week and another ~30% in week 4–5. Other fabrication parameters that have been shown to affect RA release from PLGA MSs include the surfactant MW, type of solvent, and the weight of polymer [203], and these could be explored if further tuning of release kinetics was desired.

In addition to providing sustained RA release, a mechanism to localize the MSs in apposition to the sinonasal mucosa is essential to prevent their rapid removal by mucociliary

clearance. Accordingly, the MSs were embedded in thermogel, creating TEMPS, which can be retained in rabbit sinuses for at least 1 month [157]. Importantly, the release kinetics and gelation temperature of the MSs and thermogel, respectively, were not altered when the RA-loaded MSs were combined with the gel. A thermoresponsive hydrogel is proposed to be well-suited for application along the sinonasal mucosa because the system will gel and conform upon contact with the warm tissue. Furthermore, for TEMPS removal, the phase change can be reversed by ambient temperature saline irrigation (a routine adjunct treatment for CRS patients) and TEMPS can be re-applied in a clinical setting as needed.

As TEMPS is intended to be in prolonged contact with the sinonasal epithelium, its compatibility is critical to future clinical translation. Accordingly, ciliated sinonasal tissue collected from healthy volunteers was incubated in thermogel for ~20 min to 24 h *ex vivo* to assess compatibility. Others have used similar experimental designs to assess changes in CBF following exposure to nasal drugs, excipients, preservatives, and polymers for 10–20 min and then re-evaluated CBF after a 15- or 60-min washout period [204–207]. While this time-course is consistent with the rapid clearance of nasal dosage forms, in the present study, up to 24 h incubation was evaluated as the thermogel will be maintained in apposition to the sinonasal epithelium for an extended duration. To our knowledge, this is the longest *ex vivo* compatibility testing reported using human nasal epithelium samples. At most, the effects to CBF were moderate, which has been defined as 20–50% cilio-inhibition or cilio-stimulation and statistically significant [204,205]. Overall, no trend in the change in CBF with incubation time was observed, suggesting that the thermogel is compatible with ciliary function. Although this study was limited to an incubation time of 24 h, the method of directly exposing the ciliated cells to the thermogel may be more sensitive than that encountered *in vivo* where a protective mucus layer is present [205,206].

Thus, the finding that cilia motility was maintained is promising for future studies intending to determine compatibility *in vivo* over longer durations.

A limitation of the compatibility study is that the nasal tissue samples were incubated so that the thermogel was in its gelled state, but temperature was not controlled during the measurement of CBF. In addition to affecting the physical state of the thermogel, temperature is one of several factors that influences CBF [191]. Faster CBF was observed for samples that were analyzed using a different microscopy set up (Figure 25A, Sample ID I, J, and K), which was most likely because the lamp aperture had to be opened wider for suitable brightness during video recordings. Presumably, the local temperature was elevated inducing faster CBF. Because each sample was internally controlled, the different basal CBF values should not affect the conclusions regarding compatibility of the thermogel. However, the samples were not maintained at a temperature $\geq$33 °C during imaging and whether cilia remain motile while immersed in the gelled thermogel cannot be concluded at this time.

An alternative *in vitro* model for cilia testing is the air-liquid interface (ALI) model, which may be beneficial for evaluating the effects of RA to promote durable re-ciliation and is discussed as future work in Section 6.3. In particular, others have used ALI models to culture sinonasal tissue collected from CRS patients [208,209]. We attempted to culture CRS patient samples using the non-ALI model, but the samples did not expand *in vitro,* and therefore, we believe that exploring the ALI model is a worthwhile next step. These studies should be designed to optimize the concentration and duration of RA delivery. Although evaluating the ability of RA-TEMPS to promote re-ciliation was not possible at this time, the *in vitro* bioactivity of released RA suggests that it will have its intended effect. Specifically, the mechanism for RA efficacy is its binding to nuclear retinoic acid receptors, which was demonstrated using the RARα assay. Upon receptor

binding, the transcription of mucin genes and mucin secretion is activated as well as the differentiation of ciliated cells while simultaneously inhibiting squamous differentiation [209].

Characterizing the concentration effects of RA-TEMPS is a critical next step, particularly given the toxicity to SNEC that was observed at higher concentrations. This finding is consistent with a pilot rabbit study that evaluated a bolus application of 0.01% or 0.025% RA gel. Due to the observation of more normal morphology of the rabbit mucosa, the lower concentration was recommended [193]. Others have also shown concentration-dependent growth effects when treating murine and human skin fibroblasts for RA [210,211]. Toxicity concerns related to the intake of high concentrations of dietary Vitamin A, or the application of topical VA also exist [212,213]. Retinoids, however, have less adverse effects while still maintaining beneficial therapeutic properties [213]. Thus, RA-TEMPS is promising from a safety profile standpoint because it will locally deliver a retinoid at concentrations that can be precisely controlled over time.

5.0 Shelf-Stable, Ready-to-Use TEMPS for Clinical Translation

5.1 Introduction

The thermoresponsive and controlled release capabilities of TEMPS (demonstrated in Chapters 3 and 4) are critical features of the delivery system, as is its formulation, which was developed in the following studies. To formulate the initial iteration of TEMPS, the drug-loaded microspheres must be mixed with the thermogel immediately prior to administration to prevent MS erosion and PLGA degradation that would result in premature drug release. This adds an additional step in an operating room or clinic that could hinder the ease of clinical translation of TEMPS. However, if the water content were removed, TEMPS could be available as a shelf-stable, ready-to-use product.

In the pharmaceutical industry, freeze drying (or lyophilization) is a ubiquitous method for removing water content to improve the stability, storage, and shipment of bioproducts [214,215]. The freeze-drying process consists of three stages. First, during the freezing step, water separates from the solute to form a "freeze concentrate" product that contains ~20% water (w/w). Next, during primary drying, the material is subjected to low pressures while the shelf temperature increases to supply the heat removed by ice sublimation. Within a freeze dryer, a condenser acts as a heat sink such that as ice sublimes, the water vapor crystallizes on its coils or plates that are maintained at a low temperature [214]. Finally, during secondary drying, water is desorbed from the freeze concentrate as the product temperature continues to increase. The objective for this final stage is to improve product stability by removing as much residual moisture as possible; a typical residual moisture specification is <1% (w/w) [214,216].

To explore all-in-one, shelf-stable formulations of TEMPS, we created a freeze-dried TEMPS formulation ("FD-TEMPS"). In addition to enabling shelf-stability of the combined system, it is feasible that FD-TEMPS could be applied in its dried form where contact with the mucus layer that consists of ~95% water (w/w) [9] could rehydrate the material immediately prior to gelation. The thermoresponsive behavior and drug release of mometasone furoate from FD-TEMPS were developed for consistency with the original TEMPS formulation, and here, proof-of-concept experiments were performed to demonstrate *in situ* rehydration, gelation, and mucoadhesion.

5.2 Materials & Methods

5.2.1 Preparation and Freeze Drying of TEMPS

PLGA MSs encapsulating mometasone furoate were prepared as described in Section 3.2.1. Briefly, the mometasone-loaded MSs were fabricated using a single emulsion procedure in which 10 mg mometasone and 200 mg PLGA (RG503, Sigma, St. Louis, MO) were dissolved in 4 mL dichloromethane (DCM) and homogenized at 5000 rpm in 2% polyvinyl alcohol (PVA). The DCM was allowed to evaporate, and the MSs were collected, washed, freeze dried, and stored at -20 °C.

TEMPS was prepared by combining the drug-loaded MSs with the pNIPAAm-based thermoresponsive hydrogel at 100 mg/mL. The pNIPAAm gel was prepared by aqueous free radical polymerization of NIPAAm with the addition of PEG using similar methods as described in Section 3.2.2 and previously reported [79,157]. For these studies, the thermogel was prepared

with 5% pNIPAAm and 0% PEG ("pNIPAAm only"), 5.6% PEG (MW 200; "control"), or 0.4–5% PEG (MW 2,000–8,000). These thermogel compositions were labeled by the PEG weight % and PEG MW, so a thermogel consisting of 5% pNIPAAm and 1% PEG (MW 2,000) was labeled "1% PEG2000".

TEMPS or thermogel were frozen in 5 mL glass vials at -80 °C for 24 h. The vial caps were replaced with permeable Kimwipe covers and the frozen vials were transferred to a freeze dryer operating at <100 mTorr with the condenser held at -50 °C for 3 days. The freeze-dried samples were stored in a desiccator at ambient temperature for characterization.

5.2.2 Differential Scanning Calorimetry & Thermal Gravimetric Analysis

The thermal behavior of the gel formulations was evaluated using a differential scanning calorimeter (DSC; DSC250, TA Instruments, New Castle, DE). A 5–7 mg sample of each gel was loaded in an individual aluminum pan and hermetically sealed. A heat-cool-heat cycle was used as follows: isotherm at -80 °C for 3 min, ramp to 90 °C at 10 °C/min, isotherm at 90 °C for 3 min, ramp to -80 °C at 10 °C/min, isotherm at -80 °C for 3 min, and ramp to 90 °C at 10 °C/min.

The residual moisture of freeze-dried thermogel samples was measured using a thermal gravimetric analyzer (TGA; Simultaneous Thermal Analyzer STA 6000, PerkinElmer, Waltham, MA). A 5–10 mg sample of each gel was loaded in an individual ceramic pan and heated under a nitrogen atmosphere as follows: isotherm at 40 °C for 5 min, ramp at 10 °C/min to 120 °C, and isotherm at 120 °C for 30 min. The change in weight % for each thermogel sample was calculated using a baseline curve (empty ceramic pan). For comparisons among samples, the residual moisture was determined at a specified timepoint during the hold at 120 °C.

5.2.3 Scanning Electron Microscopy

Samples of MSs, thermogel, TEMPS, freeze-dried thermogel, and FD-TEMPS were visualized by scanning electron microscopy (SEM; JEOL JSM-6510LV/LGS or Zeiss SIGMA VP). Samples were mounted on studs and sputter coated at 25–30 mAmps with gold-palladium for 35–45 s.

5.2.4 Water Content & Swelling Ratio

The amount of water in the thermogel formulations was measured gravimetrically using Equation 5-1 where W_0 and W_D are the weights of the initial gel and freeze-dried gel, respectively.

Equation 5-1: Thermogel Water Content

$$Water\ content\ (\%) = \frac{W_0 - W_D}{W_0} x\ 100\ \% \quad \text{(Equation 5-1)}$$

The freeze-dried gels were rehydrated in water or simulated nasal fluid (SNF), consisting of 8.8 mg/mL NaCl, 0.6 mg/mL $CaCl_2$, and 3 mg/mL KCl in distilled water [164], for 1 h. Excess water was removed by blotting with filter paper, the gels were weighed, and the swelling ratio was calculated using Equation 5-2 where W_S is the weight of the rehydrated gel.

Equation 5-2: Thermogel Swelling Ratio

$$Swelling\ Ratio\ (\%) = \frac{W_D - W_S}{W_D} x\ 100\ \% \quad \text{(Equation 5-2)}$$

5.2.5 Gelation Temperature & Kinetics

The sol-gel phase change was observed using a heated water bath to determine the lower critical solution temperature (LCST) of the thermogel formulations. Individual glass vials containing the gels were submerged in a water bath that was gradually heated from room temperature to 37 °C. The phase change was visually observed by a change from a clear liquid to an opaque gel.

To determine the gelation kinetics, absorbance values were measured at 415 nm and a constant temperature using a UV-Vis spectrophotometer (Molecular Devices, Sunnyvale, CA). Optical transmittance was calculated using Equation 5-3 where A_{max} and A_{min} are the maximum and minimum absorbance values and A_t is the absorbance value at time *t*.

Equation 5-3: Optical Transmittance for Gelation Kinetics

$$Transmittance\ (\%) = \frac{A_{max} - A_t}{A_{max} - A_{min}} x\ 100\ \% \quad \text{(Equation 5-3)}$$

5.2.6 Drug Release & Bioactivity Characterization

The *in vitro* release profile and bioactivity of mometasone furoate were measured using methods described in Section 3.2.3. To compare the effect of freeze drying on product stability, TEMPS was prepared in its hydrated form (MS + liquid thermogel) and its freeze-dried form (MS + liquid thermogel and freeze dried) and stored under ambient conditions for several weeks. The concentration of drug in the release medium was measured over the subsequent 5 weeks and

samples were stored at -20 °C to measure bioactivity against a Human Glucocorticoid Receptor (NR3C1, GR) Reporter Assay (Indigo Biosciences, State College, PA).

5.2.7 'Drip Transfer' Assay

The mucoadhesion of thermogel, freeze-dried thermogel, TEMPS, and FD-TEMPS was evaluated using a 'drip transfer' assay on an agar and mucin surface [217]. A solution of 1% agar in phosphate buffer (pH 6) was heated to 70–80 °C, cooled to ~50 °C, and 2% mucin was added under constant mixing. The solution was poured into a glass plate to gel overnight at 4 °C. The gelled agar/mucin plates were warmed to 37 °C in an incubator and oriented at a fixed angle. Liquid (50–100 μL) or freeze-dried (1–2 mg) thermogel or TEMPS (n = 5) were added to one end of the plate and the transfer distance was measured from the starting point to the point where displacement stopped because of gelation.

5.2.8 Statistical Analyses

Statistical analyses were performed using SAS JMP® Pro 14 (Cary, NC) or GraphPad Prism v7 (San Diego, CA). Descriptive statistics were used to describe the mean and standard deviations (S.D.) and values are reported as the mean ± S.D. Comparisons among groups with continuous data were performed by one-way ANOVA using JMP. After assessing the variances by Levene's test, Wilcoxon Method (unequal variance), Tukey (equal variance), or Student's t-test (equal variance) post-hoc testing was performed. For all analyses, $p < 0.05$ was considered as significant. For the *in vitro* bioactivity assay, EC50 values and 95% confidence intervals (CI) were determined by nonlinear 3-parameter logistic regression using GraphPad.

5.3 Results

5.3.1 Determining the Thermogel Phase Transition Temperatures by DSC

Evaluation of the thermal behavior of pNIPAAm and PEG thermogel formulations revealed three or four phase transitions. The phase transitions, labeled in the example DSC curves (Figure 27A–C), indicated the presence of free water (i.e., water that is not chemically or physically associated with the polymer), and freezing bound water (i.e., the water fraction associated with the polymer matrix) [218], the sol-gel transition, and, in some samples, the glass transition temperature of the maximally freeze concentrated solution (T_g'). The melting of free water was evident by the endotherm occurring near 0 °C (Figure 27A,B #3), and the endotherm near -25 °C (Figure 27A,B #1) indicated the melting of freezing bound water. The thermal features associated with the freezing bound water fraction include considerable supercooling and reduced enthalpy, which are indicated by the lower melting temperature and smaller area under the peak compared to free water [218]. The crystallization exotherm of the freezing bound water (Figure 27C #1) appeared as a loop, which was likely an artifact of the exothermic reaction countering the rapid, continuous cooling by the DSC. Endotherms were also observed near 33 °C (Figure 27A,B #4), which is consistent with the sol-gel transition of pNIPAAm-based gels [219]. Due to the addition of the various concentrations and MW of PEG, the peaks of the sol-gel transitions varied from 31.8–32.6 °C (Figure 27D and Table 7). The fourth phase transition that represents T_g' is critical to designing a freeze-drying process because this is the temperature below which the product must be maintained during the freezing and primary drying stages to achieve an adequate lyophilized cake [220]. This transition, however, was not detected in all gel formulations. For those with a detectable T_g', it occurred at approximately -10 °C (Figure 27A,B #2). While there was no

T_g' detected for the control gel, a broad transition that spanned more than 7 °C was detected for pure pNIPAAm. In contrast, a well-defined T_g' was detected for the 5% PEG2000 gel (Figure 27E). Values for T_g' are summarized in Table 7.

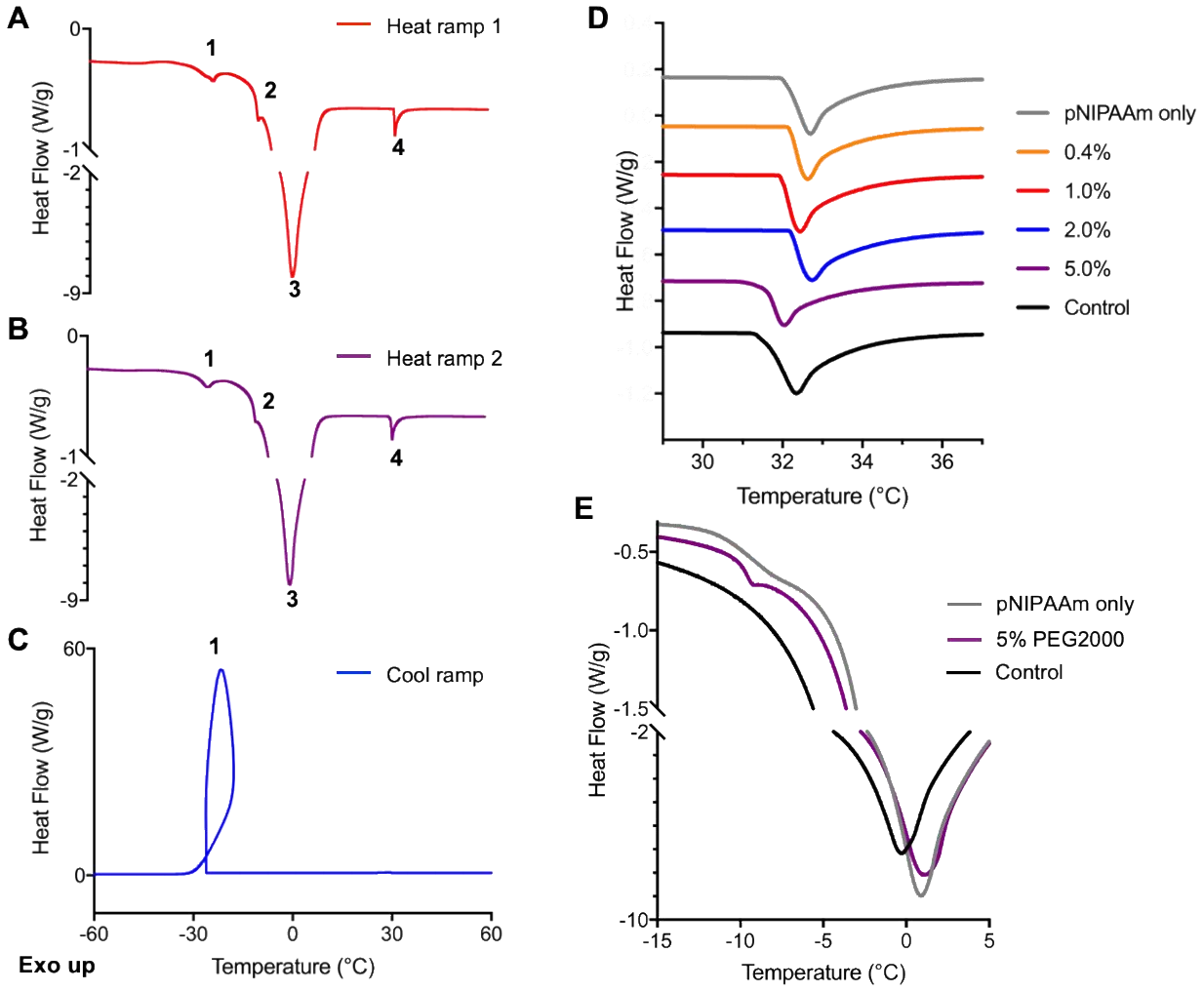

Figure 27. Thermal Behavior of Gels as Measured by DSC Thermograms.(A–C) Heat flow of 5% PEG2000 gel sample for (A) heat ramp 1, (B) heat ramp 2, and (C) cool ramp. Feature 1 shows the (A,B) melting and (C) crystallization of freezing bound water at -25 °C. (A,B) Feature 2 shows the T_g' of the gel at -9.7 °C. Feature 3 shows the melting of free water at 0 °C. Feature 4 shows the sol-gel endotherm at 32.6 °C. (D) Sol-gel endotherms for thermogels with varying concentrations of PEG2000. (E) Comparison of T_g' for the pNIPAAm only, 5% PEG2000, and control gels.

Table 7. Thermogel Transition Temperatures

Thermogel Formulation		Tg'	Sol-gel	$LCST_0$	$LCST_{FD-H20}$	$LCST_{FD-SNF}$
PEG MW (Da)	[PEG w/v)] (%)	(°C)	endotherm (°C)	(°C)	(°C)	(°C)
–	0.0	-9.9	32.5	33.0	33.0	30.4
200	5.6	N/A	32.0	32.5	33.0	30.3
2000	0.4	-9.1	32.4	33.4	NM	NM
	1.0	-9.7	32.2	33.1	NM	NM
	2.0	-9.5	32.5	33.1	NM	NM
	5.0	-9.7	32.6	32.3	33.0	30.4
4000	0.4	-8.6	32.5	32.9	NM	NM
	1.0	-9.0	32.3	32.9	NM	NM
	2.0	-9.2	32.4	32.9	NM	NM
	5.0	-9.0	31.8	33.0	NM	NM
6000	0.4	-8.6	32.6	33.2	NM	NM
	1.0	-9.0	32.6	33.2	NM	NM
	2.0	-9.2	32.4	32.9	NM	NM
8000	0.4	-8.9	32.5	32.7	NM	NM
	1.0	-9.1	32.2	32.5	NM	NM
	2.0	-8.4	32.6	33.2	NM	NM

NM = not measured; T_g' = glass transition temperature of the maximally freeze concentrated solution. N/A = T_g' was not detected. $LCST_0$, $LCST_{FD-H20}$, and $LCST_{FD-SNF}$ = lower critical solution temperature of the initial hydrated gel, freeze-dried gel rehydrated in water or Simulated Nasal Fluid (SNF), respectively

5.3.2 Texture, Residual Moisture, and Gelation of Freeze-Dried Thermogel

The various thermogel formulations were freeze dried and the texture, pore structure, and residual moisture were evaluated. The freeze-dried control gel was pliable (Figure 28A) while the 5% PEG2000 gel had a brittle texture (Figure 28B). SEM analysis revealed pores or sheet-like structures in all samples except for the control gel (Figure 29). The water content of the initial hydrated pNIPAAm only, control, and 5% PEG2000 gels was measured gravimetrically and found

to be >91% (w/w) for all 3 formulations (Figure 30A) The efficiency of freeze drying to remove the water content was determined by TGA (Figure 30B) to measure the residual moisture, which was 10.2 ± 0.6% (n = 2) for the pNIPAAm only gel, while that of the control and 5% PEG2000 gels was decreased to 3.3 ± 0.5% (n = 3) and 2.8 ± 1.0% (n = 3), respectively.

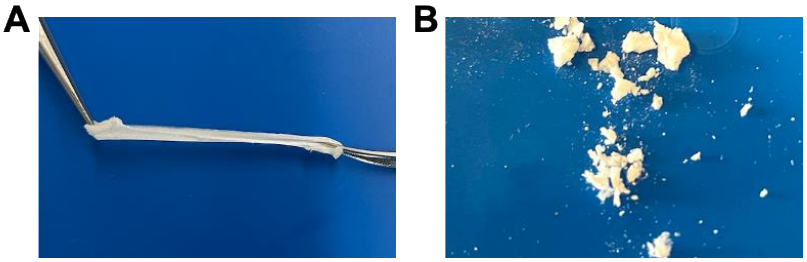

Figure 28. Photographs Showing the Textures of Freeze-Dried Gels.

(A) Control and (B) 5% PEG2000 freeze-dried gels

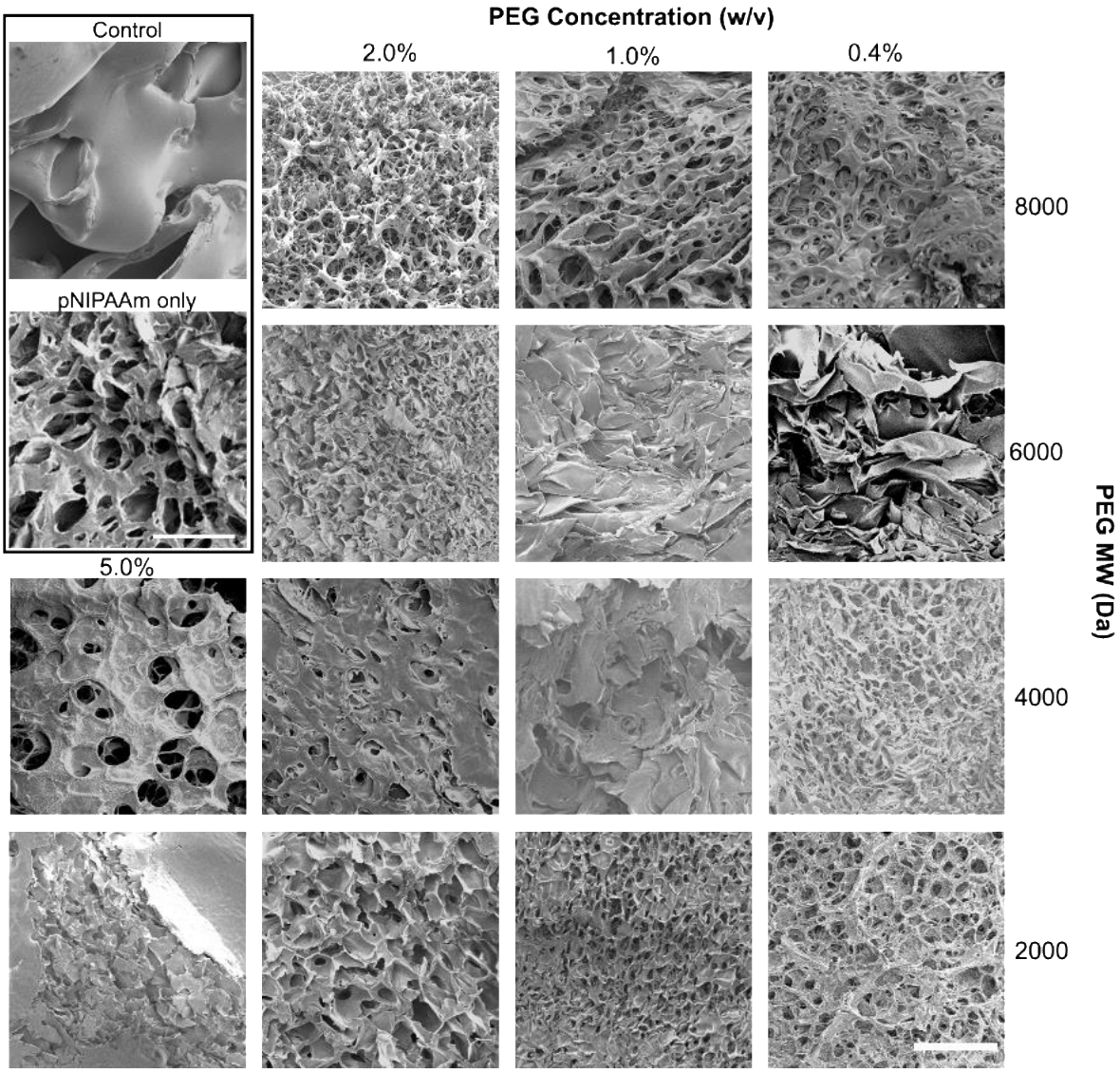

Figure 29. SEM Images of Freeze-Dried Gel Formulations.

(scale bar = 100 μm)

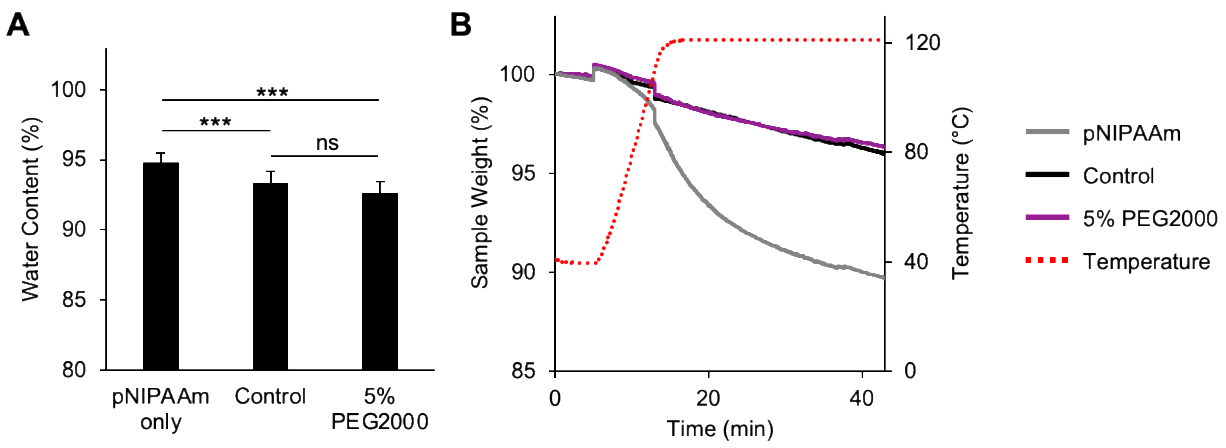

Figure 30. Analysis of the Thermogel Water Content and Residual Moisture.(A) The original water content of the hydrated thermogels was determined by measuring the weight loss after freeze drying. Error bars represent mean ± S.D. (n = 11). Statistical significance was determined by ANOVA with Tukey post hoc testing, ***p < 0.001, ns = not significant. (B) The residual moisture after freeze drying was measured using TGA, where the weight loss was determined as the dried gels were held at 120 °C.

Following rehydration, the swelling ratio and gelation properties of the freeze-dried gel formulations were characterized and showed that the freeze-drying process did not alter the thermoresponsive behavior of the gel. When immersed in SNF, the freeze-dried control gel appeared to rehydrate in approximately 10 min, while the pNIPAAm only and 5% PEG2000 gels rehydrated gradually over 60 min (Figure 31A). All gels exhibited a similar swelling ratio when rehydrated in water or SNF (Figure 31B), however the LCST was influenced by the rehydration medium (Table 7). In SNF, the LCST of the 3 gel formulations was ~30 °C, while in water it was ~33 °C, which was similar to the LCST of the initial hydrated gels. Finally, the gelation kinetics of the 5% PEG2000 gel after rehydration in SNF was investigated at 33–35 °C (the temperature range of the sinuses [13]). The sol-gel transition occurred more rapidly at higher temperatures, likely as a result of faster heat transfer (Figure 31C).

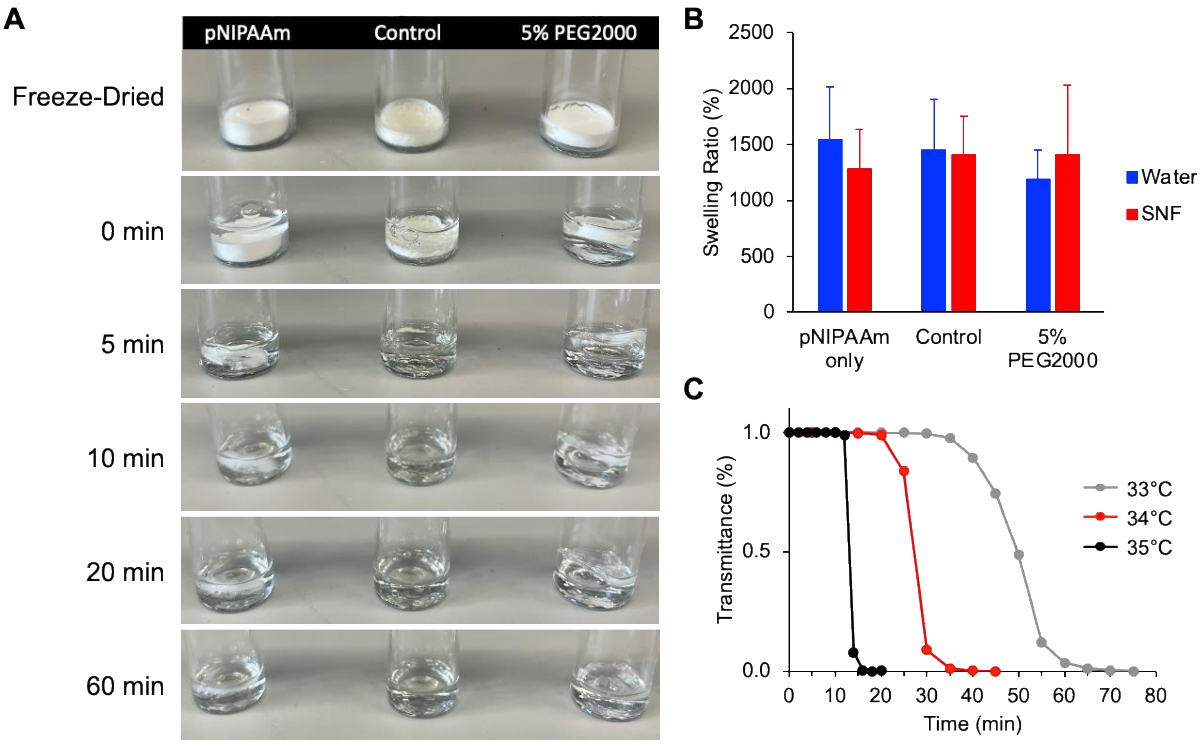

Figure 31. Rehydration, Swelling, and Gelation of Freeze-Dried Thermogels. (A) Photographs of the freeze-dried gels as they rehydrated in Simulated Nasal Fluid (SNF). (B) Swelling ratio of gels rehydrated with water or SNF. Error bars represent the mean ± S.D. (n = 4). All differences were not statistically significant. (C) Gelation kinetics of 5% PEG2000 rehydrated in SNF were measured by optical transmittance at 2- or 5-minute intervals for the indicated temperature.

5.3.3 Shelf-Stability and Mucoadhesion of FD-TEMPS

Selected for its desirable properties post freeze drying, the 5% PEG2000 gel was used for proof-of-concept studies by combining it with extended-release MSs and freeze drying the system to create FD-TEMPS. As TEMPS has been previously developed for the extended release of mometasone furoate [157], a corticosteroid that is commonly used for CRS treatment, mometasone-loaded FD-TEMPS was evaluated. The mometasone-loaded MSs had a smooth, spherical shape (Figure 32A), which was maintained after mixing with thermogel and freeze

drying (Figure 32B). To estimate if there was a change in the MS size due to formulation in FD-TEMPS, MSs (which were freeze dried after fabrication) were rehydrated in water and freeze dried a second time. The median diameter of the MSs after a 2nd freeze-drying cycle was reduced by ~1 μm (Figure 33).

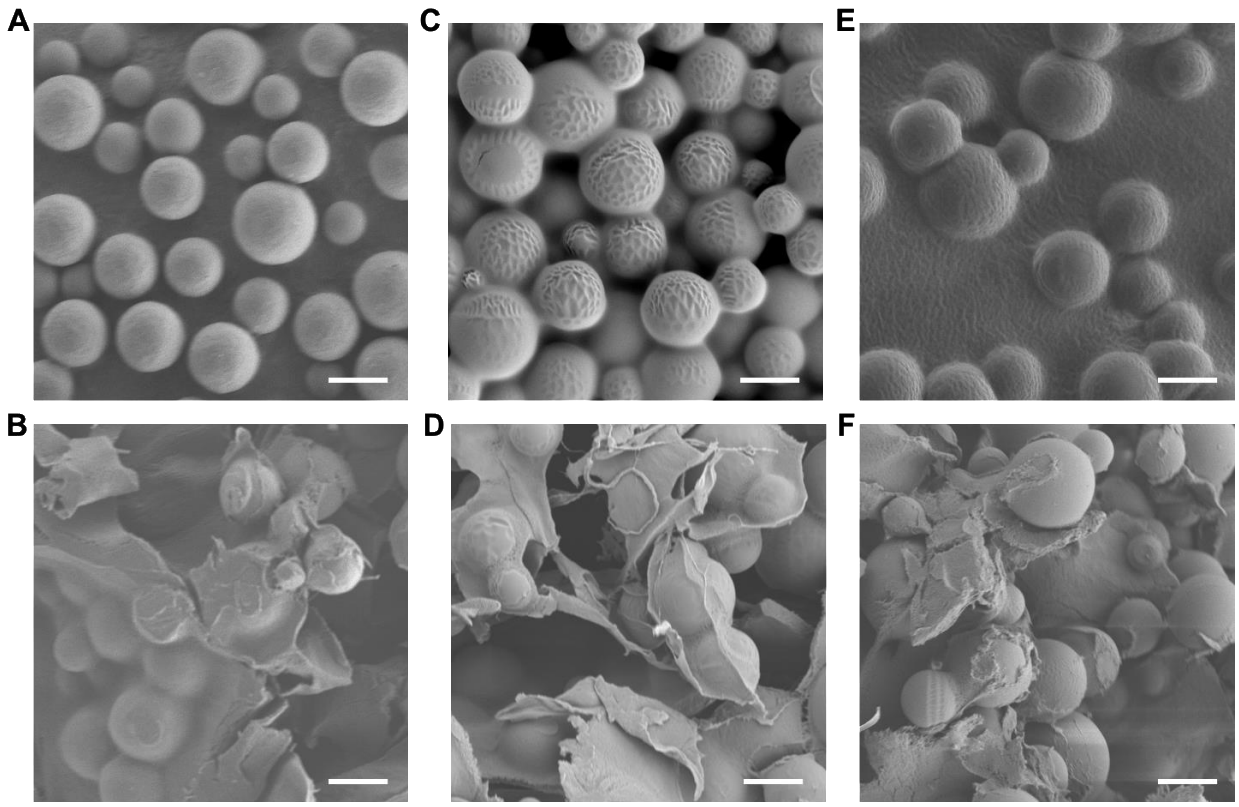

Figure 32. SEM of TEMPS and FD-TEMPS. (A) MSs alone have a smooth spherical morphology, (B) which was maintained after preparation of FD-TEMPS. Following storage (under ambient conditions) of (C) TEMPS for 3 weeks or (E) 6 weeks, the MS surface was no longer smooth, while storage of (D) FD-TEMPS for 3 weeks or (F) 6 weeks did not appear to alter the MS surface (scale bar = 5 μm).

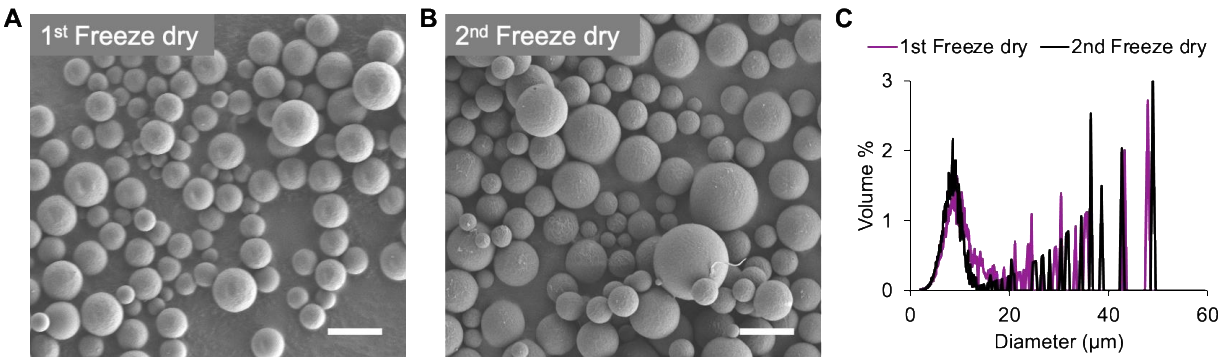

Figure 33. Characterization of Mometasone MSs After 1st and 2nd Freeze-Drying Cycle.

(A,B) SEM images of MSs after (a) 1st and (B) 2nd cycle of freeze drying (scale bar = 10 µm). (C) The size distribution of MSs following a 2nd cycle of freeze drying was ~1 µm smaller (median diameter = 8.6 µm) compared to the 1st cycle (median diameter = 9.6 µm).

The shelf-stability of TEMPS and FD-TEMPS were evaluated by comparing MS surface morphology and drug release kinetics after storage under ambient conditions. Following storage of TEMPS (i.e., MSs combined with the thermogel and stored in a hydrated state), erosion of the MS surface was apparent after 3 and 6 weeks (Figure 32C and E, respectively). In contrast, MS surface morphology remained unchanged when the freeze-dried formulation was stored for 3 and 6 weeks (Figure 32D and F, respectively). Despite the difference in MS morphologies, the storage state did not have a large effect on the release kinetics of bioactive drug. The cumulative release profiles of the 3-weeks stored FD-TEMPS and TEMPS were very similar (Figure 34A) with a small, but insignificant ($p > 0.05$) decrease in the early release of mometasone from 3-week stored TEMPS (Figure 34B). Following storage for 6 weeks, the amount of mometasone released from stored TEMPS for the first 2 days was significantly reduced ($p < 0.05$) compared to 6-weeks stored FD-TEMPS (Figure 34C), however the remainder of the cumulative release profile was not statistically different. The bioactivity of mometasone released from the 3-week stored formulations

was similar to a control consisting of mometasone that was reconstituted the day of the assay (Figure 34D).

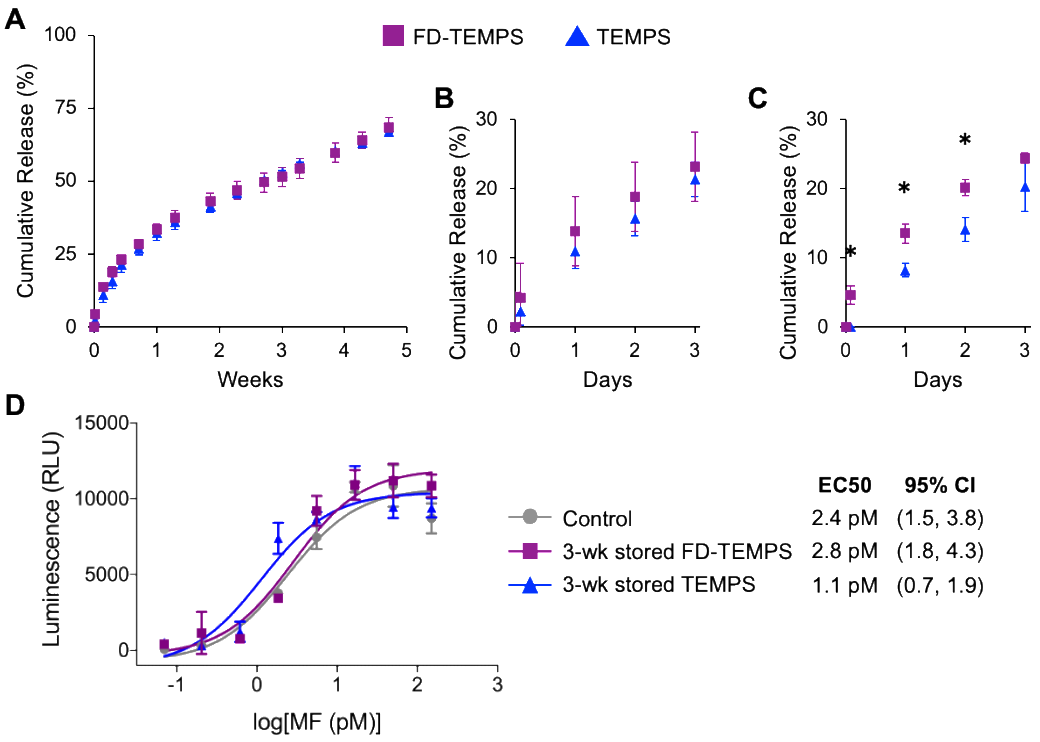

Figure 34. Cumulative Release and Bioactivity of Mometasone from FD-TEMPS and TEMPS.(A, B) Drug release after 3 weeks of storage under ambient conditions and (C) 6 weeks of storage. Error bars indicate the mean ± S.D. (n = 3). Statistical significance was determined by Student's t-test or Wilcoxon Rank Sum test, *p < 0.05. (D) The bioactivity of released mometasone after 1 day of *in vitro* incubation of the 3-week stored FD-TEMPS or TEMPS was comparable to control drug.

In addition to characterizing storage stability, the ability of FD-TEMPS to be applied directly to a mucosal surface was evaluated by measuring its transfer distance on an inclined agar and mucin surface. Both the thermogel and TEMPS were displaced several centimeters from the application site as the sol-gel transition occurred. In contrast, the freeze-dried thermogel and FD-

TEMPS remained in place after application as they rehydrated and gelled (Figure 35). Additionally, the freeze-dried material was still in place 6 hours after initiation of the assay.

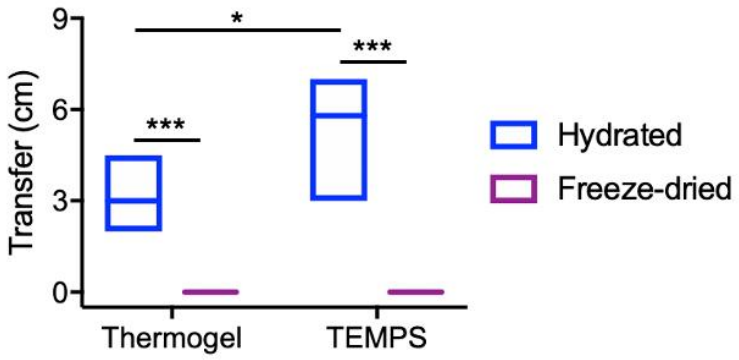

Figure 35. Transfer Distance of Thermogel and TEMPS in Hydrated or Freeze-Dried Form. The lower, upper, and middle bars represent the minimum, maximum, and mean transfer distance, respectively (n = 5). Statistical significance was determined by ANOVA, ***p < 0.0001, *p < 0.05.

5.4 Discussion

The ability to freeze dry a thermoresponsive hydrogel with embedded polymer microspheres was explored to produce a ready-to-use drug delivery system (FD-TEMPS). This enhanced formulation is proposed to be well-suited for the paranasal sinuses because the dry, powder-like product could be directly applied to the sinonasal mucosa where the water content of the overlying mucus would rehydrate the thermoresponsive polymer as it gels. Importantly, in this form, the ability to achieve a uniform distribution of the delivery system is decoupled from the gelation kinetics as was demonstrated by *in vitro* drip transfer testing (Figure 35). On a simulated mucosal surface, FD-TEMPS effectively remained in place as it rehydrated and gelled, which could reduce the possibility of dripping and pooling *in vivo*. This is a critical design requirement

for a sinonasal delivery system because any material that could potentially occlude the sinus ostia would pose the risk of blocking drainage and exacerbating local inflammation.

The process of freeze drying and rehydrating the thermogel (with water) did not affect the LCST, which is consistent with prior studies characterizing freeze-dried pNIPAAm microgel beads or microspheres [221,222]; however, the rehydration medium did have an effect. Specifically, when rehydrated in SNF, which consists of 1.2% (w/w) salt, the LCST was decreased by ~3 °C. This 'salting out' effect has been previously reported for copolymers of pNIPAAm in aqueous salt solution where the decreased LCST was attributed to either more favorable hydrogen bonding among hydrophilic portions of pNIPAAm compared to hydrogen bonding between water and hydrophilic portions or increased hydrophobic-hydrophobic interactions [223]. Both interactions can increase the tendency for the pNIPAAm chains to associate, which drives the sol-gel phase change. For application in the sinuses, where the physiological temperature is ~34 °C [13] and the overlying mucus contains ~1% salt [224], the reduced LCST of the rehydrated thermogel further ensures that the material will be maintained as a gel apposed to the mucosa.

In addition to *in situ* rehydration of the freeze-dried delivery system, another benefit of FD-TEMPS is that the minimal water content improves shelf-stability. Freeze drying is a preferred operation for drying bioproducts as it is less likely to damage the drug cargo due to the use of low temperatures [215]. As the system is cooled and ice crystallization occurs, the solute increases in concentration and viscosity. At the point where ice crystallization essentially stops, the solution is referred to as "maximally freeze concentrated" and the temperature at which this happens is T_g'. T_g' is a critical temperature for the freeze-drying process because increasing the product temperature above T_g' during primary drying can result in viscous flow of the solute causing collapse and irreversible damage to the final product [215,220,225]. Thus, T_g' was measured for

the various thermogel formulations and determined to be around -10 °C for all gels except the control. Because the research-grade freeze dryer used for these experiments did not provide control of the shelf temperature, the thermogels were frozen in a -80 °C freezer, so that after transfer to the freeze dryer, the product would take longer to equilibrate to ambient temperature as it dried. Despite the inability to control the product temperature during primary drying, a low residual moisture (2.8 ± 1.0% for the 5% PEG2000 gel) was achieved. It is expected that the residual moisture could be further reduced to the specification of <1% with improved control of the product temperature during drying, as is standard on industry-grade freeze-drying equipment.

As mentioned previously, a T_g' was not detected for the control gel (with PEG200) and after freeze drying, this gel formulation had a pliable texture and lacked pores. These observations support the plasticizing effects of the low MW PEG, which has been well characterized for thermogel formulations consisting of pNIPAAm, chitosan, and PEG over a range of MW [226]. With low MW PEG, there are a larger number of polar end groups that interact with pNIPAAm and chitosan, leading to a higher degree of plasticization because of the weakened physical crosslinking between chitosan and pNIPAAm. In contrast, high MW PEG interacts less with the other copolymers such that the free segments of PEG chains can move and crystallize [226]. However, a limitation to the effects of high MW PEGs was noted as they can restrict the mobility of pNIPAAm chains and inhibit the sol-gel phase transition. This phenomenon was observed in the present study in pNIPAAm gels formulated with 5% PEG (MW 6,000 or 8,000), which did not exhibit a typical sol-gel phase transition, so they were not further evaluated. However, an investigation of freeze drying cosolvent systems containing PEG has shown that including higher MW PEG enhanced the ability to freeze dry lower MW PEG [227]. In a mixture with PEG8000, increasing concentrations of PEG400 resulted in a decreasing trend of T_g', which is expected as

T_g decreases with decreasing molecular weight [225]. Additionally, after freeze drying, the combination of PEG8000 with PEG400 resulted in a solid lyophilized cake with interconnected pores that are indicative of the efficient escape of water vapor. Similar observations were made in the present study via SEM where pores were observed in thermogels prepared with PEG of 2,000–8,000 MW, but not with PEG200.

For proof-of-concept studies of the complete FD-TEMPS product, the release of an anti-inflammatory corticosteroid, mometasone furoate, from stored FD-TEMPS was compared to stored TEMPS. We anticipated that when TEMPS was stored under ambient conditions, the water content of the thermogel would cause erosion of the MSs because PLGA is susceptible to hydrolysis [228]. As a result, either a large initial burst release or very small release concentrations (if the drug was quickly degraded after its release into an aqueous medium) would be observed. It was also expected that the stability of the MSs in FD-TEMPS would be improved because of the low residual moisture, which would be observed as a sustained release profile consistent with prior development of TEMPS [157]. Somewhat unexpectedly, the release kinetics and bioactivity of mometasone released from the 3-week stored freeze-dried or hydrated systems were very similar to each other and prior release characterization of TEMPS. It is noteworthy, however, that mometasone furoate is a highly lipophilic drug that is stable at acidic pH [189]. Thus, any erosion of PLGA MSs that would have occurred would create an acidic microenvironment [228] that would serve to maintain the stability of this corticosteroid. Upon investigation of longer storage times, the release kinetics did deviate after 6 weeks of storage under ambient conditions. A reduced release in the first few days from TEMPS compared to FD-TEMPS was observed. With even longer storage times, the deviation in release kinetics would be expected to increase. Additionally, although the stability of mometasone is conducive to the acidic environment of the degradable

polyesters in FD-TEMPS (or TEMPS), when designed for the delivery of more labile drugs or proteins, the freeze-dried product would likely provide a considerable advantage for storage and stability.

Others have proposed similar concepts of freeze-dried polymer matrices for local drug delivery to mucosal surfaces, though with much shorter release profiles. For example, a lyophilized nasal insert composed of chitosan and gellan gum was designed for systemic administration of an anti-nausea medication. The drug was incorporated within the polymer matrix and *in vitro* release was demonstrated over 8 h with minimal displacement (0.7 ± 0.1 cm) over the same time frame [229]. Another lyophilized polymeric matrix consisting of carrageenan, Pluronic acid, and PEG600 was created for buccal delivery of model soluble or insoluble drugs where the drug dissolution was demonstrated over 10 min or 2 h, respectively. In this study, an annealing process was used during freeze drying whereby the frozen sample was heated above its T_g', but below the ice melting temperature (the eutectic temperature) to allow for large ice crystal formation. The resulting wafers had larger pores and were stable for 6 months with residual moisture values between 1.5% and 0.6% [230]. Incorporating an annealing process may be beneficial for FD-TEMPS if faster rehydration time were desired. With the formation of larger ice crystals during freezing, larger pores are formed that allow for more rapid ingress of water into the freeze-dried matrix. In comparison to these two lyophilized drug inserts, FD-TEMPS achieved drug release for several weeks because the drug release kinetics were controlled by the PLGA MSs. As a result, the delivery system can be applied in a clinical setting and local drug release will be continuous for the subsequent month, which reduces the need for daily application and enhances patient adherence.

6.0 Conclusions and Future Work

A reversibly conformable delivery system for the paranasal sinuses is a promising strategy for enhancing local therapeutic delivery for the management of chronic sinonasal disease. Herein, we have developed TEMPS (**T**hermogel, **E**xtended-release **Mi**crosphere-based-delivery to the **P**aranasal **S**inuses), which is composed of a thermoresponsive, pNIPAAm-based hydrogel with controlled-release PLGA MSs. TEMPS is cyto-compatible *in vitro* and is well-tolerated in rabbits *in vivo*. Due to its temperature-sensitive nature, TEMPS can provide unique apposition to tissue architecture, like the paranasal sinuses. Moreover, while the thermogel matrix is non-biodegradable, the system is temporary and can be readily removed and reapplied as needed. In Chapters 1 and 2, we motivated the need for new delivery technology for the sinuses, leading to the development of TEMPS, which was introduced in Chapter 3. We showed that TEMPS could provide sustained release of a corticosteroid, mometasone furoate, that effectively reduced sinonasal inflammation in rabbit sinuses. We furthered this characterization in Chapter 4 by demonstrating compatibility of the thermogel with human ciliated nasal epithelial tissue as well as showing that the PLGA MS component can be re-designed for the sustained release of another small molecule, retinoic acid. While the standard of care for managing chronic sinonasal inflammation is treatment with corticosteroids, retinoic acid can promote cilia differentiation. Thus, it is an attractive adjunct therapy that could help promote the regeneration of healthy mucosa following the injury associated with chronic inflammation or sinus surgery.

With regards to the formulation of TEMPS for future clinical use, freeze drying the complete delivery system was proposed for better ease of clinical translation. In the first iteration of TEMPS, the MSs must be mixed with the thermogel immediately prior to use because the water

content of the gel will hydrate the PLGA MSs initiating swelling of the polymer matrix and polymer chain erosion, which lead to drug release. Instead, through freeze drying, the water content was efficiently removed via ice sublimation without collapse of the polymer matrix. We showed that the incorporation of PEG2000 with pNIPAAm created a suitable thermogel that could be freeze dried to a brittle material with low residual moisture. Furthermore, the freeze-dried thermogel could rehydrate and gel at the temperature of the sinuses. When combined with corticosteroid-loaded MSs, the full product, FD-TEMPS, demonstrated sustained release of bioactive drug and remained in place after application to a simulated mucosal surface. The consistent thermoresponsive and drug release characteristics with the original TEMPS system, along with the ability for the freeze-dried product to be stored in a ready-to-use format could provide greater ease of clinical translation. Toward the goal of clinical translation and advancing CRS treatment options, there are several proposed next steps for the further development and characterization of TEMPS.

6.1 Rabbit Maxillary Antrostomy for TEMPS Application

To advance preclinical testing, performing a more clinically-representative maxillary antrostomy procedure in rabbits for TEMPS application would enable observations of its *in vivo* thermo-reversibility. The maxillary antrostomy would be performed on sedated and intubated rabbits using an endonasal approach. The maxillary sinus opening would be expanded by removing a small portion of non-structural bone, as is done during FESS on CRS patients. This would allow visualization and transnasal application of TEMPS, in comparison to the prior method of percutaneously injecting the material into the sinuses, which appeared to cause iatrogenic trauma

[157]. The expanded opening into the maxillary sinuses will allow for the distribution and gelation of TEMPS to be observed *in situ.* Furthermore, this procedure could be used with freeze-dried TEMPS to confirm *in vitro* findings that the material rehydrates, gels, and remains in place. As the rehydration of FD-TEMPS is a critical step to its ultimate clinical success, it is necessary that this be tested in rabbits to advance the clinical translation. To assess maintenance and thermo-reversibility of TEMPS, 30 days after application, the rabbits would be sedated for endoscopic visualization of the apposition of TEMPS as well as any gross tissue observations. Additionally, the material could be removed by ambient temperature (~25 °C) saline irrigation to confirm the thermo-reversibility of the delivery system. The mucosal tissue could then be harvested for histopathology analysis as described in Chapter 3.

In tandem with the thermo-reversibility studies, additional rabbits could be included in the study design to assess *in vivo* drug distribution. The subjects would be treated with mometasone-loaded TEMPS applied following the maxillary antrostomy. At regular intervals, such as day 1, 7, 14, 21, and 30, rabbits would be sacrificed to collect the mucosal tissue and measure local drug concentration by liquid chromatography with tandem mass spectrometry [161]. (This work could be supported by the Small Molecule Biomarker Core at the University of Pittsburgh.) As demonstrated by similar studies that measured corticosteroid concentrations in rabbit sinonasal tissue following release from local drug delivery systems [93,161], it is expected that the corticosteroid would be detected in the sinus mucosal tissue, but not the nasal tissue due to the local nature of the drug release. Additionally, mometasone is not expected to be detected in the blood because of its degradation at neutral pH [189]. These studies would confirm that a clinically-effective dose of mometasone is reaching the sinonasal mucosa, and if necessary, could prompt

optimization of the drug loading or release kinetics by changing PLGA MS formulation parameters.

Applying mometasone-loaded TEMPS via maxillary antrostomy could also be performed in rabbits with induced disease to further assess its anti-inflammatory effects. For disease induction, the additional recommendations previously discussed (see Section 3.4) should be implemented (these include performing microCT measurements at the acute disease timepoint and ensuring that the sinuses are maintained in hypoxic conditions for chronic disease induction). Thirty days after applying mometasone-loaded TEMPS, the methods previously established for measuring sinus opacification by microCT and histopathology scoring of tissue sections should be performed. Additionally, inflammatory markers and cell populations could be further characterized using qRT-PCR and ELISA analysis of the harvested mucosal tissue. This analysis should focus on characterizing changes in Th1 cytokines (IL-2, IFN-γ) in comparison to those associated with Th2 cells (IL-4, IL-5, IL-13) following treatment with mometasone-TEMPS or controls (no treatment, vehicle-only TEMPS, and daily nasal drops). We did previously attempt to measure cytokine levels in rabbit nasal secretions. The secretions were collected by inserting a trimmed Merocel sponge in the nasal cavity of rabbits for about 1 min, then incubating the sponge in PBS with a protease inhibitor cocktail and collecting the liquid. Most samples yielded results below the limit of quantification for the cytokine ELISA kits (IL-4 and TNF-α), and therefore, using mucosal tissue for cytokine analysis is recommended in the future.

6.2 TEMPS Integrity in the Presence of Respiratory Bacteria

A potential issue that may arise during *in vivo* thermo-reversibility testing is the maintenance of thermogel integrity following 30 days in the sinuses. While in our prior work, material recovered from the rabbit sinuses post-mortem appeared to be TEMPS in SEM images (Figure 21B,C), additional studies may be warranted to understand if any degradation is occurring. Notably, recent work by Yu *et al.* has demonstrated that hydrogels can be susceptible to bacteria-triggered degradation [231]. Although the hydrogel was intentionally designed with a β-lactam core that would degrade in response to β-lactamase, an enzyme produced by some bacterial strains, this enzyme is produced by *Pseudomonas aeruginosa*, a common respiratory pathogen [191]. Sinus microbiome characterization has identified *Pseudomonadales* in rabbits with induced CRS [166] and *P. aeruginosa* can be found in biofilm-associated CRS in patients [24]. As such, investigating the integrity and thermo-reversibility of the pNIPAAm gel following *in vitro* incubation with *P. aeruginosa* may be worthwhile. If thermogel degradation is problematic, a possible solution would be to adapt TEMPS for the controlled release of antibiotics. Indeed, others have developed a sinus stent coated with PLGA NPs designed to release of ciprofloxacin and ivacaftor, two antibiotics with activity against *P. aeruginosa* [151,152] (discussed further in Section 2.2.5). In addition to preventing possible thermogel degradation, this may be a strategy beneficial for treating biofilm-associated CRS particularly as bacterial toxins have been shown to inhibit ciliary function [191].

6.3 Air-Liquid Interface Compatibility Studies

The cilia-related studies presented in Chapter 4 could be advanced by using another *in vitro* model that creates an air-liquid interface (ALI). Human nasal tissue samples would be cultured on collagen-coated transwell inserts to establish ciliated epithelial cultures. By feeding media to the basolateral compartment only, the apical surface is exposed to air, but the culture can be maintained for extended durations. In fact, recent work has shown that creating grooves on the collagen substrate induces ciliary alignment, and the cultures can maintain transport for months [232]. This experimental set up would enable TEMPS compatibility testing with ciliated epithelium for up to, or even longer than, 30 days. Additionally, mucin proteins could be added to the apical surface to characterize the interaction of TEMPS with mucus and the effects on mucociliary transport (MCT) and CBF. The method for quantifying MCT and CBF must be compatible with the transwells, and therefore a fluorescent bead method is recommended. Specifically, small fluorescent beads are deposited on the apical ciliated surface and the distance they travel can be tracked using a Nikon Ti-E microscope and Tokai-Hit environmental chamber (which are available at the Center of Biologic Imaging at the University of Pittsburgh) to measure MCT. Additionally, the sinusoidal beat frequency of cilia can be detected in the bead motion for measurement of CBF. An advantage of this experimental set up is that the temperature can be controlled such that TEMPS could be maintained in its gelled state at >33 °C enabling the analysis of cilia exposed to the gelled thermogel.

Using the ALI culture, the ability to promote durable reciliation from CRS patient samples following treatment with RA-TEMPS could also be evaluated. Previous work has shown that the ALI model can be used to study cilia motility of CRS patient samples [204,206,233]. Notably, another study that compared basal CBF of sinonasal tissue collected from control and CRS patients

showed that there was no statistically significant difference between the two groups, however the samples exhibited different responses to ATP [17]. Specifically, control samples responded with an increase in beat frequency within 1 minute of exposure to the exogenous stimulus (100 μmol/L ATP), but CRS patient samples displayed no change or deceleration [17]. These results suggest that cilia from CRS patients do not have the same functional response to stimuli, which could contribute to the well-established pathophysiology of ineffective MCC. We hypothesize that by treating CRS patient samples with a sustained concentration of RA, functional re-ciliation will be improved that will display this *in vitro* response to external stimuli and show enhanced differentiation to ciliated cells. To investigate this hypothesis, ALI cultures could be created with nasal tissue samples collected from healthy volunteers and CRS patients and treated with RA-TEMPS to provide a continuous concentration of RA. Control conditions, including no treatment, a one-time, or daily boluses of soluble RA would also be included to compare the effect of sustained RA concentration. The effects of RA treatment would be assessed by measuring the change in CBF before and after dosing with ATP. Healthy samples are expected to respond to the stimulus with an increase in CBF whether or not they have been treated with RA. CRS samples treated with RA are also expected to show a similar increase in beat frequency in response to ATP, while CRS samples without treatment or a single dose of soluble RA are expected to show no response. In parallel, these samples could be evaluated by immunofluorescence staining for βIV tubulin, which is an indicator of cilia differentiation [234], to confirm that treatment with RA does lead to enhanced differentiation of ciliated cells.

6.4 Stability and Sterilization of FD-TEMPS

Along with the future work described in the previous sections that will further support the efficacy and compatibility of TEMPS, additional studies on the stability and sterilization of the freeze-dried form are recommended. With regards to stability, prior studies have shown that mometasone-loaded FD-TEMPS maintains its release kinetics following 6 weeks of storage (see Section 5.3.3). This work should be expanded to establish the stability of the freeze-dried product with characterization of MS morphology, release kinetics, and bioactivity at regular intervals for storage over 2 years. Additionally, exploring the ability of FD-TEMPS to enhance stability of more labile drugs, and proteins in particular, would support the versatility of the delivery system. Another aspect critical to the clinical translation of FD-TEMPS is selecting a sterilization method that does not compromise its safety or efficacy. There are two general approaches to sterilization of biomedical products. First is aseptic manufacturing, in which each material, container, and closure is sterilized individually and then assembled in a controlled, high-quality environment. The second approach is terminal sterilization, whereby the product is packaged in its final container and subjected to sterilization via heat, chemical sterilant, or ionizing radiation [235]. If a single method for terminal sterilization that is compatible with both the drug-loaded PLGA MSs and the thermogel is identified, then the system could be combined, freeze-dried, packaged, and sterilized. However, if a single sterilization method is not compatible, then the components would need to be sterilized separately and combined in an aseptic process. For safety purposes, terminal sterilization is preferred, if feasible, for preventing microbial contamination [236].

Currently available nasal products use a range of methods to prevent microbial contamination. For example, the mometasone furoate nasal spray, Nasonex, is formulated with a preservative, benzalkonium chloride (BAC), to prevent microbial contamination after repeat use

[235]. BAC is a widely used preservative, however, preservatives can cause adverse effects on the nasal mucosa. BAC, in fact, has been shown to significantly affect ciliary function [206]. Even at dilute concentrations and a short exposure time (15 min) to BAC, *in vitro* ciliary activity of hNECs was significantly impaired. Additionally, following 5 days of a single short exposure to BAC, ciliostasis was observed at all concentrations evaluated. As a result of compatibility concerns related to preservatives, preservative-free nasal products are currently being explored, particularly focusing on the design of applicators that prevent or filter air that may enter the container upon administration [235]. Alternatively, a notable benefit of the single administration of controlled release sinonasal systems is that a preservative is not necessary.

The controlled-release sinus stent, Propel, is terminally sterilized via irradiation, as indicated in the product's Instructions for Use. According to the recommendation for sterilization of healthcare products (ISO 11137), the recommended dosing for gamma irradiation is 25 kGy or 15 kGy. It is noteworthy that Propel is fabricated from PLGA, and therefore, irradiation may be suitable for sterilization of the PLGA MS component of TEMPS. In fact, irradiated PLGA MSs have been shown to maintain consistent size, drug encapsulation, and release kinetics with non-irradiated batches [237].

Another method for sterilizing PLGA is the use of pulsed ozone [238]. In this study, PLGA nanofiber scaffolds were subjected to up to 8 pulses of ~40 min of ozone exposure at low pressures. Importantly, no significant effects to the morphology, physicochemical, thermal, and mechanical properties, as well as cell-material interactions were observed after ozone sterilization. Use of ozone is an example of a terminal sterilization method with a chemical sterilant, whereby microbial contaminates are oxidized by readily available monoatomic oxygen molecules [235]. The sterilization study of PLGA nanofibers demonstrates the full range of testing that is required to

ensure that the sterilization process does not compromise the product integrity. In addition to showing that the growth of microorganism on spore strips was effectively prevented, SEM analysis was performed to show that the morphology of the PLGA scaffolds was maintained. The surface chemistry of the PLGA was evaluated by Fourier transform infrared spectroscopy as well as TGA and DSC to show that the thermal decomposition and glass transition characteristics of the polymer were unchanged by the sterilization method [238]. For controlled release PLGA MSs, additional testing should be performed to ensure that the drug loading, release kinetics, and bioactivity of the released drug are not altered by sterilization.

While there have been many investigations of suitable methods for sterilizing PLGA, the literature identifying, and fully characterizing, sterilization of pNIPAAm-based hydrogels is limited. Literature describing the range of sterilization methods explored for a variety of natural and synthetic hydrogels has been reviewed [236]. With respect to pNIPAAm hydrogels, one study used ethylene oxide sterilization, however the effects of the sterilization process were not characterized, nor was it confirmed that the gel was effectively sterilized [239]. Another study showed that ultraviolet irradiation was not effective for preventing bacterial growth in a pNIPAAm-based hydrogel [240]. Another synthetic-based thermoresponsive hydrogel fabricated with poloxamers was shown to be better suited for sterilization by autoclaving, rather than using dry heat [241]. These methods will need to be screened with the pNIPAAm hydrogel to determine the best method for its effective sterilization without compromising critical properties such as its LCST, thermo-reversibility, and cytocompatibility.

Finally, along with the selection of a sterilization method, a sterile applicator must be designed for FD-TEMPS. Ideally, such a device would consist of a catheter that could be inserted through the naris, similar to the delivery system for the Propel stent (see Section 2.2.2). Such a

device would enable direct application of the dry powder-like material to the sinonasal mucosa by a physician under endoscopic visualization in the operating room or clinic.

6.5 Treg-TEMPS: An Immunoengineering Approach for CRS Treatment

Another direction for the future development of TEMPS is to take a new and more specific approach to treat CRS via immunoengineering. Although the exact etiology of CRS remains to be fully elucidated, studies suggest that a breakdown in immunologic homeostasis is what leads to dysregulated inflammation and catalytic tissue deformation. As introduced in Section 1.2.3, this damage is either manifest through a mixed tissue infiltrate of Th1 and Th2 cells (CRSsNP) or a Th2-biased response with eosinophilic infiltrate and presence of nasal polyps (CRSwNP) [35,242]. Notably, in the healthy, homeostatic-state, regulatory T cells (Treg) naturally promote a balance of inflammation in several ways, including suppressing proliferation and cytokine production of effector T cells [243]. Several clinical studies investigating Treg populations in CRS patients have reported reduced numbers and functionality of Tregs in nasal polyp tissue [244], as well as reduced *in vitro* migratory response [245]. Others have reported lower Treg numbers in the peripheral blood of CRS patients relative to control subjects, along with reduced levels of regulatory cytokines and increased expression of inflammatory cytokines [246]. In contrast, studies evaluating the effects of corticosteroids for CRS have found a specific increase in the numbers and activity of Tregs [247,248] suggesting that they may mediate one of the many anti-inflammatory effects of steroid treatment. Given the prominent role of effector T cells in CRS [35,242] and the importance of regulatory T cells in controlling inflammatory responses [243], alteration of Treg numbers or function may improve the inflammatory imbalance of CRS. Therefore, promoting restoration of

this immunological homeostasis (such as through targeted restoration of Treg prevalence) has the potential to address or at least improve the underlying imbalance seen in CRS as compared to current treatments that only temporarily suppress inflammation (i.e., corticosteroids).

For this immunoengineering approach, TEMPS could be developed for the targeted recruitment of endogenous Tregs, mimicking the manner in which tumors promote immunological homeostasis [249]. Using this method, our laboratories have previously shown therapeutic success with corresponding increases in Treg cells and regulatory cytokines in multiple disease models of dysregulated inflammation, including periodontitis, dry eye disease, and even allograft transplantation models [250–252]. Given that CRS appears to exhibit similar forms of dysregulated inflammation, this biomimetic approach to recruit a patient's endogenous Tregs could also be applied for the sinonasal mucosa. Specifically, local Treg recruitment is accomplished by creating a gradient of the chemokine CCL22 from PLGA MSs that is released over 30 days [249] and results in the preferential migration of Tregs *in vitro* [251]. A Treg-TEMPS formulation would consist of Treg-recruiting MSs combined with the thermogel for application along the sinonasal mucosa. In contrast to corticosteroid treatment that requires local concentrations in the range of mg/kg for a therapeutic effect, this approach has previously demonstrated efficacy at concentrations 10^6-fold less (i.e., pg/kg). This is due to the fact that the released agent does not directly act to produce a pharmacological effect, but instead recruits a patient's own population of regulatory cells, which then employ sophisticated and dynamic mechanisms for naturally controlling inflammation.

In previous work by our laboratory, we have shown that local administration of Treg recruiting-MSs in murine models resulted in a site-specific increase of mRNA expression of the hallmark Treg transcription factor, forkhead box P3 (FoxP3), as well as anti-inflammatory

cytokines IL-10 and TGF-β1. These findings were confirmed by measurement of protein levels by ELISA (Fig. 9B) [250]. Additionally, following treatment with Treg recruiting-MSs in the murine lacrimal gland, the population of Treg cells ($FoxP3^+$ (%$CD4^+$)) was increased relative to Teff cells (IFN-γ^+ (%$CD4^+$)) (Fig. 9C) [252]. This local increase in the prevalence of Tregs has also demonstrated robust ability to address dysregulated inflammation *in vivo.* For example, in a canine model of periodontal disease, treatment with Treg-recruiting MSs reduced bone resorption demonstrating the suppression of destructive inflammation in the periodontal tissue and alveolar bone [250]. In another inflammatory disease driven by influx of $CD4^+$ lymphocytes, dry eye disease, local injection of Treg recruiting-MSs in the murine lacrimal gland prevented the destruction of the ocular epithelial barrier and improved aqueous tear production [252]. Most notably, administration of Treg-recruiting MSs has even been shown to prevent rodent allograft rejection indefinitely [251].

Given these promising results in other inflammatory disease models, we propose to test the ability of Treg-TEMPS to increase sinonasal Treg numbers in CRS-induced rabbits. The rabbit model used in Aim I with additional modifications described in Section 6.1 would be used to induce disease and apply Treg-TEMPS. The performance of Treg-TEMPS in comparison to no treatment and a blank vehicle would be evaluated by microCT, histopathology, and several additional complementary methods. Using flow cytometry, the relative abundance of both regulatory and effector T-cell subsets in sinonasal mucosa and/or draining lymph nodes from rabbits in each treatment group could be evaluated. In particular, $CD4^+$ $FoxP3^+$ Treg, $CD4^+$ T-bet^+ Th1, and $CD4^+$ GATA-3^+ Th2 populations, as well as $CD8^+$ T-bet^+ Tc1 cells, should be identified and quantified in terms of relative frequency and total number per mass of tissue [251]. The phenotype of TEMPS-recruited Tregs could be further characterized by staining for key functional

markers (e.g., CD25 (IL-2Rα), CTLA-4, LAP (TGF-β1), CD39, and CD73). Suppressive function of FACS-sorted $CD4^{+}$ $CD25^{high}$ $CD127^{low}$ Tregs from draining lymph nodes and/or sinonasal mucosa would be evaluated using *in vitro* Treg suppression assays, as previously reported by our group [251]. To complement the immunophenotypic analysis, RNA could be extracted from sinonasal mucosa for qRT-PCR analysis to measure inflammatory and regulatory cytokine levels. Treatment with Treg-TEMPS is expected to show an elevated response of regulatory T cells and regulatory cytokines relative to effector T cells and inflammatory cytokines. If Treg recruitment is successful, we would expect to see a corresponding reduction in inflammation, as assessed by microCT and histopathology scoring.

While prior research using Treg-recruiting MSs has demonstrated a therapeutic effect in multiple species (including mice, rats, and dogs) and inflammatory disease models [250–252], this will represent (to our knowledge) the first study of Treg-recruitment in rabbits and in a disease model of sinonasal inflammation. The proposed experiments will use rhCCL22, which is effective in a canine model [250], where Canine and Human CCL22 share 71% of amino acid identities and score 84% positives using a BLAST analysis. Similarly, Rabbit and Human CCL22 share 72% identities and score 80% positives, thus efficacy is anticipated. However, if a therapeutic response is not observed, optimization of the CCL22 MSs formulation or mucosal permeation could be explored. For example, the loading or release of CCL22 could be tuned by adjusting PLGA molecular weight, MS size, or porosity. Another possible cause for insufficient Treg recruitment could be that CCL22 has limited transport across the mucosal barrier. If this is suspected, *ex vivo* permeation studies can be conducted using a Franz diffusion apparatus with nasal mucosa sandwiched between the donor and receiver compartments [253]. The nasal mucosa samples could be obtained via the Tissue Bank that is maintained by our clinical co-investigator or harvested

from healthy or CRS-induced rabbits. Models of sinusitis suggest that tight junctions are reduced in CRS, therefore permeation of CCL22 across disease-induced tissue may be enhanced relative to healthy control tissue. Permeation of CCL22 released from TEMPS or MSs would be compared to soluble CCL22 by measuring the concentrations in the receiver well at regular intervals by ELISA. If necessary, the TEMPS formulation could be altered to enhance drug absorption as has been explored for intranasal insulin delivery [254]. Permeation enhancers, such as bile salts, surfactants, and fatty acids, can improve paracellular or transcellular drug transport, although care must be taken to ensure that they do not damage the mucosa. Alternatively, bioadhesive or mucoadhesive polymers, such as hyaluronic acid or chitosan, can increase contact time and further augment drug permeation.

If the approaches described above do not address the challenges of Treg recruitment *in vivo,* alternatively, our laboratories have previously demonstrated that the local release of 3 factors, IL-2, TGF-β1, and rapamycin, can effectively induce differentiation of Tregs from a highly prevalent population of naïve $CD4^+$ lymphocytes [255]. This alternative approach would include developing the 3-factor Treg-TEMPS formulation and demonstrating sustained release prior to conducting *in vivo* studies. Given the versatility of TEMPS to be engineered for the sustained release of any number of therapeutics, adapting the formulation for local immunoengineering is an attractive direction for this delivery system as it could have a more targeted impact on reversing chronic sinonasal inflammation.

Bibliography

[1] R. Pawankar, G.W. Canonica, S.T. Holgate, R.F. Lockey, M.S. Blaiss, WAO White Book on Allergy (Update. 2013), n.d.

[2] N. Bhattacharyya, Incremental Health Care Utilization and Expenditures for Chronic Rhinosinusitis in the United States, Ann Otology Rhinology Laryngology. 120 (2011) 423–427. https://doi.org/10.1177/000348941112000701.

[3] National Center for Health Statistics. Crude percentages of sinusitis for adults aged 18 and over, United States, 2015-2018, National Health Interview Survey. (2011).

[4] E.O. Meltzer, D.A. Bukstein, The economic impact of allergic rhinitis and current guidelines for treatment, Ann Allergy Asthma Immunol. 106 (2011) S12–S16. https://doi.org/10.1016/j.anai.2010.10.014.

[5] A. Sahin-Yilmaz, R.M. Naclerio, Anatomy and Physiology of the Upper Airway, Proc Am Thorac Soc. 8 (2011) 31–39. https://doi.org/10.1513/pats.201007-050rn.

[6] N. Jones, The nose and paranasal sinuses physiology and anatomy, Adv Drug Deliv Rev. 51 (2001) 5–19. https://doi.org/10.1016/s0169-409x(01)00172-7.

[7] J. Leal, H.D.C. Smyth, D. Ghosh, Physicochemical properties of mucus and their impact on transmucosal drug delivery, Int J Pharm. 532 (2017) 555–572. https://doi.org/10.1016/j.ijpharm.2017.09.018.

[8] P.G. Djupesland, Nasal drug delivery devices: characteristics and performance in a clinical perspective—a review, Drug Deliv Transl Re. 3 (2013) 42–62. https://doi.org/10.1007/s13346-012-0108-9.

[9] S. Gizurarson, The Effect of Cilia and the Mucociliary Clearance on Successful Drug Delivery, Biological Pharm Bulletin. 38 (2015) 497–506. https://doi.org/10.1248/bpb.b14-00398.

[10] J.-A. Schwab, M. Zenkel, Filtration of Particulates in the Human Nose, Laryngoscope. 108 (1998) 120–124. https://doi.org/10.1097/00005537-199801000-00023.

[11] D.M. Dalgorf, R.J. Harvey, Sinonasal Anatomy and Function, Am J Rhinol Allergy. 27 (2013) S3–S6. https://doi.org/10.2500/ajra.2013.27.3888.

[12] A. Parikh, U. Anand, M.C. Ugwu, T. Feridooni, E. Massoud, R.U. Agu, Drug-Eluting Nasal Implants: Formulation, Characterization, Clinical Applications and Challenges, Pharm. 6 (2014) 249–267. https://doi.org/10.3390/pharmaceutics6020249.

[13] T. Keck, R. Leiacker, H. Riechelmann, G. Rettinger, Temperature Profile in the Nasal Cavity, Laryngoscope. 110 (2000) 651–654. https://doi.org/10.1097/00005537-200004000-00021.

[14] J.M. Pinto, Olfaction, Proc Am Thorac Soc. 8 (2011) 46–52. https://doi.org/10.1513/pats.201005-035rn.

[15] N. Mygind, R. Dahl, Anatomy, physiology and function of the nasal cavities in health and disease, Adv Drug Deliv Rev. 29 (1998) 3–12. https://doi.org/10.1016/s0169-409x(97)00058-6.

[16] S.K. Lai, Y.-Y. Wang, D. Wirtz, J. Hanes, Micro- and macrorheology of mucus, Adv Drug Deliv Rev. 61 (2009) 86–100. https://doi.org/10.1016/j.addr.2008.09.012.

[17] N.A. Cohen, Sinonasal Mucociliary Clearance in Health and Disease, Ann Otology Rhinol Laryngol Suppl. 196 (2006) 20–26. https://doi.org/10.1177/00034894061150s904.

[18] J.O.N. Lundberg, T. Farkas-Szallasi, E. Weitzberg, J. Rinder, J. Lidholm, A. Änggård, T. Hökfelt, J.M. Lundberg, K. Alving, High nitric oxide production in human paranasal sinuses, Nat Med. 1 (1995) 370–373. https://doi.org/10.1038/nm0495-370.

[19] P.J. Conway, N.S. Jones, The nose and nitric oxide: a review., Clin Otolaryngol. 25 (2000) 337. https://doi.org/10.1046/j.1365-2273.2000.00378.x.

[20] C. Bogdan, Nitric oxide and the immune response., Nat Immunol. 2 (2001) 907. https://doi.org/10.1038/ni1001-907.

[21] T. Runer, S. Lindberg, Effects of Nitric Oxide on Blood Flow and Mucociliary Activity in the Human Nose, Ann Otology Rhinology Laryngology. 107 (1998) 40–46. https://doi.org/10.1177/000348949810700108.

[22] J.L. Brożek, J. Bousquet, I. Agache, A. Agarwal, C. Bachert, S. Bosnic-Anticevich, R. Brignardello-Petersen, G.W. Canonica, T. Casale, N.H. Chavannes, J.C. de Sousa, A.A. Cruz, C.A. Cuello-Garcia, P. Demoly, M. Dykewicz, I. Etxeandia-Ikobaltzeta, I.D. Florez, W. Fokkens, J. Fonseca, P.W. Hellings, L. Klimek, S. Kowalski, P. Kuna, K.-T. Laisaar, D.E. Larenas-Linnemann, K.C.L. Carlsen, P.J. Manning, E. Meltzer, J. Mullol, A. Muraro, R. O'Hehir, K. Ohta, P. Panzner, N. Papadopoulos, H.-S. Park, G. Passalacqua, R. Pawankar, D. Price, J.J. Riva, Y. Roldán, D. Ryan, B. Sadeghirad, B. Samolinski, P. Schmid-Grendelmeier, A. Sheikh, A. Togias, A. Valero, A. Valiulis, E. Valovirta, M. Ventresca, D. Wallace, S. Waserman, M. Wickman, W. Wiercioch, J.J. Yepes-Nuñez, L. Zhang, Y. Zhang, M. Zidarn, T. Zuberbier, H.J. Schünemann, Allergic Rhinitis and its Impact on Asthma (ARIA) guidelines—2016 revision, J Allergy Clin Immun. 140 (2017) 950–958. https://doi.org/10.1016/j.jaci.2017.03.050.

[23] J. Bousquet, N. Khaltaev, A.A. Cruz, J. Denburg, W.J. Fokkens, A. Togias, T. Zuberbier, C.E. Baena-Cagnani, G.W. Canonica, C.V. Weel, I. Agache, N. Aït-Khaled, C. Bachert, M.S. Blaiss, S. Bonini, L.-P. Boulet, P.-J. Bousquet, P. Camargos, K.-H. Carlsen, Y. Chen, A. Custovic, R. Dahl, P. Demoly, H. Douagui, S.R. Durham, R.G.V. Wijk, O. Kalayci, M.A.

Kaliner, Y.-Y. Kim, M.L. Kowalski, P. Kuna, L.T.T. Le, C. Lemiere, J. Li, R.F. Lockey, S. Mavale-Manuel, E.O. Meltzer, Y. Mohammad, J. Mullol, R. Naclerio, R.E. O'Hehir, K. Ohta, S. Ouedraogo, S. Palkonen, N. Papadopoulos, G. Passalacqua, R. Pawankar, T.A. Popov, K.F. Rabe, J. Rosado-Pinto, G.K. Scadding, F.E.R. Simons, E. Toskala, E. Valovirta, P.V. Cauwenberge, D.-Y. Wang, M. Wickman, B.P. Yawn, A. Yorgancioglu, O.M. Yusuf, H. Zar, I. Annesi-Maesano, E.D. Bateman, A.B. Kheder, D.A. Boakye, J. Bouchard, P. Burney, W.W. Busse, M. Chan-Yeung, N.H. Chavannes, A. Chuchalin, W.K. Dolen, R. Emuzyte, L. Grouse, M. Humbert, C. Jackson, S.L. Johnston, P.K. Keith, J.P. Kemp, J.-M. Klossek, D. Larenas-Linnemann, B. Lipworth, J.-L. Malo, G.D. Marshall, C. Naspitz, K. Nekam, B. Niggemann, E. Nizankowska-Mogilnicka, Y. Okamoto, M.P. Orru, P. Potter, D. Price, S.W. Stoloff, O. Vandenplas, G. Viegi, D. Williams, Allergic Rhinitis and its Impact on Asthma (ARIA) 2008, Allergy. 63 (2008) 8–160. https://doi.org/10.1111/j.1398-9995.2007.01620.x.

[24] R.R. Orlandi, T.T. Kingdom, P.H. Hwang, T.L. Smith, J.A. Alt, F.M. Baroody, P.S. Batra, M. Bernal-Sprekelsen, N. Bhattacharyya, R.K. Chandra, A. Chiu, M.J. Citardi, N.A. Cohen, J. DelGaudio, M. Desrosiers, H. Dhong, R. Douglas, B. Ferguson, W.J. Fokkens, C. Georgalas, A. Goldberg, J. Gosepath, D.L. Hamilos, J.K. Han, R. Harvey, P. Hellings, C. Hopkins, R. Jankowski, A.R. Javer, R. Kern, S. Kountakis, M.L. Kowalski, A. Lane, D.C. Lanza, R. Lebowitz, H. Lee, S.Y. Lin, V. Lund, A. Luong, W. Mann, B.F. Marple, K.C. McMains, R. Metson, R. Naclerio, J.V. Nayak, N. Otori, J.N. Palmer, S.R. Parikh, D. Passali, A. Peters, J. Piccirillo, D.M. Poetker, A.J. Psaltis, H.H. Ramadan, V.R. Ramakrishnan, H. Riechelmann, H. Roh, L. Rudmik, R. Sacks, R.J. Schlosser, B.A. Senior, R. Sindwani, J.A. Stankiewicz, M. Stewart, B.K. Tan, E. Toskala, R. Voegels, D.Y. Wang, E.K. Weitzel, S. Wise, B.A. Woodworth, P. Wormald, E.D. Wright, B. Zhou, D.W. Kennedy, International Consensus Statement on Allergy and Rhinology: Rhinosinusitis, Int Forum Allergy Rhinol. 6 (2017) S22–S209. https://doi.org/10.1002/alr.21695.

[25] M.S. Dykewicz, D.L. Hamilos, Rhinitis and sinusitis, J Allergy Clin Immun. 125 (2010) S103–S115. https://doi.org/10.1016/j.jaci.2009.12.989.

[26] A.S. DeConde, Z.M. Soler, Chronic Rhinosinusitis: Epidemiology and Burden of Disease, Am J Rhinol Allergy. 30 (2016) 134–139. https://doi.org/10.2500/ajra.2016.30.4297.

[27] M.S. Benninger, B.J. Ferguson, J.A. Hadley, D.L. Hamilos, M. Jacobs, D.W. Kennedy, D.C. Lanza, B.F. Marple, J.D. Osguthorpe, J.A. Stankiewicz, J. Anon, J. Denneny, I. Emanuel, H. Levine, Adult chronic rhinosinusitis: Definitions, diagnosis, epidemiology, and pathophysiology, Otolaryngol Head Neck Surg. 129 (2003) S1–S32. https://doi.org/10.1016/s0194-5998(03)01397-4.

[28] L.M. Wheatley, A. Togias, Allergic Rhinitis, New Engl J Medicine. 372 (2015) 456–463. https://doi.org/10.1056/nejmcp1412282.

[29] F.M. Baroody, R.M. Naclerio, Antiallergic effects of H1-receptor antagonists, Allergy. 55 (2000) 17–27. https://doi.org/10.1034/j.1398-9995.2000.00803.x.

[30] D.V. Wallace, M.S. Dykewicz, D.I. Bernstein, J. Blessing-Moore, L. Cox, D.A. Khan, D.M. Lang, R.A. Nicklas, J. Oppenheimer, J.M. Portnoy, C.C. Randolph, D. Schuller, S.L. Spector, S.A. Tilles, The diagnosis and management of rhinitis: An updated practice parameter, J Allergy Clin Immun. 122 (2008) S1–S84. https://doi.org/10.1016/j.jaci.2008.06.003.

[31] R.M. Rosenfeld, J.F. Piccirillo, S.S. Chandrasekhar, I. Brook, K.A. Kumar, M. Kramper, R.R. Orlandi, J.N. Palmer, Z.M. Patel, A. Peters, S.A. Walsh, M.D. Corrigan, Clinical practice guideline (update): Adult sinusitis, Otolaryngology Head Neck Surg. 152 (2015) S1–S39. https://doi.org/10.1177/0194599815572097.

[32] Z.M. Soler, E. Wittenberg, R.J. Schlosser, J.C. Mace, T.L. Smith, Health state utility values in patients undergoing endoscopic sinus surgery, Laryngoscope. 121 (2011) 2672–2678. https://doi.org/10.1002/lary.21847.

[33] P. Piromchai, Kasemsiri, Laohasiriwong, Thanaviratananich, Chronic rhinosinusitis and emerging treatment options, Int J Gen Medicine. Volume 6 (2013) 453–464. https://doi.org/10.2147/ijgm.s29977.

[34] K. Snidvongs, S. Thanaviratananich, Update on Intranasal Medications in Rhinosinusitis, Curr Allergy Asthm R. 17 (2017) 47. https://doi.org/10.1007/s11882-017-0720-3.

[35] R.P. Schleimer, Immunopathogenesis of Chronic Rhinosinusitis and Nasal Polyposis, Annu Rev Pathology Mech Dis. 12 (2017) 331–357. https://doi.org/10.1146/annurev-pathol-052016-100401.

[36] J.H. Fastenberg, W.D. Hsueh, A. Mustafa, N.A. Akbar, W.M. Abuzeid, Biofilms in chronic rhinosinusitis: Pathophysiology and therapeutic strategies, World J Otorhinolaryngol Head Neck Surg. 2 (2016) 219–229. https://doi.org/10.1016/j.wjorl.2016.03.002.

[37] K.E. Hulse, Immune Mechanisms of Chronic Rhinosinusitis, Curr Allergy Asthm R. 16 (2015) 1. https://doi.org/10.1007/s11882-015-0579-0.

[38] S. Lee, A.P. Lane, Chronic Rhinosinusitis as a Multifactorial Inflammatory Disorder, Curr Infect Dis Rep. 13 (2011) 159–168. https://doi.org/10.1007/s11908-011-0166-z.

[39] S.H. Lee, Mechanisms of Glucocorticoid Action in Chronic Rhinosinusitis, Allergy Asthma Immunol Res. 7 (2015) 534–537. https://doi.org/10.4168/aair.2015.7.6.534.

[40] J. Sastre, R. Mosges, Local and systemic safety of intranasal corticosteroids, J Invest Allerg Clin. 22 (2012) 1–12.

[41] H. Kumar, R. Jain, R.G. Douglas, M.H. Tawhai, Airflow in the Human Nasal Passage and Sinuses of Chronic Rhinosinusitis Subjects, Plos One. 11 (2016) e0156379. https://doi.org/10.1371/journal.pone.0156379.

[42] J.K. Han, B.F. Marple, T.L. Smith, A.H. Murr, B.J. Lanier, J.W. Stambaugh, A.S. Mugglin, Effect of steroid-releasing sinus implants on postoperative medical and surgical interventions: an efficacy meta-analysis, Int Forum Allergy Rhinol. 2 (2012) 271–279. https://doi.org/10.1002/alr.21044.

[43] A.S. DeConde, J.C. Mace, J.M. Levy, L. Rudmik, J.A. Alt, T.L. Smith, Prevalence of polyp recurrence after endoscopic sinus surgery for chronic rhinosinusitis with nasal polyposis, Laryngoscope. 127 (2017) 550–555. https://doi.org/10.1002/lary.26391.

[44] D. Mendelsohn, G. Jeremic, E.D. Wright, B.W. Rotenberg, Revision Rates after Endoscopic Sinus Surgery: A Recurrence Analysis, Ann Otology Rhinology Laryngology. 120 (2011) 162–166. https://doi.org/10.1177/000348941112000304.

[45] W. Moller, U. Schuschnig, G. Celik, W. Munzing, P. Bartenstein, K. Haussinger, W.G. Kreyling, M. Knoch, M. Canis, S. Becker, Topical Drug Delivery in Chronic Rhinosinusitis Patients before and after Sinus Surgery Using Pulsating Aerosols, Plos One. 8 (2013) e74991. https://doi.org/10.1371/journal.pone.0074991.

[46] W. Möller, U. Schuschnig, P. Bartenstein, G. Meyer, K. Häussinger, O. Schmid, S. Becker, Drug Delivery to Paranasal Sinuses Using Pulsating Aerosols, J Aerosol Med Pulm D. 27 (2014) 255–263. https://doi.org/10.1089/jamp.2013.1071.

[47] F.G. Torres, O.P. Troncoso, A. Pisani, F. Gatto, G. Bardi, Natural Polysaccharide Nanomaterials: An Overview of Their Immunological Properties, Int J Mol Sci. 20 (2019) 5092. https://doi.org/10.3390/ijms20205092.

[48] D. Klemm, B. Heublein, H.-P. Fink, A. Bohn, Cellulose: Fascinating Biopolymer and Sustainable Raw Material, Angew Chem Int Ed Engl. 44 (2005) 3358–3393. https://doi.org/10.1002/anie.200460587.

[49] C.J. Massey, J.D. Suh, B. Tessema, S.T. Gray, A. Singh, Biomaterials in Rhinology, Otolaryngol Head Neck Surg. 154 (2016) 606–617. https://doi.org/10.1177/0194599815627782.

[50] H.C. Arca, L.I. Mosquera-Giraldo, V. Bi, D. Xu, L.S. Taylor, K.J. Edgar, Pharmaceutical Applications of Cellulose Ethers and Cellulose Ether Esters, Biomacromolecules. 19 (2018) 2351–2376. https://doi.org/10.1021/acs.biomac.8b00517.

[51] X. Xu, A.K. Jha, D.A. Harrington, M.C. Farach-Carson, X. Jia, Hyaluronic acid-based hydrogels: from a natural polysaccharide to complex networks, Soft Matter. 8 (2012) 3280–3294. https://doi.org/10.1039/c2sm06463d.

[52] M. Casale, A. Moffa, L. Sabatino, A. Pace, G. Oliveto, M. Vitali, P. Baptista, F. Salvinelli, Hyaluronic Acid: Perspectives in Upper Aero-Digestive Tract. A Systematic Review, Plos One. 10 (2015) 1–17. https://doi.org/10.1371/journal.pone.0130637.

[53] G.A. Martău, M. Mihai, D.C. Vodnar, The Use of Chitosan, Alginate, and Pectin in the Biomedical and Food Sector-Biocompatibility, Bioadhesiveness, and Biodegradability, Polymers-Basel. 11 (2019) 1837. https://doi.org/10.3390/polym11111837.

[54] H.H. Tønnesen, J. Karlsen, Alginate in Drug Delivery Systems., Drug Dev Ind Pharm. 28 (2002) 621–630. https://doi.org/10.1081/ddc-120003853.

[55] H.M. Ibrahim, E.M.R.E.- Zairy, Chitosan as a Biomaterial — Structure, Properties, and Electrospun Nanofibers, in: V. Bobbarala (Ed.), Concepts, Compounds and the Alternatives of Antibacterials, IntechOpen, Rijeka, 2015. https://doi.org/10.5772/61300.

[56] T.M.M. Ways, W.M. Lau, V.V. Khutoryanskiy, Chitosan and Its Derivatives for Application in Mucoadhesive Drug Delivery Systems, Polymers-Basel. 10 (2018) 267. https://doi.org/10.3390/polym10030267.

[57] R.J.A. England, J.J. Homer, L.C. Knight, S.R. Ell, Nasal pH measurement: a reliable and repeatable parameter., Clin Otolaryngology. 24 (1999) 67–68. https://doi.org/10.1046/j.1365-2273.1999.00223.x.

[58] B.-G. Kim, J.-H. Kim, S.-W. Kim, S.-W. Kim, K.-S. Jin, J.-H. Cho, J.-M. Kang, S.-Y. Park, Nasal pH in patients with chronic rhinosinusitis before and after endoscopic sinus surgery, Am J Otolaryngol. 34 (2013) 505–507. https://doi.org/10.1016/j.amjoto.2013.04.015.

[59] M.C. Gohel, R.K. Parikh, S.A. Nagori, S.N. Shah, M.R. Dabhi, Preparation and evaluation of soft gellan gum gel containing paracetamol, Indian J Pharm Sci. 71 (2009) 120–124. https://doi.org/10.4103/0250-474x.54273.

[60] A.H. Bacelar, J. Silva-Correia, J.M. Oliveira, R.L. Reis, Recent progress in gellan gum hydrogels provided by functionalization strategies, J Mater Chem B. 4 (2016) 6164–6174. https://doi.org/10.1039/c6tb01488g.

[61] J.N. BeMiller, An Introduction to Pectins: Structure and Properties, in: M.L. Fishman, J.J. Jen (Eds.), Chemistry and Function of Pectins, American Chemical Society, 1986: pp. 2–12. https://doi.org/10.1002/chin.198648383.

[62] B.R. Thakur, R.K. Singh, A.K. Handa, Dr.M.A. Rao, Chemistry and uses of pectin — A review, Crit Rev Food Sci. 37 (1997) 47–73. https://doi.org/10.1080/10408399709527767.

[63] T. Rajangam, S.S.A. An, Fibrinogen and fibrin based micro and nano scaffolds incorporated with drugs, proteins, cells and genes for therapeutic biomedical applications, Int J Nanomed. 8 (2013) 3641–3662. https://doi.org/10.2147/ijn.s43945.

[64] J.W. Weisel, R.I. Litvinov, Fibrin Formation, Structure and Properties, Subcell Biochem. 82 (2017) 405–456. https://doi.org/10.1007/978-3-319-49674-0_13.

[65] M.C. Catoira, L. Fusaro, D.D. Francesco, M. Ramella, F. Boccafoschi, Overview of natural hydrogels for regenerative medicine applications, J Mater Sci Mater Medicine. 30 (2019) 115. https://doi.org/10.1007/s10856-019-6318-7.

[66] B. Tyler, D. Gullotti, A. Mangraviti, T. Utsuki, H. Brem, Polylactic acid (PLA) controlled delivery carriers for biomedical applications, Adv Drug Deliv Rev. 107 (2016) 163–175. https://doi.org/10.1016/j.addr.2016.06.018.

[67] J.M. Anderson, M.S. Shive, Biodegradation and biocompatibility of PLA and PLGA microspheres, Adv Drug Deliv Rev. 64 (2012) 72–82. https://doi.org/10.1016/s0169-409x(97)00048-3.

[68] S.N. Rothstein, W.J. Federspiel, S.R. Little, A unified mathematical model for the prediction of controlled release from surface and bulk eroding polymer matrices, Biomaterials. 30 (2009) 1657–1664. https://doi.org/10.1016/j.biomaterials.2008.12.002.

[69] S.N. Rothstein, S.R. Little, A "tool box" for rational design of degradable controlled release formulations, J Mater Chem. 21 (2011) 29–39. https://doi.org/10.1039/c0jm01668c.

[70] H. Seyednejad, A.H. Ghassemi, C.F. {van Nostrum}, T. Vermonden, W.E. Hennink, Functional aliphatic polyesters for biomedical and pharmaceutical applications, J Control Release. 152 (2011) 168–176. https://doi.org/10.1016/j.jconrel.2010.12.016.

[71] T.K. Dash, V.B. Konkimalla, Poly-ϵ-caprolactone based formulations for drug delivery and tissue engineering: A review, J Control Release. 158 (2012) 15–33. https://doi.org/10.1016/j.jconrel.2011.09.064.

[72] U. Sharma, D. Concagh, L. Core, Y. Kuang, C. You, Q. Pham, G. Zugates, R. Busold, S. Webber, J. Merlo, R. Langer, G.M. Whitesides, M. Palasis, The development of bioresorbable composite polymeric implants with high mechanical strength, Nat Mater. 17 (2018) 96–103. https://doi.org/10.1038/nmat5016.

[73] J. Herzberger, K. Niederer, H. Pohlit, J. Seiwert, M. Worm, F.R. Wurm, H. Frey, Polymerization of Ethylene Oxide, Propylene Oxide, and Other Alkylene Oxides: Synthesis, Novel Polymer Architectures, and Bioconjugation, Chem Rev. 116 (2016) 2170–2243. https://doi.org/10.1021/acs.chemrev.5b00441.

[74] K. Knop, R. Hoogenboom, D. Fischer, U.S. Schubert, Poly(ethylene glycol) in Drug Delivery: Pros and Cons as Well as Potential Alternatives, Angew Chem Int Ed Engl. 49 (2010) 6288–6308. https://doi.org/10.1002/anie.200902672.

[75] C.-C. Lin, K.S. Anseth, PEG Hydrogels for the Controlled Release of Biomolecules in Regenerative Medicine, Pharmaceut Res. 26 (2009) 631–643. https://doi.org/10.1007/s11095-008-9801-2.

[76] S.K. Lai, Y.-Y. Wang, J. Hanes, Mucus-penetrating nanoparticles for drug and gene delivery to mucosal tissues, Adv Drug Deliv Rev. 61 (2009) 158–171. http://www.sciencedirect.com/science/article/pii/S0169409X08002652.

[77] E. Giuliano, D. Paolino, M. Fresta, D. Cosco, Mucosal Applications of Poloxamer 407-Based Hydrogels: An Overview, Pharm. 10 (2018) 159. https://doi.org/10.3390/pharmaceutics10030159.

[78] E. Russo, C. Villa, Poloxamer Hydrogels for Biomedical Applications, Pharm. 11 (2019) 671. https://doi.org/10.3390/pharmaceutics11120671.

[79] E. Bellotti, M.V. Fedorchak, S. Velankar, S.R. Little, Tuning of thermoresponsive pNIPAAm hydrogels for the topical retention of controlled release ocular therapeutics, J Mater Chem B. 7 (2019) 1276–1283. https://doi.org/10.1039/c8tb02976h.

[80] L. Klouda, A.G. Mikos, Thermoresponsive hydrogels in biomedical applications, Eur J Pharm Biopharm. 68 (2008) 34–45. https://doi.org/10.1016/j.ejpb.2007.02.025.

[81] S. Lanzalaco, E. Armelin, Poly(N-isopropylacrylamide) and Copolymers: A Review on Recent Progresses in Biomedical Applications, Prog Coll Pol Sci S. 3 (2017) 36. https://doi.org/10.3390/gels3040036.

[82] J.Y. Cherng, T.Y. Hou, M.F. Shih, H. Talsma, W.E. Hennink, Polyurethane-based drug delivery systems, Int J Pharm. 450 (2013) 145–162. https://doi.org/10.1016/j.ijpharm.2013.04.063.

[83] R. Shi, D. Chen, Q. Liu, Y. Wu, X. Xu, L. Zhang, W. Tian, Recent advances in synthetic bioelastomers, Int J Mol Sci. 10 (2009) 4223–4256. https://doi.org/10.3390/ijms10104223.

[84] M.I. Baker, S.P. Walsh, Z. Schwartz, B.D. Boyan, A review of polyvinyl alcohol and its uses in cartilage and orthopedic applications, J Biomed Mater Res B Appl Biomater. 100B (2012) 1451–1457. https://doi.org/10.1002/jbm.b.32694.

[85] P. Franco, I.D. Marco, The Use of Poly(N-vinyl pyrrolidone) in the Delivery of Drugs: A Review, Polymers-Basel. 12 (2020) 1114. https://doi.org/10.3390/polym12051114.

[86] A.A. Attama, Y.A. Aguilar-López, L. Villafuerte-Robles, Functional Performance of Chitosan/Carbopol 974P NF Matrices in Captopril Tablets, J Pharm. 2016 (2016) 3240290. https://doi.org/10.1155/2016/3240290.

[87] D. Mastropietro, K. Park, H. Omidian, 4.23 Polymers in Oral Drug Delivery, in: P. Ducheyne (Ed.), Comprehensive Biomaterials II, Elsevier, Oxford, 2017: pp. 430–444. https://doi.org/10.1016/b978-0-12-803581-8.09291-2.

[88] V. Poscher, Y. Salinas, Trends in Degradable Mesoporous Organosilica-Based Nanomaterials for Controlling Drug Delivery: A Mini Review, Materials. 13 (2020) 3668. https://doi.org/10.3390/ma13173668.

[89] H. Jaganathan, B. Godin, Biocompatibility assessment of Si-based nano- and micro-particles, Adv Drug Deliv Rev. 64 (2012) 1800–1819. https://doi.org/10.1016/j.addr.2012.05.008.

[90] L.K. Dkhar, J. Bartley, D. White, A. Seyfoddin, Intranasal drug delivery devices and interventions associated with post-operative endoscopic sinus surgery, Pharm Dev Technol. 23 (2018) 282–294. https://doi.org/10.1080/10837450.2017.1389956.

[91] K. Szczygielski, P. Rapiejko, A. Wojdas, D. Jurkiewicz, Use of CMC foam sinus dressing in FESS, Eur Arch Otorhinolaryngol. 267 (2010) 537–540. https://doi.org/10.1007/s00405-009-1117-2.

[92] L. Rudmik, J. Mace, B. Mechor, Effect of a dexamethasone Sinu-FoamTM middle meatal spacer on endoscopic sinus surgery outcomes: A randomized, double-blind, placebo-controlled trial, Int Forum Allergy Rhinol. 2 (2012) 248–251. https://doi.org/10.1002/alr.21011.

[93] V.S. Patel, E. Walgama, A. Psaltis, F. Lavigne, S.D. Pletcher, P.H. Hwang, Biocompatibility and Pharmacokinetics of Fluticasone-Eluting Sinus Implant in a Rabbit Model, Am J Rhinol Allergy. 31 (2017) 382–388. https://doi.org/10.2500/ajra.2017.31.4481.

[94] G.F.J.P.M. Adriaensen, K.-H. Lim, W.J. Fokkens, Safety and efficacy of a bioabsorbable fluticasone propionate–eluting sinus dressing in postoperative management of endoscopic sinus surgery: a randomized clinical trial, Int Forum Allergy Rhinol. 7 (2017) 813–820. https://doi.org/10.1002/alr.21963.

[95] C.S. Hwang, S.S. Sharhan, B.R. Kim, S.I. Kim, J.W. Kim, H. Cho, J. Yoon, C. Kim, Randomized controlled trial of steroid-soaked absorbable calcium alginate nasal packing following endoscopic sinus surgery, Laryngoscope. 128 (2018) 311–316. https://doi.org/10.1002/lary.26871.

[96] Y.L. Sow, I.P. Tang, J. Kho, P. Narayanan, Pilot study comparing steroid-impregnated and non- steroid-impregnated absorbable nasal dressing following endoscopic sinus surgery, Med J Malaysia. 73 (2018) 244–248.

[97] J.J. Xu, G.-M. Busato, C. McKnight, J.M. Lee, Absorbable Steroid-Impregnated Spacer After Endoscopic Sinus Surgery to Reduce Synechiae Formation, Ann Otology Rhinology Laryngology. 125 (2016) 195–198. https://doi.org/10.1177/0003489415606446.

[98] D.W.J. Côté, E.D. Wright, Triamcinolone-impregnated nasal dressing following endoscopic sinus surgery: A randomized, double-blind, placebo-controlled study, Laryngoscope. 120 (2010) 1269–1273. https://doi.org/10.1002/lary.20905.

[99] J.F. Dautremont, B. Mechor, L. Rudmik, The Role of Immediate Postoperative Systemic Corticosteroids When Utilizing a Steroid-eluting Spacer Following Sinus Surgery, Otolaryngol Head Neck Surg. 150 (2014) 689–695. https://doi.org/10.1177/0194599814521373.

[100] K. Zhao, Y. Yu, H. Yu, Effects of mometasone furoate–impregnated biodegradable nasal dressing on endoscopic appearance in healing process following endoscopic sinus surgery: a randomized, double-blind, placebo-controlled study, Int Forum Allergy Rhinol. 8 (2018) 1233–1241. https://doi.org/10.1002/alr.22213.

[101] V. Sabarinath, M.R. Harish, S. Divakaran, Triamcinolone Impregnated Nasal Pack in Endoscopic Sinus Surgery: Our Experience, Indian J Otolaryngol. 69 (2017) 88–92. https://doi.org/10.1007/s12070-016-1041-x.

[102] X. Zhao, A. Grewal, M. Briel, J.M. Lee, A systematic review of nonabsorbable, absorbable, and steroid-impregnated spacers following endoscopic sinus surgery, Int Forum Allergy Rhinol. 3 (2013) 896–904. https://doi.org/10.1002/alr.21201.

[103] J. Wang, C. Cai, S. Wang, Merocel versus Nasopore for Nasal Packing: A Meta-Analysis of Randomized Controlled Trials, Plos One. 9 (2014) e93959. https://doi.org/10.1371/journal.pone.0093959.

[104] W. Li, H. Lu, H. Wang, X. Sun, D. Wang, Efficacy and safety of steroid-impregnated implants following sinus surgery: A meta-analysis, Laryngoscope. 130 (2019) 2754–2759. https://doi.org/10.1002/lary.28388.

[105] M.S. Maccabee, D.R. Trune, P.H. Hwang, Effects of Topically Applied Biomaterials on Paranasal Sinus Mucosal Healing, Am J Rhinol Allergy. 17 (2003) 203–207. https://doi.org/10.1177/194589240301700405.

[106] R.R. Orlandi, D.C. Lanza, Is Nasal Packing Necessary Following Endoscopic Sinus Surgery?, Laryngoscope. 114 (2004) 1541–1544. https://onlinelibrary.wiley.com/doi/abs/10.1097/00005537-200409000-00007.

[107] A.H. Murr, T.L. Smith, P.H. Hwang, N. Bhattacharyya, B.J. Lanier, J.W. Stambaugh, A.S. Mugglin, Safety and efficacy of a novel bioabsorbable, steroid-eluting sinus stent, Int Forum Allergy Rhinol. 1 (2011) 23–32. https://doi.org/10.1002/alr.20020.

[108] T.L. Smith, A. Singh, A. Luong, R.A. Ow, S.D. Shotts, N.B. Sautter, J.K. Han, J. Stambaugh, A. Raman, Randomized controlled trial of a bioabsorbable steroid-releasing implant in the frontal sinus opening, Laryngoscope. 126 (2016) 2659–2664. https://doi.org/10.1002/lary.26140.

[109] G.D. Santarelli, J.K. Han, Evaluation of the PROPEL® mini sinus implant for the treatment of frontal sinus disease, Expert Opin Drug Del. 13 (2016) 1789–1793. https://doi.org/10.1080/17425247.2016.1250740.

[110] J.K. Han, K.D. Forwith, T.L. Smith, R.C. Kern, W.J. Brown, S.K. Miller, R.A. Ow, D.M. Poetker, B. Karanfilov, K.E. Matheny, J. Stambaugh, A.K. Gawlicka, RESOLVE: a randomized, controlled, blinded study of bioabsorbable steroid-eluting sinus implants for in-office treatment of recurrent sinonasal polyposis, Int Forum Allergy Rhinol. 4 (2014) 861–870. https://doi.org/10.1002/alr.21426.

[111] C.C. Wei, D.W. Kennedy, Mometasone implant for chronic rhinosinusitis, Med Devices (Auckl). 5 (2012) 75–80. https://doi.org/10.2147/mder.s33916.

[112] J.K. Han, R.C. Kern, Topical therapies for management of chronic rhinosinusitis: steroid implants., Int Forum Allergy Rhinol. 9 (2019) S22–S26. https://doi.org/10.1002/alr.22344.

[113] J. Shen, K. Welch, R. Kern, Mometasone furoate sinus implant – a new targeted approach to treating recurrent nasal polyp disease, Expert Rev Clin Phar. 11 (2018) 1163--1170. https://doi.org/10.1080/17512433.2018.1549485.

[114] A. Luong, R.A. Ow, A. Singh, R.L. Weiss, J.K. Han, R. Gerencer, J.P. Stolovitzky, J.W. Stambaugh, A. Raman, Safety and Effectiveness of a Bioabsorbable Steroid-Releasing Implant for the Paranasal Sinus Ostia: A Randomized Clinical Trial, JAMA Otolaryngol Head Neck Surg. 144 (2018) 28–35. https://doi.org/10.1001/jamaoto.2017.1859.

[115] K.E. Matheny, K.B.C. Jr., E.Y. Tseng, K.J. Fong, Safety, feasibility, and efficacy of placement of steroid-eluting bioabsorbable sinus implants in the office setting: a prospective case series, Int Forum Allergy Rhinol. 4 (2014) 808–815. https://doi.org/10.1002/alr.21416.

[116] K.D. Forwith, R.K. Chandra, P.T. Yun, S.K. Miller, H.D. Jampel, ADVANCE: A multisite trial of bioabsorbable steroid-eluting sinus implants, Laryngoscope. 121 (2011) 2473–2480. https://doi.org/10.1002/lary.22228.

[117] K.D. Forwith, J.K. Han, J.P. Stolovitzky, D.M. Yen, R.K. Chandra, B. Karanfilov, K.E. Matheny, J.W. Stambaugh, A.K. Gawlicka, RESOLVE: bioabsorbable steroid-eluting sinus implants for in-office treatment of recurrent sinonasal polyposis after sinus surgery: 6-month outcomes from a randomized, controlled, blinded study, Int Forum Allergy Rhinol. 6 (2016) 573–581. https://doi.org/10.1002/alr.21741.

[118] R.C. Kern, J.P. Stolovitzky, S.L. Silvers, A. Singh, J.T. Lee, D.M. Yen, A.M.C.I. Jr., F.P.J. Langford, B. Karanfilov, K.E. Matheny, J.W. Stambaugh, A.K. Gawlicka, A phase 3 trial of mometasone furoate sinus implants for chronic sinusitis with recurrent nasal polyps, Int Forum Allergy Rhinol. 8 (2018) 471–481. https://doi.org/10.1002/alr.22084.

[119] D.Y. Cho, K. Hoffman, D. Skinner, C. Mackey, D.J. Lim, G.C. Alexander, C.Y. Bae, D.K. Han, H.W. Jun, B.A. Woodworth, Tolerance and pharmacokinetics of a ciprofloxacin-coated sinus stent in a preclinical model, Int Forum Allergy Rhinol. 7 (2017) 352–358. https://doi.org/10.1002/alr.21892.

[120] D.-Y. Cho, D. Lim, C. Mackey, D. Skinner, C. Weeks, G.S. Gill, R.W. Hergenrother, W.E. Swords, B.A. Woodworth, Preclinical therapeutic efficacy of the ciprofloxacin-eluting sinus stent for Pseudomonas aeruginosa sinusitis, Int Forum Allergy Rhinol. 8 (2018) 482–489. https://doi.org/10.1002/alr.22081.

[121] R.G. Douglas, A.J. Psaltis, J. Rimmer, T. Kuruvilla, A. Cervin, Y. Kuang, Phase 1 clinical study to assess the safety of a novel drug delivery system providing long-term topical steroid therapy for chronic rhinosinusitis, Int Forum Allergy Rhinol. 9 (2019) 378–387. https://doi.org/10.1002/alr.22288.

[122] M. Palasis, C. You, D. Concagh, L. Core, K. Ho, U. Sharma, G.T. Zugates, Drug Eluting Medical Implant, 2018.

[123] B.F. Marple, T.L. Smith, J.K. Han, A.R. Gould, H.D. Jampel, J.W. Stambaugh, A.S. Mugglin, Advance II: A Prospective, Randomized Study Assessing Safety and Efficacy of Bioabsorbable Steroid-Releasing Sinus Implants, Otolaryngol Head Neck Surg. 146 (2012) 1004–1011. https://doi.org/10.1177/0194599811435968.

[124] F. Lavigne, S.K. Miller, A.R. Gould, B.J. Lanier, J.L. Romett, Steroid-eluting sinus implant for in-office treatment of recurrent nasal polyposis: A prospective, multicenter study, Int Forum Allergy Rhinol. 4 (2014) 381–389. https://doi.org/10.1002/alr.21309.

[125] S. Al-Halifa, L. Gauthier, D. Arpin, S. Bourgault, D. Archambault, Nanoparticle-Based Vaccines Against Respiratory Viruses, Front Immunol. 10 (2019) 22. https://doi.org/10.3389/fimmu.2019.00022.

[126] J. Far, M. Abdel-Haq, M. Gruber, A.A. Ammar, Developing Biodegradable Nanoparticles Loaded with Mometasone Furoate for Potential Nasal Drug Delivery, ACS Omega. 5 (2020) 7432--7439. https://doi.org/10.1021/acsomega.0c00111.

[127] M.A. Sallam, H.M. Helal, S.M. Mortada, Rationally designed nanocarriers for intranasal therapy of allergic rhinitis: influence of carrier type on in vivo nasal deposition, Int J Nanomed. 11 (2016) 2345–2357. https://doi.org/10.2147/ijn.s98547.

[128] A. Abruzzo, T. Cerchiara, F. Bigucci, G. Zuccheri, C. Cavallari, B. Saladini, B. Luppi, Cromolyn-crosslinked chitosan nanoparticles for the treatment of allergic rhinitis, Eur J Pharm Sci. 131 (2019) 136–145. https://doi.org/10.1016/j.ejps.2019.02.015.

[129] M. Sun, X. Yu, T. Wang, S. Bi, Y. Liu, X. Chen, Nasal adaptive chitosan-based nano-vehicles for anti-allergic drug delivery, Int J Biol Macromol. 135 (2019) 1182–1192. https://doi.org/10.1016/j.ijbiomac.2019.05.188.

[130] S.K. Lai, J.S. Suk, A. Pace, Y.-Y. Wang, M. Yang, O. Mert, J. Chen, J. Kim, J. Hanes, Drug carrier nanoparticles that penetrate human chronic rhinosinusitis mucus, Biomaterials. 32 (2011) 6285–6290. https://doi.org/10.1016/j.biomaterials.2011.05.008.

[131] M. Lee, C.G. Park, B.K. Huh, S.-N. Kim, S.H. Lee, R. Khalmuratova, J.-W. Park, H.-W. Shin, Y.B. Choy, Sinonasal Delivery of Resveratrol via Mucoadhesive Nanostructured Microparticles in a Nasal Polyp Mouse Model, Sci Rep-Uk. 7 (2017) 40249. https://doi.org/10.1038/srep40249.

[132] J. Pandey, P.K. Tripathi, Formulation and evaluation of levocetirizine loaded mucoadhesive microspheres for nasal delivery, Int J Pharm Sci Res. 7 (2016) 2242–2251. https://doi.org/10.13040/IJPSR.0975-8232.7(5). 2242-51.

[133] S. Wang, Y. Sun, J. Zhang, X. Cui, Z. Xu, D. Ding, L. Zhao, W. Li, W. Zhang, Astragalus Polysaccharides/Chitosan Microspheres for Nasal Delivery: Preparation, Optimization, Characterization, and Pharmacodynamics, Front Pharmacol. 11 (2020) 230. https://doi.org/10.3389/fphar.2020.00230.

[134] Y. Zheng, W. Ren, L. Zhang, Y. Zhang, D. Liu, Y. Liu, A Review of the Pharmacological Action of Astragalus Polysaccharide, Front Pharmacol. 11 (2020) 349. https://doi.org/10.3389/fphar.2020.00349.

[135] J.-E. Kim, H.-J. Cho, D.-D. Kim, Budesonide/cyclodextrin complex-loaded lyophilized microparticles for intranasal application., Drug Dev Ind Pharm. 40 (2014) 743–748. https://doi.org/10.3109/03639045.2013.782503.

[136] C. Shi, P. Liu, X. Liu, X. Feng, D. Fu, The effects of mPEG proportion and LA/GA ratio on degradation and drug release behaviors of PLGA-mPEG microparticles, Pharmazie. 71 (2016) 243--246. https://doi.org/10.1691/ph.2016.5179.

[137] W.M. Abuzeid, V.M. Girish, J.H. Fastenberg, A.R. Draganski, A.Y. Lee, J.D. Nosanchuk, J.M. Friedman, Nitric oxide-releasing microparticles as a potent antimicrobial therapeutic against chronic rhinosinusitis bacterial isolates, Int Forum Allergy Rhinol. 8 (2018) 1190–1198. https://doi.org/10.1002/alr.22185.

[138] C. Yang, G.V. Mavelli, P. Nacharaju, K. Li, L.G. Cleare, J.D. Nosanchuk, J.M. Friedman, W.M. Abuzeid, Novel nitric oxide–generating platform using manuka honey as an anti-biofilm strategy in chronic rhinosinusitis, International Forum of Allergy & Rhinology. 10 (2020) 223–232. https://doi.org/10.1002/alr.22472.

[139] M.H. Mahdi, B.R. Conway, A.M. Smith, Development of mucoadhesive sprayable gellan gum fluid gels, Int J Pharm. 488 (2015) 12–19. https://doi.org/10.1016/j.ijpharm.2015.04.011.

[140] L. Nižić, I. Ugrina, D. Špoljarić, V. Saršon, M.S. Kučuk, I. Pepić, A. Hafner, Innovative sprayable in situ gelling fluticasone suspension: development and optimization of nasal deposition, Int J Pharm. 563 (2019) 445–456. https://doi.org/10.1016/j.ijpharm.2019.04.015.

[141] E. Altuntaş, G. Yener, Formulation and Evaluation of Thermoreversible In Situ Nasal Gels Containing Mometasone Furoate for Allergic Rhinitis, AAPS PharmSciTech. 18 (2017) 2673–2682. https://doi.org/10.1208/s12249-017-0747-8.

[142] C. Karavasili, D.G. Fatouros, Smart materials: in situ gel-forming systems for nasal delivery, Drug Discov Today. 21 (2016) 157–166. https://doi.org/10.1016/j.drudis.2015.10.016.

[143] M. Agrawal, S. Saraf, S. Saraf, S.K. Dubey, A. Puri, U. Gupta, P. Kesharwani, V. Ravichandiran, P. Kumar, V.G.M. Naidu, U.S. Murty, Ajazuddin, A. Alexander, Stimuli-responsive In situ gelling system for nose-to-brain drug delivery, J Control Release. 327 (2020) 235–265. https://doi.org/10.1016/j.jconrel.2020.07.044.

[144] E. Bellotti, A.L. Schilling, S.R. Little, P. Decuzzi, Injectable thermoresponsive hydrogels as drug delivery system for the treatment of central nervous system disorders: A review, J Control Release. 329 (2021) 16–35. https://doi.org/10.1016/j.jconrel.2020.11.049.

[145] E. Altuntaş, G. Yener, R. Doğan, F. Aksoy, M.Ş. Aydın, E. Karataş, Effects of a Thermosensitive In Situ Gel Containing Mometasone Furoate on a Rat Allergic Rhinitis Model, Am J Rhinol Allergy. 32 (2018) 132–138. https://doi.org/10.1177/1945892418764951.

[146] F. Aksoy, R. Dogan, O. Ozturan, E. Altuntas, F.G. Yener, G. Topcu, B. Guler, Effect of a combination of mometasone furoate, levofloxacin, and retinyl palmitate with an in situ gel-forming nasal delivery system on nasal mucosa damage repair in an experimental rabbit model, Biomed Pharmacother. 96 (2017) 603–611. https://doi.org/10.1016/j.biopha.2017.10.023.

[147] P. Pandey, P.J. Cabot, B. Wallwork, B.J. Panizza, H.S. Parekh, Formulation, functional evaluation and ex vivo performance of thermoresponsive soluble gels - A platform for therapeutic delivery to mucosal sinus tissue, Eur J Pharm Sci. 96 (2017) 499--507. https://doi.org/10.1016/j.ejps.2016.10.017.

[148] K. Chu, L. Chen, W. Xu, H. Li, Y. Zhang, W. Xie, J. Zheng, Preparation of a Paeonol-Containing Temperature-Sensitive In Situ Gel and Its Preliminary Efficacy on Allergic Rhinitis, Int J Mol Sci. 14 (2013) 6499–6515. https://doi.org/10.3390/ijms14036499.

[149] C. Cao, C. Yan, Z. Hu, S. Zhou, Potential application of injectable chitosan hydrogel treated with siRNA in chronic rhinosinusitis therapy, Mol Med Rep. 12 (2015) 6688–6694. https://doi.org/10.3892/mmr.2015.4237.

[150] S. Cao, X. Ren, Q. Zhang, E. Chen, F. Xu, J. Chen, L.-C. Liu, X. Jiang, In situ gel based on gellan gum as new carrier for nasal administration of mometasone furoate, Int J Pharm. 365 (2009) 109–115. https://doi.org/10.1016/j.ijpharm.2008.08.042.

[151] D.Y. Cho, D.J. Lim, C. Mackey, C.G. Weeks, J.A.P. Garcia, D. Skinner, S. Zhang, J. McCormick, B.A. Woodworth, In-vitro evaluation of a ciprofloxacin- and ivacaftor-coated sinus stent against Pseudomonas aeruginosa biofilms, Int Forum Allergy Rhinol. 9 (2019) 486–492. https://doi.org/10.1002/alr.22285.

[152] D. Lim, J. McCormick, D. Skinner, S. Zhang, J.B. Elder, J.G. McLemore, M. Allen, J.M. West, J.W. Grayson, S.M. Rowe, B.A. Woodworth, D. Cho, Controlled delivery of ciprofloxacin

and ivacaftor via sinus stent in a preclinical model of Pseudomonas sinusitis, Int Forum Allergy Rhinol. 10 (2020) 481–488. https://doi.org/10.1002/alr.22514.

[153] Z. Chen, Z. Cai, C. Zhu, X. Song, Y. Qin, M. Zhu, T. Zhang, W. Cui, H. Tang, H. Zheng, Injectable and Self-Healing Hydrogel with Anti-Bacterial and Anti-Inflammatory Properties for Acute Bacterial Rhinosinusitis with Micro Invasive Treatment, Adv Healthc Mater. 9 (2020) 2001032. https://doi.org/10.1002/adhm.202001032.

[154] S.S. Garakani, S.M. Davachi, Z. Bagher, A.H. Esfahani, N. Jenabi, Z. Atoufi, M. Khanmohammadi, A. Abbaspourrad, H. Rashedi, M. Jalessi, Fabrication of chitosan/polyvinylpyrrolidone hydrogel scaffolds containing PLGA microparticles loaded with dexamethasone for biomedical applications, Int J Biol Macromol. 164 (2020) 356–370. https://doi.org/10.1016/j.ijbiomac.2020.07.138.

[155] Y. Su, B. Sun, X. Gao, S. Liu, R. Hao, B. Han, Chitosan Hydrogel Doped with PEG-PLA Nanoparticles for the Local Delivery of miRNA-146a to Treat Allergic Rhinitis, Pharm. 12 (2020) 907. https://doi.org/10.3390/pharmaceutics12100907.

[156] B.F. Marple, T.L. Smith, J.K. Han, A.R. Gould, H.D. Jampel, J.W. Stambaugh, A.S. Mugglin, Advance II: A Prospective, Randomized Study Assessing Safety and Efficacy of Bioabsorbable Steroid-Releasing Sinus Implants, Otolaryngol Head Neck Surg. 146 (2012) 1004–1011. https://doi.org/10.1177/0194599811435968.

[157] A.L. Schilling, Y. Kulahci, J. Moore, E.W. Wang, S.E. Lee, S.R. Little, A thermoresponsive hydrogel system for long-acting corticosteroid delivery into the paranasal sinuses, J. Control. Release. 330 (2021) 889–897. https://doi.org/10.1016/j.jconrel.2020.10.062.

[158] S.K. Gadkaree, V.K. Rathi, G.A. Scangas, M.R. Naunheim, R. Metson, Use of Corticosteroid-Eluting Sinus Stents Between 2012 and 2017, JAMA Otolaryngol Head Neck Surg. 145 (2019) 90–91. https://doi.org/10.1001/jamaoto.2018.2944.

[159] L. Rudmik, T.L. Smith, Economic Evaluation of a Steroid-Eluting Sinus Implant following Endoscopic Sinus Surgery for Chronic Rhinosinusitis, Otolaryngol Head Neck Surg. 151 (2014) 359–366. https://doi.org/10.1177/0194599814533779.

[160] C. Li, C. Guo, V. Fitzpatrick, A. Ibrahim, M.J. Zwierstra, P. Hanna, A. Lechtig, A. Nazarian, S.J. Lin, D.L. Kaplan, Design of biodegradable, implantable devices towards clinical translation, Nat Rev Mater. 5 (2020) 61–81. https://doi.org/10.1038/s41578-019-0150-z.

[161] P.M.M.C. Li, P.F. Li, D. Downie, P.H. Hwang, Controlled steroid delivery via bioabsorbable stent: Safety and performance in a rabbit model, Am J Rhinol Allergy. 23 (2009) 591–596. https://doi.org/10.2500/ajra.2009.23.3391.

[162] D.M. Tang, C.R. Roxbury, R. Sindwani, V.R. Kshettry, P. Recinos, T.D. Woodard, Multiple bioabsorbable corticosteroid-eluting stent placement with associated skull base injury, Laryngoscope. 129 (2019) 1494–1496. https://doi.org/10.1002/lary.27659.

[163] M.V. Fedorchak, I.P. Conner, J.S. Schuman, A. Cugini, S.R. Little, Long Term Glaucoma Drug Delivery Using a Topically Retained Gel/Microsphere Eye Drop, Sci Rep-Uk. 7 (2017) 8639. https://doi.org/10.1038/s41598-017-09379-8.

[164] U.C. Galgatte, A.B. Kumbhar, P.D. Chaudhari, Development of in situ gel for nasal delivery: design, optimization, in vitro and in vivo evaluation, Drug Deliv. 21 (2014) 62–73. https://doi.org/10.3109/10717544.2013.849778.

[165] A.A. Ammar, M. Gruber, P. Martin, O. Stern, F. Jahshan, O. Ertracht, E. Sela, S. Srouji, E. Zussman, Local delivery of mometasone furoate from an eluting endotracheal tube, J Control Release. 272 (2018) 54–61. https://doi.org/10.1016/j.jconrel.2018.01.005.

[166] D.-Y. Cho, C. Mackey, W.J.V.D. Pol, D. Skinner, C.D. Morrow, T.R. Schoeb, S.M. Rowe, W.E. Swords, G.J. Tearney, B.A. Woodworth, Sinus Microanatomy and Microbiota in a Rabbit Model of Rhinosinusitis, Front Cell Infect Mi. 7 (2018) 540. https://doi.org/10.3389/fcimb.2017.00540.

[167] A. Bar-Ilan, The pattern of distribution of intraocular pressure in the albino rabbit, Graefe's Archive Clin Exp Ophthalmol. 224 (1986) 469–472. https://doi.org/10.1007/bf02173366.

[168] I. Alava, S. Isaacs, A. Luong, M.J. Citardi, S. Fakhri, Mometasone furoate gel: A novel in-office treatment of recalcitrant postoperative chronic rhinosinusitis, J Otolaryngology - Head Neck Surg Le J D'oto-Rhino-Laryngologie Et De Chir Cervico-Faciale. 41 (2012) 183–188. https://doi.org/10.2310/7070.2012.00023.

[169] P. Pandey, P.J. Cabot, B. Wallwork, B.J. Panizza, H.S. Parekh, Formulation, functional evaluation and ex vivo performance of thermoresponsive soluble gels - A platform for therapeutic delivery to mucosal sinus tissue, Eur J Pharm Sci. 96 (2017) 499--507. https://doi.org/10.1016/j.ejps.2016.10.017.

[170] S.N. Rothstein, J.E. Kay, F.J. Schopfer, B.A. Freeman, S.R. Little, A Retrospective Mathematical Analysis of Controlled Release Design and Experimentation, Mol Pharmaceut. 9 (2012) 3003–3011. https://doi.org/10.1021/mp300388w.

[171] J. Far, M. Abdel-Haq, M. Gruber, A.A. Ammar, Developing Biodegradable Nanoparticles Loaded with Mometasone Furoate for Potential Nasal Drug Delivery, ACS Omega. 5 (2020) 7432--7439. https://doi.org/10.1021/acsomega.0c00111.

[172] L.K. Dkhar, J. Bartley, D. White, A. Seyfoddin, Intranasal drug delivery devices and interventions associated with post-operative endoscopic sinus surgery, Pharm Dev Technol. 23 (2018) 282–294. https://doi.org/10.1080/10837450.2017.1389956.

[173] S.N. Rothstein, S.R. Little, A "tool box" for rational design of degradable controlled release formulations, J Mater Chem. 21 (2011) 29–39. https://doi.org/10.1039/c0jm01668c.

[174] J. Xi, X.A. Si, J. Kim, Y. Zhang, R.E. Jacob, S. Kabilan, R.A. Corley, Anatomical Details of the Rabbit Nasal Passages and Their Implications in Breathing, Air Conditioning, and Olfaction, Anatomical Rec. 299 (2016) 853–868. https://doi.org/10.1002/ar.23367.

[175] S.L. Ball, M.I. Suwara, L.A. Borthwick, J.A. Wilson, D.A. Mann, A.J. Fisher, How reliable are sino-nasal cell lines for studying the pathophysiology of chronic rhinosinusitis?, Ann Otology Rhinology Laryngology. 124 (2015) 437–442. https://doi.org/10.1177/0003489414565003.

[176] A. Alexander, Ajazuddin, J. Khan, S. Saraf, S. Saraf, Polyethylene glycol (PEG)–Poly(N-isopropylacrylamide) (PNIPAAm) based thermosensitive injectable hydrogels for biomedical applications, Eur J Pharm Biopharm. 88 (2014) 575–585. https://doi.org/10.1016/j.ejpb.2014.07.005.

[177] A.A. Al-Sayed, R.U. Agu, E. Massoud, Models for the study of nasal and sinus physiology in health and disease: A review of the literature, Laryngoscope Investig Otolaryngol. 2 (2017) 398–409. https://doi.org/10.1002/lio2.117.

[178] A. Şimşek, C. Bayraktar, S. Doğan, M. Karataş, Y. Sarıkaya, The effect of long-term use of intranasal steroids on intraocular pressure, Clin Ophthalmol. 10 (2016) 1079–1082. https://doi.org/10.2147/opth.s106392.

[179] D. Bross-Soriano, C. Hanenberg-Milver, J. Schimelmitz-Idi, J.R. Arrieta-Gomez, R.A.D. Toro, G. Bravo-Escobar, Effects of three nasal topical steroids in the intraocular pressure compartment, Otolaryngology Head Neck Surg. 130 (2004) 187–191. https://doi.org/10.1016/j.otohns.2003.09.020.

[180] S.J. Zinreich, Imaging for staging of rhinosinusitis, Ann Otology Rhinology Laryngology. 113 (2004) 19–23. https://doi.org/10.1177/00034894041130s506.

[181] K.M. Ozcan, I. Ozcan, A. Selcuk, O. Akdogan, S.G. Gurgen, T. Deren, S. Koparal, C. Ozogul, H. Dere, Comparison of Histopathological and CT Findings in Experimental Rabbit Sinusitis, Indian J Otolaryngol. 63 (2011) 56–59. https://doi.org/10.1007/s12070-011-0120-2.

[182] J.E. Kerschner, M.J. Cruz, D.J. Beste, K.M. Donahue, K.S. Kehl, Computed tomography vs. magnetic resonance imaging of acute bacterial sinusitis: A rabbit model, Am J Otolaryng. 21 (2000) 298–305. https://doi.org/10.1053/ajot.2000.9874.

[183] G.N. Hounsfield, Computed Medical Imaging, Science. 210 (1980) 22–28.

[184] S.H. Cho, H.J. Min, H.X. Han, S.S. Paik, K.R. Kim, CT analysis and histopathology of bone remodeling in patients with chronic rhinosinusitis, Otolaryngology - Head Neck Surg. 135 (2006) 404–408. https://doi.org/10.1016/j.otohns.2006.04.005.

[185] S.J. Szefler, Pharmacokinetics of intranasal corticosteroids, J Allergy Clin Immun. 108 (2001) S26–S31. https://doi.org/10.1067/mai.2001.115563.

[186] A.L. Schilling, J. Moore, Y. Kulahci, S.R. Little, L.H. Rigatti, E.W. Wang, S.E. Lee, Evaluating inflammation in an obstruction-based chronic rhinosinusitis model in rabbits, Int Forum Allergy Rhinol. 11 (2021) 807–809. https://doi.org/10.1002/alr.22729.

[187] A.L. Schilling, S.R. Little, E.W. Wang, S.E. Lee, In Reply: A Preclinical Model to Tackle Chronic Rhinosinusitis, Int Forum Allergy Rhinol. 11 (2021) 828–829. https://doi.org/10.1002/alr.22769.

[188] W. Xianmin, Z. Yue, C. Xiaoyun, C. Jun, J. Minghui, Inflammatory immune response in rabbits with Staphylococcus aureus biofilm–associated sinusitis, Int Forum Allergy Rhinol. 8 (2018) 1226–1232. https://doi.org/10.1002/alr.22175.

[189] X.W. Teng, D.C. Cutler, N.M. Davies, Degradation kinetics of mometasone furoate in aqueous systems, Int J Pharm. 259 (2003) 129–141. https://doi.org/10.1016/s0378-5173(03)00226-6.

[190] A.C. Doty, D.G. Weinstein, K. Hirota, K.F. Olsen, R. Ackermann, Y. Wang, S. Choi, S.P. Schwendeman, Mechanisms of in vivo release of triamcinolone acetonide from PLGA microspheres, J Control Release. 256 (2017) 19--25. https://doi.org/10.1016/j.jconrel.2017.03.031.

[191] D. Gudis, K.Q. Zhao, N.A. Cohen, Acquired cilia dysfunction in chronic rhinosinusitis, Am J Rhinol Allergy. 26 (2012) 1–6. https://doi.org/10.2500/ajra.2012.26.3716.

[192] Y.Y. Li, C.W. Li, S.S. Chao, F.G. Yu, X.M. Yu, J. Liu, Y. Yan, L. Shen, W. Gordon, L. Shi, D.Y. Wang, Impairment of cilia architecture and ciliogenesis in hyperplastic nasal epithelium from nasal polyps., J Allergy Clin Immun. 134 (2014) 1282–1292. https://doi.org/10.1016/j.jaci.2014.07.038.

[193] M.S. Maccabee, D.R. Trune, P.H. Hwang, Paranasal Sinus Mucosal Regeneration: The Effect of Topical Retinoic Acid, Am J Rhinol Allergy. 17 (2003) 133–137. https://doi.org/10.1177/194589240301700304.

[194] M.-K. Leung, P.H. Hwang, Rehabilitation of Surgically Traumatized Paranasal Sinus Mucosa using Retinoic Acid, Am J Rhinol. 21 (2007) 271–275. https://doi.org/10.2500/ajr.2007.21.3035.

[195] P.H. Hwang, J.M. Chan, Retinoic acid improves ciliogenesis after surgery of the maxillary sinus in rabbits, Laryngoscope. 116 (2006) 1080–1085. https://doi.org/10.1097/01.mlg.0000224352.50256.99.

[196] V.R. Erickson, M. Antunes, B. Chen, N.A. Cohen, P.H. Hwang, The Effects of Retinoic Acid on Ciliary Function of Regenerated Sinus Mucosa, Am J Rhinol Allergy. 22 (2008) 334–336. https://doi.org/10.2500/ajr.2008.22.3176.

[197] K.M. Fang, C.T. Wang, Y.W. Chen, T.W. Huang, Reduction of adhesions and antrostomy stenosis with topical Vitamin A after endoscopic sinus surgery, Am J Rhinol Allergy. 29 (2015) 430–434. https://doi.org/10.2500/ajra.2015.29.4235.

[198] M. Zahid, A. Bais, X. Tian, W. Devine, D.M. Lee, C. Yau, D. Sonnenberg, L. Beerman, O. Khalifa, C.W. Lo, Airway ciliary dysfunction and respiratory symptoms in patients with transposition of the great arteries, Plos One. 13 (2018) 1–12. https://doi.org/10.1371/journal.pone.0191605.

[199] D. Chopra, Squamous Metaplasia in Organ Cultures of Vitamin A-Deficient Hamster Trachea: Cytokinetic and Ultrastructural Alterations, J Natl Cancer Inst. 69 (1982) 895–905. https://doi.org/10.1093/jnci/69.4.895.

[200] E.M. McDowell, K.P. Keenan, M. Huang, Restoration of mucociliary tracheal epithelium following deprivation of vitamin A. A quantitative morphologic study., Virchows Archiv B Cell Pathol Incl Mol Pathol. 45 (1984) 221–240. https://doi.org/10.1007/bf02889866.

[201] T. Ehtezazi, C. Washington, Controlled release of macromolecules from PLA microspheres: using porous structure topology, J Control Release. 68 (2000) 361–372. https://doi.org/10.1016/s0168-3659(00)00270-4.

[202] Y. Çirpanli, N. ünlü, S. Çaliş, A.A. Hincal, Formulation and in-vitro characterization of retinoic acid loaded poly (lactic-co-glycolic acid) microspheres, J Microencapsul. 22 (2005) 877–889. https://doi.org/10.1080/02652040500273878.

[203] J. Young-Il, S. Jin-Gyu, K. Sam-Suk, R. Hyang-Hwa, L. Young-Hwa, C. Chan, S. Boo-Ahn, K. Kyung-Keun, A. Kyu-Youn, J. Shin, Preparation of poly(dl-lactide-co-glycolide) microspheres encapsulating all-trans retinoic acid, Int J Pharmaceut. 259 (2003) 79. https://doi.org/10.1016/s0378-5173(03)00207-2.

[204] T.F. Palmberger, P. Augustijns, A. Vetter, A. Bernkop-Schunrch, Safety assessment of thiolated polymers: Effect on ciliary beat frequency in human nasal epithelial cells, Drug Dev Ind Pharm. 37 (2011) 1455–1462. https://doi.org/10.3109/03639045.2011.584537.

[205] C. Menzel, M. Jelkmann, F. Laffleur, A. Bernkop-Schnurch, Nasal drug delivery: Design of a novel mucoadhesive and in situ gelling polymer, Int J Pharmaceut. 517 (2017) 196–202. https://doi.org/10.1016/j.ijpharm.2016.11.055.

[206] R. Mallants, M. Jorissen, P. Augustijns, Effect of preservatives on ciliary beat frequency in human nasal epithelial cell culture: Single versus multiple exposure, Int J Pharmaceut. 338 (2007) 64. https://doi.org/10.1016/j.ijpharm.2007.01.029.

[207] P. Merkus, S.G. Romeijn, J.C. Verhoef, F.W.H.M. Merkus, P.F. Schouwenburg, Classification of Cilio-Inhibiting Effects of Nasal Drugs, Laryngoscope. 111 (2001) 595–602. https://doi.org/10.1097/00005537-200104000-00008.

[208] B.S. Bleier, R.M. Mulligan, R.J. Schlosser, Primary human sinonasal epithelial cell culture model for topical drug delivery in patients with chronic rhinosinusitis with nasal polyposis, J Pharm Pharmacol. 64 (2012) 449–456. https://doi.org/10.1111/j.2042-7158.2011.01409.x.

[209] K. Million, F. Tournier, O. Houcine, P. Ancian, U. Reichert, F. Marano, Effects of Retinoic Acid Receptor–Selective Agonists on Human Nasal Epithelial Cell Differentiation, Am J Resp Cell Mol. 25 (2001) 744–750. https://doi.org/10.1165/ajrcmb.25.6.4549.

[210] A.M. Jetten, M.E.R. Jetten, S.S. Shapiro, J.P. Poon, Characterization of the action of retinoids on mouse fibroblast cell lines, Experimental Cell Research. 119 (1979) 289–299. https://www.sciencedirect.com/science/article/pii/0014482779903562.

[211] V. James, M. S Raj, G. Douglas, P. H Sem, D. M Vishva, M. Rajorshi, W. Tamara, S. J Karl, N. J Brian, V. J John, All-Trans Retinoic Acid Stimulates Growth and Extracellular Matrix Production in Growth-Inhibited Cultured Human Skin Fibroblasts, J Invest Dermatol. 94 (1990) 717–723. https://doi.org/10.1111/1523-1747.ep12876294.

[212] K.L. Penniston, T. A Sherry, The acute and chronic toxic effects of vitamin A, Am J Clin Nutrition. 83 (2006) 191. https://doi.org/10.1093/ajcn/83.2.191.

[213] Retinoids, in: LiverTox: Clinical and Research Information on Drug-Induced Liver Injury, National Institute of Diabetes and Digestive and Kidney Diseases, 2020.

[214] X. (Charlie) Tang, M.J. Pikal, Design of Freeze-Drying Processes for Pharmaceuticals: Practical Advice, Pharmaceut Res. 21 (2004) 191–200. https://doi.org/10.1023/b:pham.0000016234.73023.75.

[215] F. Franks, Freeze-drying of bioproducts: putting principles into practice, Eur J Pharm Biopharm. 45 (1998) 221–229. https://doi.org/10.1016/s0939-6411(98)00004-6.

[216] J.F. Carpenter, M.J. Pikal, B.S. Chang, T.W. Randolph, Rational Design of Stable Lyophilized Protein Formulations: Some Practical Advice, Pharmaceut Res. 14 (1997) 969–975. https://doi.org/10.1023/a:1012180707283.

[217] S. Lungare, J. Bowen, R. Badhan, Development and Evaluation of a Novel Intranasal Spray for the Delivery of Amantadine, J Pharm Sci. 105 (2016) 1209–1220. https://doi.org/10.1016/j.xphs.2015.12.016.

[218] H. Hatakeyama, T. Hatakeyama, Interaction between water and hydrophilic polymers, Thermochimica Acta. 308 (1998) 3–22. https://doi.org/10.1016/s0040-6031(97)00325-0.

[219] S. H.G., Poly(N-isopropylacrylamide): experiment, theory and application, Prog Polym Sci. 17 (1992) 163–249. https://doi.org/10.1016/0079-6700(92)90023-r.

[220] S.K. Pansare, S.M. Patel, Practical Considerations for Determination of Glass Transition Temperature of a Maximally Freeze Concentrated Solution, AAPS PharmSciTech. 17 (2016) 805–819. https://doi.org/10.1208/s12249-016-0551-x.

[221] L. Shan-Yang, C. Ko-Shao, R.-C. Liang, Drying methods affecting the particle sizes, phase transition, deswelling/reswelling processes and morphology of poly(N-isopropylacrylamide) microgel beads, Polymer. 40 (1999) 6307. https://doi.org/10.1016/s0032-3861(98)00872-6.

[222] C. Chang-Jing, C. Liang-Yin, Z. Jie, W. Hai-Dong, W. Gang, Effect of freeze-drying and rehydrating treatment on the thermo-responsive characteristics of poly(N-isopropylacrylamide) microspheres, Colloid Polym Sci. 286 (2008) 571. https://doi.org/10.1007/s00396-007-1817-3.

[223] X.-M. Liu, L.-S. Wang, L. Wang, J. Huang, C. He, The effect of salt and pH on the phase-transition behaviors of temperature-sensitive copolymers based on N-isopropylacrylamide, Biomaterials. 25 (2004) 5659–5666. https://doi.org/10.1016/j.biomaterials.2004.01.019.

[224] L. K. Samuel, W. Ying-Ying, W. Denis, H. Justin, Micro- and macrorheology of mucus, Adv Drug Deliver Rev. 61 (2009) 86–100. https://doi.org/10.1016/j.addr.2008.09.012.

[225] H. Lih-Min, S.L. Nail, Measurement of Glass Transition Temperatures of Freeze-Concentrated Solutes by Differential Scanning Calorimetry, Pharmaceut Res. 11 (1994) 54. https://doi.org/10.1023/a:1018989509893.

[226] G. Sun, X.Z. Zhang, C.C. Chu, Effect of the molecular weight of polyethylene glycol (PEG) on the properties of chitosan-PEG-poly(N-isopropylacrylamide) hydrogels, J Mater Sci Mater Med. 19 (2008) 2865–2872. https://doi.org/10.1007/s10856-008-3410-9.

[227] K. Amin, R. Dannenfelser, J. Zielinski, B. Wang, Lyophilization of polyethylene glycol mixtures, J Pharm Sci. 93 (2004) 2244–2249. https://doi.org/10.1002/jps.20135.

[228] M.L. Houchin, E.M. Topp, Chemical degradation of peptides and proteins in PLGA: A review of reactions and mechanisms, J Pharm Sci. 97 (2008) 2395–2404. https://doi.org/10.1002/jps.21176.

[229] A.G. Sonje, H.S. Mahajan, Nasal inserts containing ondansetron hydrochloride based on Chitosan–gellan gum polyelectrolyte complex: In vitro–in vivo studies, Mater Sci Eng C Mater Biol Appl. 64 (2016) 329–335. https://doi.org/10.1016/j.msec.2016.03.091.

[230] F. Kianfar, M. Antonijevic, B. Chowdhry, J.S. Boateng, Lyophilized wafers comprising carrageenan and pluronic acid for buccal drug delivery using model soluble and insoluble drugs, Colloids Surf. B: Biointerfaces. 103 (2013) 99–106. https://doi.org/10.1016/j.colsurfb.2012.10.006.

[231] Y. Chao, A. Dahlia, S. Anita, β-Lactamase Responsive Supramolecular Hydrogels with Host–Guest Self-Healing Capability, Acs Appl Polym Mater. 2 (2020) 55–65. https://doi.org/10.1021/acsapm.9b00879.

[232] P.R. Sears, X.M. Bustamante-Marin, H. Gong, M.R. Markovetz, R. Superfine, D.B. Hill, L.E. Ostrowski, Induction of ciliary orientation by matrix patterning and characterization of mucociliary transport, Biophys J. 120 (2021) 1387–1395. https://doi.org/10.1016/j.bpj.2021.01.041.

[233] B. Mieke, J. Mark, J. Martine, A. Patrick, V. L. François, P. Marijke, D.B. Kris, The Influence of Nebulized Drugs on Nasal Ciliary Activity, J Aerosol Med Pulm D. 29 (2016) 378–385. https://doi.org/10.1089/jamp.2015.1229.

[234] D.S. Lazard, A. Moore, V. Hupertan, C. Martin, V. Escabasse, P. Dreyfus, B. P.-R., A. S., E. E., C. A., Muco-ciliary differentiation of nasal epithelial cells is decreased after wound healing in vitro, Allergy. 64 (2009) 1136–1143. https://doi.org/10.1111/j.1398-9995.2009.02003.x.

[235] E. D. Jason, S. A. Samir, S. Charles, K. S. Vitthal, C. Intira, D. Samiran, S. D. Julie, Considerations for the Development of Nasal Dosage Forms, in: Springer New York, New York, NY, 2013: pp. 99–144. https://doi.org/10.1007/978-1-4614-7978-9_5.

[236] G. Raquel, P. A. Terezinha J., C. Rogério, S. Paula Ana, Sterilization of hydrogels for biomedical applications: A review, J Biomed Mater Res Part B Appl Biomaterials. 106 (2018) 2472–2492. https://doi.org/10.1002/jbm.b.34048.

[237] Y. Yang, G. Yongliang, M. Xingguo, Effects of formulation parameters on encapsulation efficiency and release behavior of thienorphine loaded PLGA microspheres, Pharm Dev Technol. 18 (2013) 1169–1174. https://doi.org/10.3109/10837450.2011.618948.

[238] R. Fracalossi Carolina, de J.A.P. Terezinha, B.-C. Araci Nadia, G. Raquel, de A. Barros Gabriel Lima, do N.P. Tatiana, M.-E. Stuchi Silvya, D.B. A. Paul, Ozone Gas as a Benign Sterilization Treatment for PLGA Nanofiber Scaffolds, Tissue Eng Part C Methods. 22 (2016) 338–347. https://doi.org/10.1089/ten.tec.2015.0298.

[239] Z. Cui, B.H. Lee, C. Pauken, B.L. Vernon, Degradation, cytotoxicity, and biocompatibility of NIPAAm-based thermosensitive, injectable, and bioresorbable polymer hydrogels, J Biomed Mater Res A. 98A (2011) 159–166. https://doi.org/10.1002/jbm.a.33093.

[240] N. Huebsch, M. Gilbert, K.E. Healy, Analysis of sterilization protocols for peptide-modified hydrogels, J Biomed Mater Res Part B Appl Biomaterials. 74B (2005) 440–447. https://doi.org/10.1002/jbm.b.30155.

[241] D. Rafael, F. Andrade, F. Martinez-Trucharte, J. Basas, J. Seras-Franzoso, M. Palau, X. Gomis, M. Pérez-Burgos, A. Blanco, A. López-Fernández, R. Vélez, I. Abasolo, M. Aguirre, J. Gavaldà, S. Schwartz, Sterilization Procedure for Temperature-Sensitive Hydrogels Loaded with Silver Nanoparticles for Clinical Applications, Nanomaterials-Basel. 9 (2019) 380. https://doi.org/10.3390/nano9030380.

[242] S. W. Whitney, L. J. Robert, S. P. Robert, C. A. Noam, Chronic rhinosinusitis pathogenesis, J Allergy Clin Immun. 136 (2015) 1442–1453. https://doi.org/10.1016/j.jaci.2015.10.009.

[243] T. Qizhi, B. A Jeffrey, The Foxp3+ regulatory T cell: a jack of all trades, master of regulation, Nat Immunol. 9 (2008) 239–244. https://doi.org/10.1038/ni1572.

[244] C. Palmer, J.K. Mulligan, S.E. Smith, C. Atkinson, The Role of Regulatory T Cells in the Regulation of Upper Airway Inflammation, Am J Rhinol Allergy. 31 (2017) 345–351. https://doi.org/10.2500/ajra.2017.31.4472.

[245] K. Min Yong, M. Amanda, H. H. Peter, N. C. Kari, Migration of regulatory T cells toward airway epithelial cells is impaired in chronic rhinosinusitis with nasal polyposis, Clin Immunol. 137 (2010) 111–121. https://doi.org/10.1016/j.clim.2010.05.013.

[246] S. Sharma, S. Watanabe, A. Sivam, J. Wang, S.J. Neuwirth, R.I. Perez, M.D. Tineo, F.M. Baroody, R.M. Naclerio, J.M. Pinto, Peripheral Blood and Tissue T Regulatory Cells in Chronic Rhinosinusitis, Am J Rhinol Allergy. 26 (2012) 371–379. https://doi.org/10.2500/ajra.2012.26.3800.

[247] H.B. Li, K.M. Cai, Z. Liu, J.H. Xia, Y. Zhang, R. Xu, G. Xu, Foxp3+ T regulatory cells (Tregs) are increased in nasal polyps (NP) after treatment with intranasal steroid, Clin Immunol. 129 (2008) 394–400. https://doi.org/10.1016/j.clim.2008.07.031.

[248] E. A Justin, S. Mrinmoy, L. Wei, S. Ethan, R. R Vijay, B. T Dawn, N. L Alan, Z. David, K. T Todd, H. H Peter, G.F. C, N. V Jayakar, Selective expansion of human regulatory T cells in nasal polyps, and not adjacent tissue microenvironments, in individual patients exposed to steroids, Clin Immunol. 179 (2017) 66–76. https://doi.org/10.1016/j.clim.2017.02.002.

[249] S. Jhunjhunwala, G. Raimondi, A.J. Glowacki, S.J. Hall, D. Maskarinec, S.H. Thorne, A.W. Thomson, S.R. Little, Bioinspired Controlled Release of CCL22 Recruits Regulatory T Cells In Vivo, Adv Mater. 24 (2012) 4735–4738. https://doi.org/10.1002/adma.201202513.

[250] A.J. Glowacki, S. Yoshizawa, S. Jhunjhunwala, A.E. Vieira, G.P. Garlet, C. Sfeir, S.R. Little, Prevention of inflammation-mediated bone loss in murine and canine periodontal disease via recruitment of regulatory lymphocytes, PNAS. 110 (2013) 18525–18530. https://doi.org/10.1073/pnas.1302829110.

[251] J.D. Fisher, W. Zhang, S.C. Balmert, A.M. Aral, A.P. Acharya, Y. Kulahci, J. Li, H.R. Turnquist, A.W. Thomson, M.G. Solari, V.S. Gorantla, S.R. Little, In situ recruitment of regulatory T cells promotes donor-specific tolerance in vascularized composite allotransplantation, Sci Adv. 6 (2020) eaax8429. https://doi.org/10.1126/sciadv.aax8429.

[252] M.L. Ratay, A.J. Glowacki, S.C. Balmert, A.P. Acharya, J. Polat, L.P. Andrews, M.V. Fedorchak, J.S. Schuman, D.A.A. Vignali, S.R. Little, Treg-recruiting microspheres prevent

inflammation in a murine model of dry eye disease, J Control Release. 258 (2017) 208–217. https://doi.org/10.1016/j.jconrel.2017.05.007.

[253] C. W. Lauren, D.A.A. Vignali, In Vitro Treg Suppression Assays, in: Humana Press, Totowa, NJ, 2011: pp. 21–37. https://doi.org/10.1007/978-1-61737-979-6_2.

[254] M. Hinchcliffe, L. Illum, Intranasal insulin delivery and therapy, Adv Drug Deliver Rev. 35 (1999) 199–234. https://doi.org/10.1016/s0169-409x(98)00073-8.

[255] S. Jhunjhunwala, S.C. Balmert, G. Raimondi, E. Dons, E.E. Nichols, A.W. Thomson, S.R. Little, Controlled release formulations of IL-2, TGF-β1 and rapamycin for the induction of regulatory T cells, J Control Release. 159 (2012) 78–84. https://doi.org/10.1016/j.jconrel.2012.01.013.